OVERCOMING RESISTANCE TO MEK INHIBITOR TREATMENT IN NF1-DEFICIENT MALIGNANT PERIPHERAL NERVE SHEATH TUMORS

by

Miguel Angel Miranda-Román

A Dissertation

Presented to the Faculty of the Louis V. Gerstner, Jr.

Graduate School of Biomedical Sciences,

Memorial Sloan Kettering Cancer Center

In Partial Fulfillment of the Requirements for the

Degree of Doctor of Philosophy

New York, NY

September, 2022

_____ _____

Ping Chi, M.D., Ph.D. Date

Dissertation Mentor

DEDICATION

I want to dedicate this thesis to the people who without their support all of this would have been impossible to achieve. To my best friend and wife, Andrea, my main listener, supporter, and motivator. Gracias por siempre estar ahí cuando lo necesitaba, dándome tu apoyo y ayuda incondicional en todo momento. To my parents and brother, Awilda, Anselmo, and Juan Pablo, always there, ready to listen and offer their unconditional support. And to my two pets, Arya and Sansa, who always were ready to help me de-stress and relax after the long days of studying and working. ¡Gracias a todos!

ABSTRACT

Malignant peripheral nerve sheath tumor (MPNST) is a highly aggressive type of soft tissue sarcoma with a high propensity to metastasize and very limited treatment options. Loss of the RAS-GAP NF1 leads to sustained RAF/MEK/ERK signaling in MPNST. However, single-agent MEK inhibitors (MEKi) have failed to elicit a good and sustained inhibition of the pathway in MPNST. Here, we report that MEKi treatment resistance in MPNST involves two pathways: direct transcriptional upregulation of the receptor tyrosine kinase (RTK) PDGFRβ, and MEKi-induced increase in RAF dimer formation and activation of downstream signaling. While the pharmacological combination of MEKi with a PDGFRβ specific inhibitor was more effective than treatment with MEKi alone, the combination of MEKi and RAF-dimer inhibitors led to a robust inhibition of the MAPK pathway signaling. Furthermore, this combination treatment was effective *in vitro* and *in vivo,* as demonstrated by the significant increase in drug synergism and its high effectiveness at decreasing MPNST viability. Our findings support the use of this combination strategy to overcome MEKi resistance and as a novel targeted therapeutic approach for NF1-deficient MPNST patients, which in turn could impact future clinical trials for this patient population.

BIOGRAPHICAL SKETCH

Miguel was born in Bayamón, Puerto Rico, in May 1992. Miguel got his bachelor's in science (B.S.) degree in Cellular and Molecular Biology from the University of Puerto Rico (UPR) – Río Piedras in 2015, with Magna Cum Laude honors and as a member of the Faculty of Natural Sciences Honor Dean's List. During this time, Miguel worked as an undergraduate researcher in four different laboratories located in the UPR – Río Piedras, UPR – Comprehensive Cancer Center, Albert Einstein College of Medicine, and the University of Pennsylvania. The NIH Maximizing Access to Research Careers (MARC) fellowship supported his research performed in Puerto Rico. Later, in the summer of 2015, Miguel moved to New York City, NY, to join the Louis V. Gerstner Jr. Graduate School of Biomedical Sciences at Memorial Sloan Kettering Cancer Center. After finishing the first year of graduate school, Miguel was awarded the Palestine Fellowship by the graduate school to support the second year of his studies. Later, in 2019, Miguel was also awarded the Department of Defense Peer Reviewed Cancer Horizon Award fellowship to support his last three years of research leading to the conclusion of his Ph.D. thesis and first author research manuscript in 2022.

ACKNOWLEDGMENTS

I want to thank my mentor, Dr. Ping Chi, for providing me with the support, feedback, and training needed to complete this work and develop as an independent researcher. I also want to thank Dr. Yu Chen for providing great feedback and support these past years.

I want to thank all members of the Ping Chi and Yu Chen laboratories, the members of my thesis advisory committee, Dr. Ross Levine and Dr. Sarat Chandarlapaty, and the members of my thesis defense Drs. Charles Rudin and Christine Pratilas, for all their support.

I would also like to thank the Department of Defense for the Peer Reviewed Cancer Horizon Award, which helped support the last years of my doctoral research.

Lastly, I would like to thank the GSK graduate school, Drs. Ken Marians, Michael Overholtzer, Linda Burnley, Tom Magaldi, David McDonagh, Iwona Abramek, and others, who also in one way or another helped make all this possible, and to the school in general which also helped support my doctoral research by selecting me to be the recipient of the Palestine Fellowship.

TABLE OF CONTENTS

LIST OF TABLES

LIST OF FIGURES

LIST OF ABBREVIATIONS

BCA	Bicinchoninic acid assay
BSA	Bovine Serum Albumin
Co-IP	Co-Immunoprecipitation
CTG	CellTiter-Glo
CRISPR	Clustered regularly interspaced short palindromic repeats
DMEM	Dulbecco's Minimum Essential Media
DTT	Dithiothreitol
EtOH	Ethanol
FBS	Fetal Bovine Serum (supplement for cell media)
H2O	Water
H3K27me	Histone H3 Lysine 27 methylation
KO	Knockout
LB	Cell Lysis Buffer
MAPK	Mitogen-activated protein kinases
MEKi	MEK inhibitor
MeOH	Methanol
MPNST	Malignant Peripheral Nerve Sheath Tumor
MOPS	3-(N-morpholino)propanesulfonic acid
NF1	Neurofibromin 1 (protein)
NP40	Nonionic polyoxyethylene surfactant
PBS	Phosphate-buffered saline

PDGFR	Platelet Derived Growth Factor Receptor
PDX	Patient derived xenograft
PI	Protease Inhibitor
PMSF	Serine protease inhibitor (phenylmethylsulfonyl fluoride)
PRC2	Polycomb repressive complex 2
PPI	Phosphatase Inhibitor
RAFi	RAF inhibitor
RPMI	Roswell Park Memorial Institute (culture medium)
RTK	Receptor tyrosine kinase
RT-qPCR	Reverse transcription quantitative polymerase chain reaction
SCID	Severe combined immune deficiency
SDS	Sodium Dodecyl Sulfate
-Seq	High-throughput sequencing
TBS	Tris-buffered saline
TBST	Tris-buffer Saline, Tween
WB	Western blot

CHAPTER 1 – INTRODUCTION

CHAPTER 1.1 – MALIGNANT PERIPHERAL NERVE SHEATH TUMORS

Malignant peripheral nerve sheath tumor (MPNST) is a highly aggressive type of soft tissue sarcoma that originates in the cellular component of the peripheral nerves. Accounting for 5-10% of all soft tissue sarcomas [1], this disease has a high propensity to metastasize, poor sensitivity to systemic chemotherapy and radiotherapy, and poor prognosis, with a 5-year survival rate of 30-40% [1,2]. Diagnostic of the disease generally occurs between ages 20-50, but cases have been reported in newborns and infants [3,4]. Patients normally present a rapidly enlarging mass that may cause neurological symptoms, such as paraesthesia or motor weakness, and that in 50% of patients has already metastasized, usually to the lung, soft tissue, bone, and liver [5]. Primary tumors are commonly located on the extremities, followed by the trunk and head/neck [1].

Complete surgical resection with wide margins remains the best treatment option for MPNST patients, which makes the disease outcome particularly detrimental in cases with unresectable or metastatic disease [1,6–8]. Also, the location of the tumors can significantly affect the ability to achieve suitable negative surgical margins without resulting in an important compromise of function [2]. In addition to surgery, the majority of patients also receive adjuvant treatment with radiation, chemotherapy, or both [1,9]. Therefore, the discovery of novel targeted therapeutic strategies for MPNST is an urgent clinical need.

Conventionally, MPNST arises through three distinct clinical settings. Around 45% of MPNSTs arise in the setting of Neurofibromatosis type I (NF1-associated), another 45% arise sporadically, and 10% are associated with previous radiotherapy treatment [7,10,11]. Patients with Neurofibromatosis type I present a 10% lifetime risk of developing MPNST.[3]

CHAPTER 1.2 – GENOMIC ALTERATIONS IN MPNST

Regardless of the clinical setting through which MPNST arises, most MPNSTs share a frequent biallelic genetic inactivation of three major tumor suppressor pathways including the NF1, CDKN2A, and PRC2 (EED or SUZ12) (Figure 1 A) [12–14]. PRC2 mutations were observed in 70% of NF1-associated, 92% of sporadic, and 90% of radiotherapy-associated MPNSTs, and loss of trimethylation at lysine 27 of histone H3 (H3K27me3) was detected in these tumors (Figure 1 B) [12]. Investigating the involvement of PRC2 in MPNST will help to determine its role in the onset and progression of the disease. On the other hand, NF1 functions as a RAS-GAP, and its absence can lead to uncontrolled activation of RAS and subsequent sustained activation of the RAF/MEK/ERK signaling [15,16], which identifies this signaling pathway as an important target for MPNST treatment. Finally, CDKN2A mutations are found in around 81% of NF1-associated, and 95% of sporadic and radiotherapy-associated MPNSTs [12]. All these data suggest that despite the clinical heterogeneity found in MPNST, at the molecular level these tumors represent a relatively homogenous group of diseases.

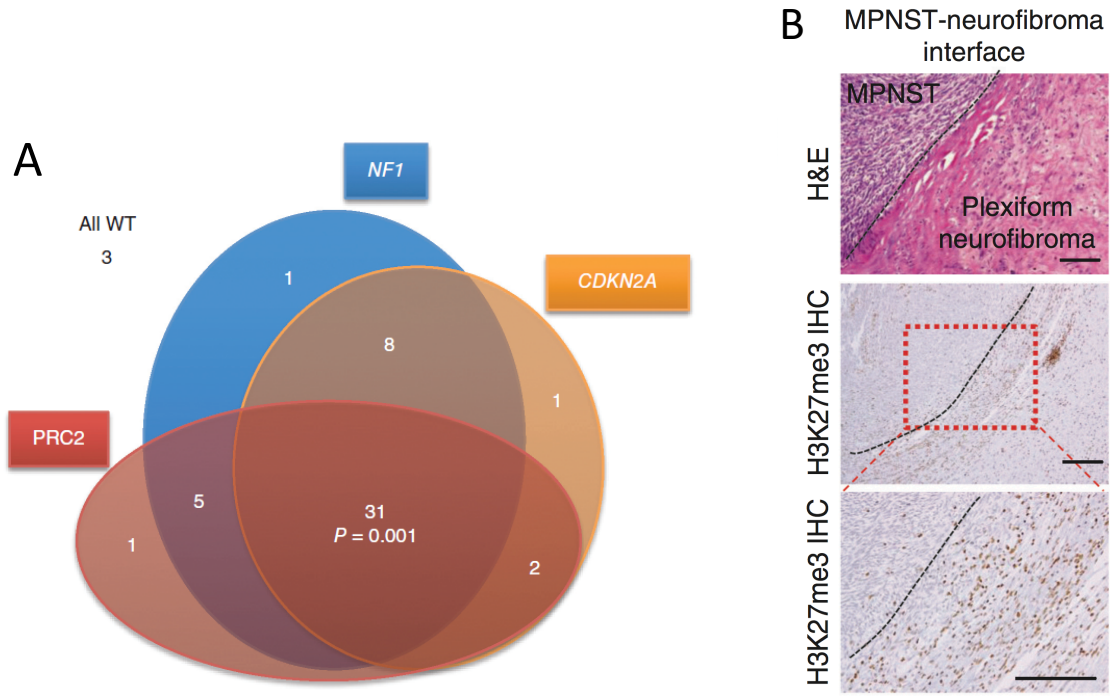

Figure 1. Common genetic alterations in MPNST

A) Inactivating mutations of NF1, CDKN2A, and PRC2 (EED or SUZ12 components) frequently co-occur in MPNST.

B) Representative H&E staining and H3K27me3 IHC images of the interface of plexiform neurofibroma transitioning into MPNST.

* Adapted from: Lee, W., et al. PRC2 is recurrently inactivated through EED or SUZ12 loss in malignant peripheral nerve sheath tumors. *Nat. Genet*. 46, 1227–1232 (2014).

CHAPTER 1.2.1 – POLYCOMB REPRESSIVE COMPLEX 2 AND MPNST

The Polycomb group (PcG) proteins are epigenetic regulators capable of forming complexes that modulate the chromatin environment in order to help establish and/or maintain targeted transcriptional repression throughout cell generations [17,18]. Disruption of these factors can result in the dysregulation of gene expression patterns, which can influence changes in cell fate to promote cancer progression [18]. Polycomb repressive complex 1 (PRC1) and Polycomb repressive complex 2 (PRC2), the best characterized PRCs, carry out post-translational modifications (PTM) of histones in order to mediate gene silencing [19].

PRC2 is a methyltransferase that establishes and maintains H3K27me2/3 in the genome and regulates chromatin structure, transcription, and cell differentiation [19] (Figure 2). Its core proteins include the mutually exclusive SET-domain containing enzymatic proteins EZH1 or EZH2, the WD40 protein EED, and the Zinc-finger protein SUZ12. This core complex can associate with additional proteins, such as JARID2, RBAP46/48, and AEBP2, and non-coding RNAs (ncRNAs) that contribute to the stability of the complex, regulate its enzymatic activity, and support its targeting to the chromatin [18,20]. PRC2 is known to be involved in the repression of developmentally-regulated genes, and loss of its function through knockouts (KO) of EZH1/EZH2, EED, or SUZ12 in mice, results in early embryonic lethality with the embryos failing to undergo gastrulation, while loss of JARID2 results in mid-late-gestation lethality [21–24].

PRC2 mutations conferring both loss- and gain-of-function have been identified in different cancers, which indicate its ability to act as either an oncogene or a tumor suppressor depending on the cancer context [18]. Cancers that present PRC2 inactivation include MPNST [12,13], melanoma [13], pediatric gliomas [25–28], invasive breast cancer [29], myeloid disorders [30,31], T-cell acute lymphocytic leukemia (ALL) [32], early T-cell precursor ALL [33], and others. Among all of these, MPNST has the highest prevalence of complete loss of PRC2 function. In MPNST, most EED and SUZ12 genetic alterations are nonsense mutations resulting in frameshift or truncations that lead to a non-functional complex [12–14,34,35].

Interestingly, recent studies in our lab have identified that the loss of PRC2 function in MPNST leads to the development of an immune desert tumor microenvironment (TME) [36]. Loss of PRC2 reprograms the chromatin landscape, leading to a cell-autonomous shift from signaling-dependent immune cellular responses (e.g., interferon γ) to development and differentiation transcriptional programs normally regulated by PRC2. This also leads to diminished tumor immune infiltrates, increased immune evasion, and decreased tumor T-cell recruitment, conferring MPNST with resistance to immune checkpoint blockade (ICB) therapies [36].

Considering all of this, it is important to determine if PRC2 loss has any role in determining the sensitivity of MPNST to targeted therapies of the MAPK pathway.

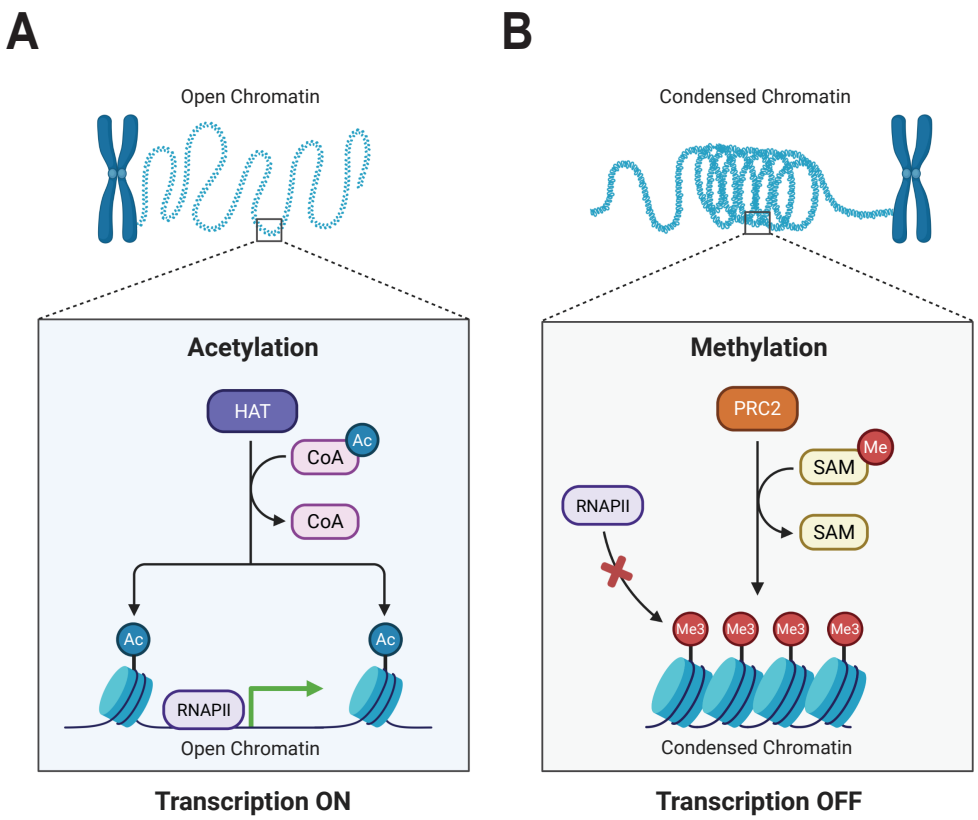

Figure 2. PRC2 regulation of chromatin state

A) H3K27 acetylation helps promote an open chromatin state with active transcription.

B) PRC2 methylates H3K27, leading to the condensation of the chromatin and inactivation of the transcription activity.

* Figure created with BioRender.com.

CHAPTER 1.2.2 – CDKN2A AND MPNST

Cell cycle progression from G1 to mitosis is regulated by various cyclin proteins and cyclin-dependent kinases [37]. At the same time, these proteins can be inhibited by different cyclin-CDK inhibitors proteins (CDIs), which include $p16^{INK4a}$, $p21^{CIP1}$, $p27^{KIP1}$, and some associated proteins that include $p15^{INK4b}$, $p18^{INK4c}$, $p19^{INK4d}$ and $p57^{KIP2}$ [37]. Therefore, these proteins act as tumor suppressors capable of regulating cell cycle progression, and their inactivation is associated with human carcinogenesis [38].

Somatic loss of CDKN2A, the gene that encodes the $p16^{INK4a}$ and $p14^{ARF}$ proteins, is a common characteristic of MPNST, with an occurrence of about 81% of NF1-associated, and 95% of sporadic and radiotherapy-associated MPNSTs [12]. $p16^{INK4a}$ inhibits the CDK4 and CDK6 cyclin-dependent kinases maintaining the retinoblastoma (RB) protein in an unphosphorylated state leading to E2F being unable to promote cell cycle progression and provoking a growth-suppressive cell state [38,39]. On the other hand, $p14^{ARF}$ binds to and inhibits the MDM2 protein and prevents the MDM2 mediates the degradation of p53, which then can also lead to a suppression of cell cycle progression or to apoptosis [40–42] (Figure 3).

While CDKN2A deletions are not found in Plexiform Neurofibromas, loss of this gene has been identified in another precursor lesion to MPNST called Atypical neurofibromas [43,44]. Atypical neurofibromas are normally slow-growing tumors,

with few mutations apart from those in NF1 and CDKN2A [45], highlighting the potential importance of CDKN2A in the development of these tumors. On the other hand, MPNST is a highly aggressive tumor that has been found to carry additional frequent mutations that may be important for the development of Atypical neurofibromas and plexiform neurofibromas into MPNST [12–14,46].

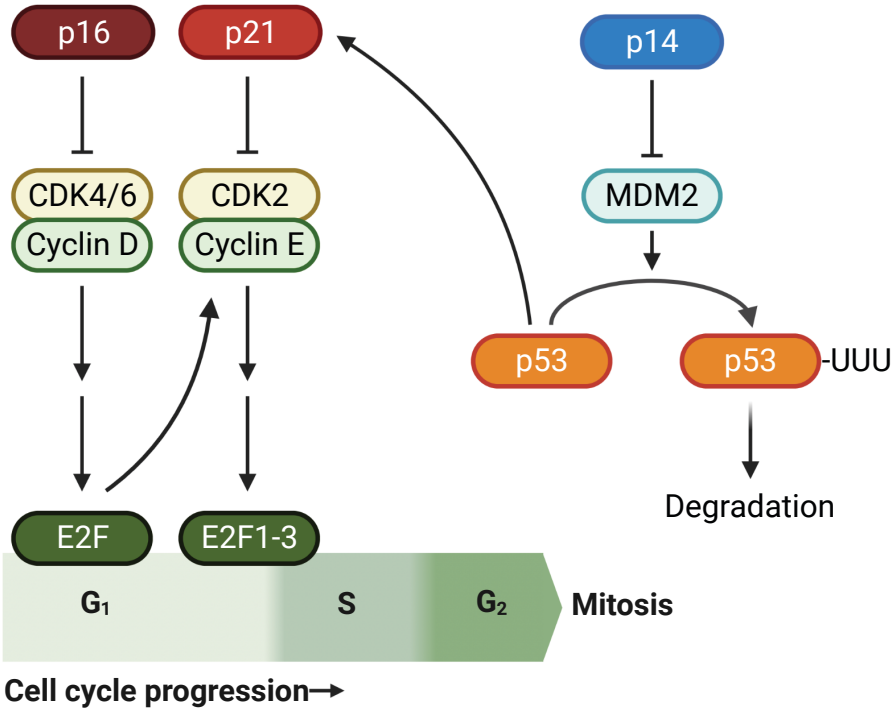

Figure 3. CDKN2A regulation of cell cycle progression and p53 levels
CDKN2A gene codes for the $p16^{INK4a}$ and $p14^{ARF}$ proteins. p16 inhibits the CDK4/6 kinases, which then indirectly suppresses the cell cycle progression, while p14 inhibits MDM2 leading to a stable p53 and arresting cell cycle progression or leading to apoptosis.
* Figure created with BioRender.com.

CHAPTER 1.2.3 – NF1 AND MPNST

The NF1 protein, neurofibromin 1, is a RAS GTPase activating protein (RAS-GAP) that limits signaling downstream of RAS by facilitating the hydrolysis of GTP to GDP [47,48] (Figure 4). The absence of this tumor suppressor can lead to uncontrolled activation of RAS and subsequent sustained activation of the RAF/MEK/ERK signaling [15,16].

Loss of NF1 is a common event in MPNST as around 45% of cases are patients with previous Neurofibromatosis type I disease that go through a two-hit mechanism in which the initiating tumor cell loses the non-mutant allele of the gene in order for the disease to progress to MPNST [49,50]. On the other hand, more than 70% of the non-NF1-associated MPNSTs also carry NF1 loss-of-function mutations [12–14], which points to the loss of the NF1's tumor suppressive abilities as a key event in MPNST pathogenesis.

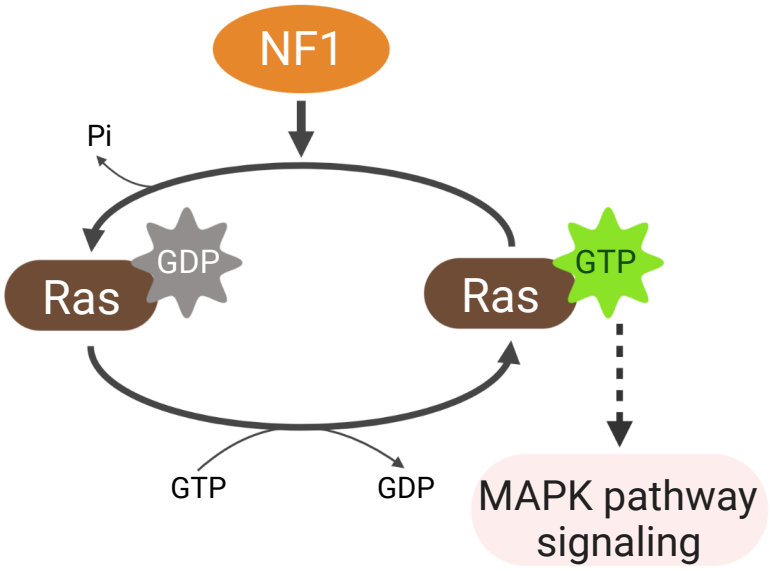

Figure 4. NF1 role as a tumor suppressor
NF1 limits RAS downstream signaling by facilitating the conversion of the active RAS-GTP to the inactive RAS-GDP form
* Figure created with BioRender.com.

CHAPTER 1.3 – MAPK SIGNALING PATHWAY IN CANCER

The mitogen-activated protein kinase (MAPK) signal transduction cascades are highly conserved critical regulators of cell growth and cell-cycle progression. The most well-studied of the MAPK signaling pathways is the RAS–RAF–MEK–ERK cascade [51] (Figure 5). This signaling pathway is dysregulated in more than one-third of all human cancers, and alterations leading to abnormal activation of the pathway can be found at almost every level of the cascade [52,53].

The RAS–ERK MAPK signaling pathway starts when receptor tyrosine kinases (RTK) are activated upon stimulation by extracellular mitogens. These active RTKs can then stimulate the RAS (H-, N-, K-RAS) small GTPase proteins. RAS proteins are activated when guanine exchange factors (GEF) mediate the binding to GTP, and are inactivated when GTPase activating proteins (GAP), like NF1, facilitate the hydrolysis of GTP to GDP [47]. Activated RAS can then recruit RAF (A-RAF, B-RAF, and C-RAF/RAF1) kinases to the plasma membrane by binding to the RAS binding domain (RBD) of RAF, in order to facilitate its activation [51,54].

Activation of RAF involves the dephosphorylation of a conserved inhibitory site in RAF (A-RAF S214, B-RAF S365, C-RAF S259), an event that facilitates the dissociation of 14-3-3 proteins and subsequent RAF dimerization [55,56]. Dephosphorylation of the conserved inhibitory site is mediated by a ternary complex comprised of SHOC2, MRAS, and PP1 [55,57,58]. Active RAF dimers are

formed by either homodimers or heterodimers containing any combination of A-RAF, B-RAF, and C-RAF.

Active RAF kinases phosphorylate and activate downstream MEK1/2 kinases. MEK1/2 then phosphorylates and activate ERK1/2 kinases, its only characterized downstream target [59]. Both MEK and ERK have identical isoforms with a high conservation of both their sequence and function, and therefore there are normally referred to as MEK1/2 and ERK1/2, or simply MEK and ERK.

After being phosphorylated by MEK, active ERK can translocate to the nucleus to regulate the transcription of numerous transcription factors and proteins that promote cell-cycle progression, cell survival, cell differentiation, angiogenesis, and others [52,60,61]. Additionally, ERK is also involved in negative feedback loops of the MAPK pathway, in which by regulating the transcription of a group of genes that negatively inhibit the pathway or by directly interacting with a set of proteins involved in the pathway, it can regulate the activity of RTKs, RAS, and RAF proteins [48,62].

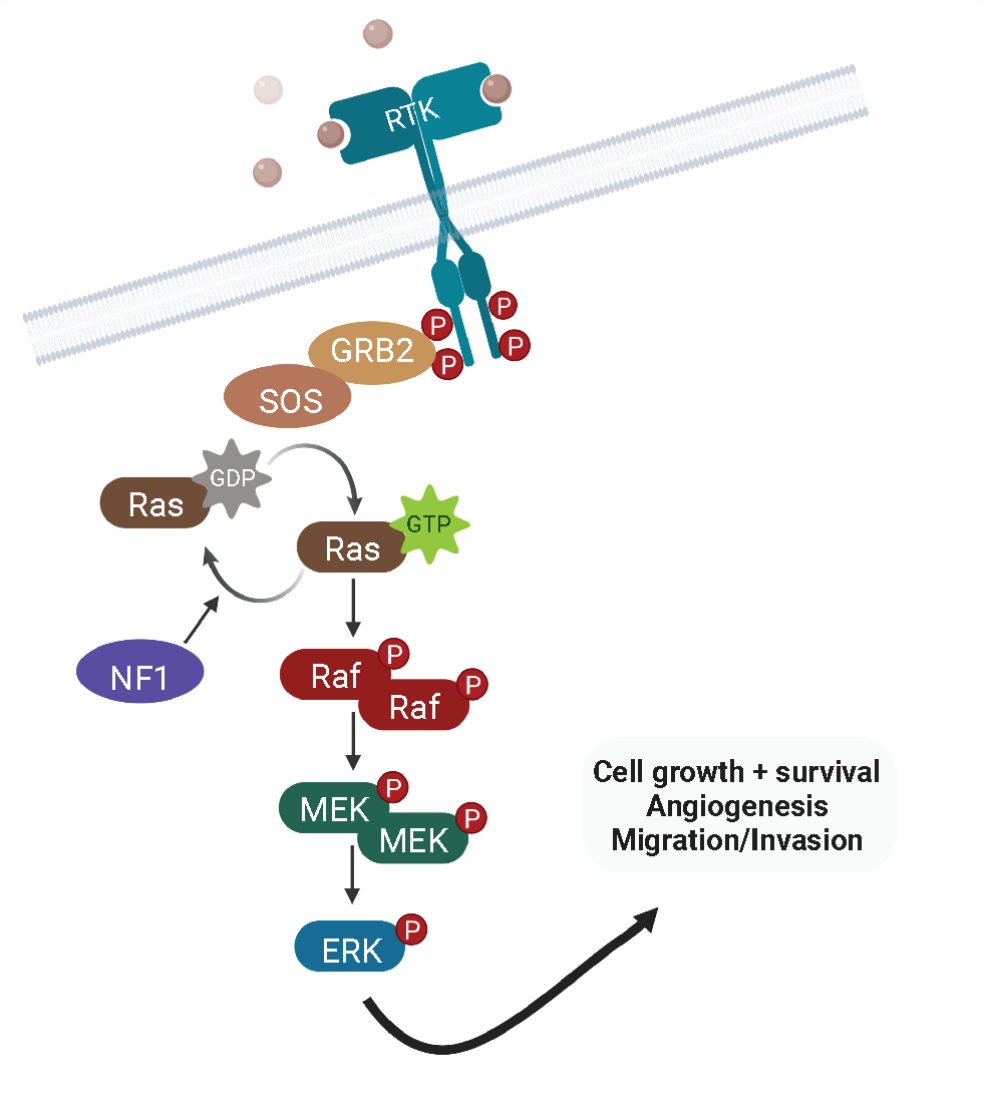

Figure 5. MAPK signaling pathway

MAPK pathway signaling involves the activation of upstream RTKs, formation of active RAS-GTP, phosphorylation and dimerization of RAF, phosphorylation of MEK, phosphorylation of ERK, and translocation of active ERK to the nucleus to promote the expression of different target genes that control cell growth, survival, angiogenesis, cell migration, and invasion.

* Figure created with BioRender.com.

CHAPTER 1.4 – MAPK PATHWAY INHIBITORS IN CLINICAL DEVELOPMENT

The RAS–ERK MAPK pathway plays a central role in most human cancers, with more than 30% of cases showing an abnormal activation of the signaling pathway [52,53]. Also, many of its components have been identified as oncogenes or tumor suppressor genes. Because of this, an immense interest has been generated in the targeting of this pathway, and numerous inhibitors of the pathway have gone into development and passed through preclinical and clinical studies [53,63,64]

However, the ability of tumors to acquire drug resistance to MAPK inhibitors has become a major issue in the treatment of these cancers [52]. For this reason, newer studies have focused on identifying combination therapies capable of inhibiting multiple targets within the same pathway in order to better regulate other interconnected signaling pathways and overcome the different resistance mechanisms that could arise after drug treatment [65].

CHAPTER 1.4.1 – MEK INHIBITORS IN CLINICAL DEVELOPMENT

While mutations in MEK are not as frequent in cancer as mutations in other members of the MAPK pathway [66,67], its central role in controlling this pathway has led to many MEK inhibitors (MEKi) entering preclinical and clinical development [52]. Currently, four MEKi have been approved by the FDA: Trametinib, Binimetinib, Selumetinib, and Cobimetinib [68]. All these are ATP non-competitive, type III allosteric inhibitors [69–71].

Trametinib, in particular, was initially described as a MEKi that preferentially binds to unphosphorylated MEK and is capable of preventing RAF-dependent MEK phosphorylation and activation [72]. Interestingly, recent studies have shown that Trametinib is more effective than either of the other MEKi mentioned above at disrupting RAF–MEK complexes and at inhibiting both MEK and ERK phosphorylation [68].

On the other hand, in contrast to most MEK inhibitors, CH5126766 was found to promote the formation of the RAF–MEK complexes and, by doing so, makes MEK become an inhibitor of RAF [73]. Recent studies have shown that CH5126766 has similar effectiveness as Trametinib at inhibiting MEK phosphorylation [68].

All these MEKi possess different properties that can affect their effectiveness depending on the cellular context, and their different pharmacokinetic profiles

could also affect their clinical activity [73–75]. Therefore, more studies need to be done to better determine which MEK inhibitors work best in what cellular context and which MEKi should be optimally used in the different pharmacological combinations.

CHAPTER 1.4.2 – RAF INHIBITORS IN CLINICAL DEVELOPMENT

The RAF kinases ARAF, BRAF, and CRAF are key players in the MAPK signaling cascade. While not activated, these kinases exist in the cell in a monomeric form and normally need to dimerize in order to be active and phosphorylate MEK [52]. However, mutations like the $BRAF^{V600E}$, which is seen in around 8% of tumors, confers BRAF with the ability to constitutively signal as a monomer [76–78]. For this reason, several RAF inhibitors (RAFi) that target RAF monomers have been developed, with Vemurafenib, Dabrafenib, and Encorafenib already approved by the FDA [79]. However, the release of the negative feedback of the MAPK pathway in response to the monomeric RAFi treatment can lead some cancer cells to rapidly form RAF dimers and subsequently become resistant to these inhibitors [76,80]. Additionally, it was also discovered that treatments with non-saturating concentrations of RAFi could lead to paradoxical activation of the MAPK pathway by binding to the RAF monomers, inducing RAF dimerization, and then not being able to effectively inhibit the other RAF in the active dimer [81,82].

To overcome the limitations of the first developed RAFi, a new type of RAFi that is equally potent against RAF monomers and dimers is being developed [83,84]. This new class of RAFi includes the LY3009120 and the TAK-632, among others. However, these equipotent RAFi have not been very successful in the clinic, and this may be due to these drugs also being potent inhibitors of dimeric $BRAF^{WT}$, a situation that could be causing many on-target toxicities in normal tissues [68].

On the other hand, recent studies identified a third class of RAFi that are more selective against RAF in its dimeric form. Some of these inhibitors include Naporafenib (LXH254), Regorafenib, and Sorafenib, among others [68]. With these advancements in RAFi development, more studies need to assess how to exploit the different allosteric properties of the RAFi when designing novel combinatorial therapies for cancer.

CHAPTER 1.4.3 – RTK INHIBITORS IN CLINICAL DEVELOPMENT

Receptor tyrosine kinases (RTK) are cell-surface receptors that regulate different cellular processes, including cell survival, proliferation, differentiation, migration, and many others. There are 58 known RTK, and while they are divided into 20 subfamilies, all of them share a similar structure comprised of an extracellular ligand binding domain, a single transmembrane helix, and intracellular regions that contain several domains that include the tyrosine kinase domain [85]. Abnormal activation of RTKs can be caused by both ligand-dependent and ligand-independent mechanisms [85–87]. One example of the latter is when MAPK pathway inhibitors relieve the negative feedback inhibition of upstream RTK signaling, leading to upregulation of the pathway and potential development of adaptive resistance to the inhibitor [62,76,88,89]. In the case of MPNST, I and others identified that the levels of the RTK PDGFRβ consistently increase after MEKi treatment [90].

Various RTK inhibitors (RTKi) have been developed and approved by the FDA for different diseases. These drugs are either small molecular inhibitors that target the intracellular tyrosine kinase domain or monoclonal antibodies that interfere with RTK upregulation [85,91,92]. Furthermore, the small molecule inhibitors can be divided into three categories: type I inhibitors like Avapritinib that bind to the active conformation of a kinase in the ATP pocket, type II inhibitors like AZD-3229 that bind an inactive conformation of the kinase, and type III inhibitors like Ripretinib that are allosteric ligands that bind to a site different from the active site [93,94].

CHAPTER 1.4 – TARGETED INHIBITION OF MAPK PATHWAY AS TREATMENT FOR MPNST

In recent years, preclinical studies have evaluated the use of single-agent MEK inhibitors (MEKi) as a treatment for MPNST [95–97]. While this strategy has been effective for plexiform neurofibromas [98–100], an MPNST precursor, it has failed to show a good and sustained inhibition of ERK activity in MPNST. As with other cancers, activation of the receptor tyrosine kinases (RTKs) or the development of adaptive resistance after the release of ERK feedback inhibition of the MAPK pathway signaling could play a major role in the development of this resistance [76,88,89,101,102]. Additionally, MEKi has also been found able to reactivate C-RAF and induce RAF/MEK complex formation, which in turn could also lead to the development of resistance [74].

In my work, I identified that MEKi treatment resistance in MPNST involves two pathways, PDGFRβ upregulation through direct transcriptional upregulation, and MEKi treatment induced RAF dimer formation which leads to an increased MAPK pathway signaling. These resistance mechanisms can be overcome by the pharmacological combination of MEK inhibition and RAF-dimer inhibitors (Figure 6). These findings support the use of this combination strategy to overcome MEKi resistance and as a novel targeted therapeutic strategy for MPNST patients.

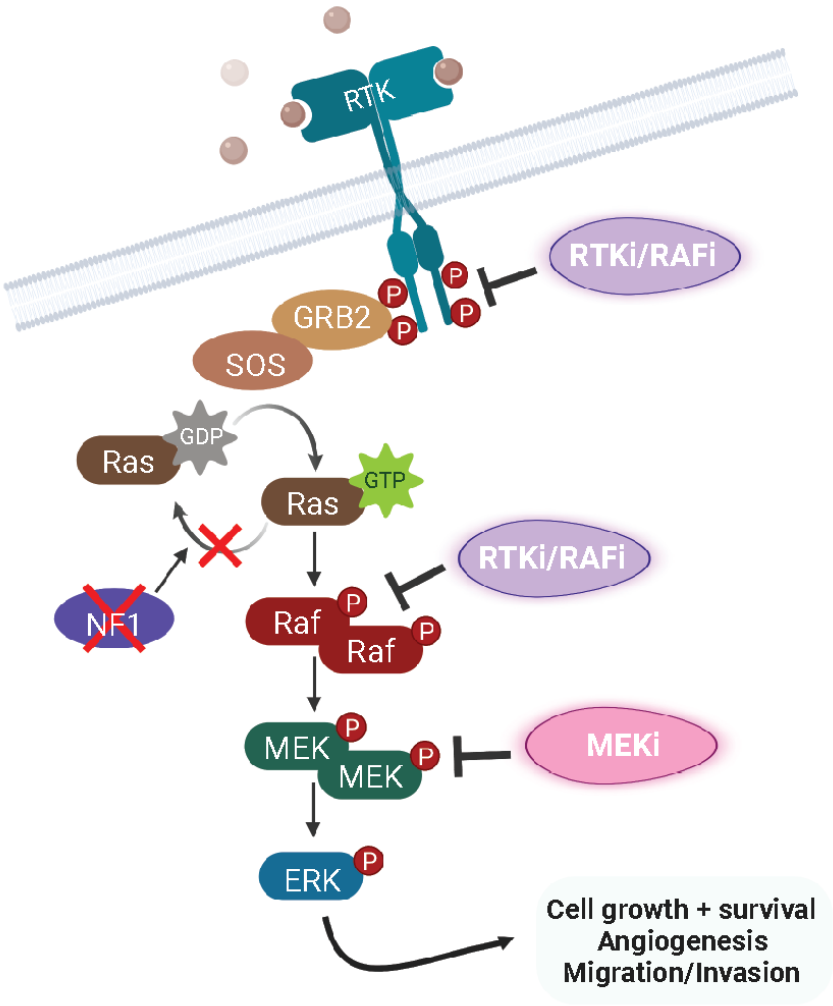

Figure 6. Graphical abstract.
MEK inhibitors lead to PDGFR pathway upregulation and increase RAF dimer formation in MPNST. Combination treatments capable of inhibiting both resistance mechanisms could prove to be an effective for the treatment of MPNST patients.
* Figure created with BioRender.com.

CHAPTER 2 – MATERIALS AND METHODS

CHAPTER 2.1 – MATERIALS

CHAPTER 2.1.1 – CELL LINES AND CELL CULTURES

The ST88-14 (RRID:CVCL_8916) and the M724 (MPNST724, RRID:CVCL_AU20) human MPNST cell lines were obtained as gifts provided by Jonathan A. Fletcher (Brigham and Women's Hospital, Harvard Medical School). The SNF96.2 (CRL-2884, RRID:CVCL_K281) human MPNST cell line and the HEK-293T (CRL-3216, RRID:CVCL_0063) cell line were purchased from ATCC. The M1, M3, M4, M5 and M6 Human NF1 associated MPNST cell lines were gifts developed by William L. Gerald and Xiaoliang L. Xu at the Memorial Sloan Kettering Cancer Center. The SK-Mel-103, SK-Mel-113, SK-Mel-217, and MeWo NF1-mutant melanoma cell lines were obtained as gifts provided by David Solit. The ST88-14, M724, SK-Mel-103, SK-Mel-113, SK-Mel-217, and MeWo cell lines were grown in RPMI supplemented with 10% FBS, the SNF96.2 cell line was grown in DME HG supplemented with 10% FBS and 1mM Sodium Pyruvate at 1.5 g/L-Sodium Bicarbonate, and the M1, M3, M4, M5, M6, and HEK-293T cell lines were grown in DMEM HG supplemented with 10% FBS. All these culture media were also supplemented with penicillin (100 U/ml), streptomycin (100 µg/ml), and L-glutamine (2 mM), and cells were cultured in 5% CO2 incubator at 37°C. All cell lines were tested negative for mycoplasma by the ABM Mycoplasma PCR Detection Kit (catalog # G238). Other relevant reagents used in this study are listed in Table 1.

CHAPTER 2.1.2 – MICE

All animal experiments were performed following the protocols approved by the MSKCC Institutional Animal Care and Use Committee (IACUC), and were in compliance with relevant ethical regulations regarding animal research. For lll xenograft studies and pharmacodynamics studies, 6-8 weeks old CB17 SCID female mice were purchased from Taconic.

CHAPTER 2.1.3 – OTHER RELEVANT REAGENTS

Table 1. Drugs, chemicals, and reagents used

Supplier	Catalog #	Item
Addgene	52962	LentiCas9-Blast plasmid
Addgene	52961	LentiCRISPR v2 plasmid
Addgene	52963	LentiGuide-Puro plasmid
Addgene	8454	pCMV-VSV-G packaging plasmid
Addgene	12260	psPAX2 packaging plasmid
Applied Biological Materials Inc.	G238	Mycoplasma PCR Detection Kit
Bio-Rad	1620115	Nitrocellulose Membrane, Roll, 0.45 µm
Cell Signaling Technology	8821	Active Ras Detection Kit
Cell Signaling Technology	7722	Blue Loading Buffer Pack
Cell Signaling Technology	9803	Cell Lysis Buffer (10X)
Corning	356237	Matrigel Basement Membrane Matrix, Phenol Red-free, LDEV-free
LI-COR Biosciences	928-60000	Chameleon Duo Pre-stained Protein Ladder

LI-COR Biosciences	927-60001	Intercept (TBS) Blocking Buffer
LI-COR Biosciences	927-85001	Intercept T20 (TBS) Protein-Free Antibody Diluent
Millipore Sigma	4693132001	cOmplete™, EDTA-free Protease Inhibitor Cocktail
Millipore Sigma	WBKLS0500	Immobilon Western Chemiluminescent HRP Substrate
Millipore Sigma	4906837001	PhosSTOP, Phosphatase Inhibitor Cocktail Tablets
New England BioLabs	N3200L	1 kb Plus DNA Ladder
New England BioLabs	R3733L	BsaI-HFv2
New England BioLabs	R0739L	BsmBI-v2
New England BioLabs	B7025S	Gel Loading Dye, Purple (6X), no SDS
New England BioLabs	C3040H	Stable Competent E. coli (High Efficiency)
Omega Bio-Tek	D6492-01	E.Z.N.A. Cycle Pure Kit (V-spin)
Omega Bio-Tek	R6834-01	E.Z.N.A. Total RNA Kit I
Omega Bio-Tek	HCR003	Homogenizer Columns
Promega	G9242	CellTiter-Glo 2.0 Cell Viability Assay
Qiagen	28706	QIAquick Gel Extraction Kit
R&D Systems	ARY001B	Proteome Profiler Human Phospho-RTK Array Kit
R&D Systems	AR002	Resazurin / Alamar Blue
Roche	6365787001	X-tremeGENE™ 9 DNA Transfection Reagent
Teknova	M1088	MOPS/SDS Running Buffer
Thermo Fisher Scientific	A1113903	Blasticidin S HCl
Thermo Fisher Scientific	26162	ChIP-grade Protein A/G magnetic beads
Thermo Fisher Scientific	17101015	Collagenase, Type II, powder
Thermo Fisher Scientific	BP172-5	Dithiothreitol (DTT)
Thermo Fisher Scientific	78444	Halt Protease and Phosphatase Inhibitor Cocktail

Thermo Fisher Scientific	4368813	High-Capacity cDNA Reverse Transcription kit
Thermo Fisher Scientific	NP0336BOX	NuPAGE 4-12% Bis-Tris gels
Thermo Fisher Scientific	NP0007	NuPAGE LDS sample buffer
Thermo Fisher Scientific	23225	Pierce BCA Protein Assay Kit
Thermo Fisher Scientific	36978	PMSF Protease Inhibitor
Thermo Fisher Scientific	A25778	PowerUp SYBR Green Master Mix
Thermo Fisher Scientific	A1113803	Puromycin Dihydrochloride
Thermo Fisher Scientific	89900	RIPA Lysis and Extraction Buffer
Thermo Fisher Scientific	26634	Spectra Multicolor Broad Range Protein Ladder
Thermo Fisher Scientific	37542	StartingBlock (TBS) Blocking Buffer
Thermo Fisher Scientific	34578	SuperSignal West Pico PLUS Chemiluminescent Substrate

Table 2. Small molecule inhibitors used

Supplier	Catalog #	Item
Deciphera Pharmaceuticals	n/a	Ripretinib (DCC-2618)
MSKCC Pharmacy	n/a	Binimetinib (MEK162) – for *in vivo* studies
SelleckChem	S8553	Avapritinib (BLU-285)
SelleckChem	S8780	AZD3229
SelleckChem	S7007	Binimetinib (MEK162) – for *in vitro* studies
SelleckChem	S7108	Encorafenib (LGX818)
SelleckChem	S7842	LY3009120
SelleckChem	S8745	Naporafenib (LXH254)
SelleckChem	S1008	Selumetinib (AZD6244)

SelleckChem	S2673	Trametinib (GSK1120212)

Table 3. sgRNAs used for CRISPR/Cas9 KOs

Species	sgRNA	20-mer Guide Sequence
n/a	sgCNT	GCTGATCTATCGCGGTCGTC
Human	sgBRAF	GGTTTCCGCTGTCAAACATG
Human	sgCRAF	GTGATGCTGTCCACTCGGAT
Human	sgPDGFRβ	GACTAACGTGACGTACTGGG
Human	sgSHOC2	TAGTTATACGATTAAAGCGA

Table 4. Primers used for RT-qPCR

Species	Primer	Sequence (5' to 3') [PAM = NGG]
Human	Fw_DUSP6	GGCGAGCTGCTGCTACACGA
Human	Rv_DUSP6	TGCCGGGCGTTCTACCTGGA
Human	Fw_PDGFRβ	ACAGACTCCAGGTGTCATCCA
Human	Rv_PDGFRβ	CCACTTTCTTTGCGGGGGTA
Human	Fw_RPL27	CATGGGCAAGAAGAAGATCG
Human	Rv_RPL27	TCCAAGGGGATATCCACAGA
Human	Fw_SPRED2	GACGTTTTTACAACAGCTACAGACA
Human	Rv_SPRED2	TGTGGGGTATGAGTCGTGGA
Human	Fw_SPRY2	ATTTGCACATCGCAGAAAGAAGA
Human	Rv_SPRY2	AGAACACATCTGAACTCCGTGA

Table 5. Antibodies used for WB and IP

Supplier	Catalog #	Target Protein	Host	Application	Dilution
Cell Signaling Technology	2128	B-Tubulin	Rabbit	Western blot	1:1000

Cell Signaling Technology	86298	B-Tubulin	Mouse	Western blot	1:1000
Cell Signaling Technology	9433	BRAF	Rabbit	Western blot	1:1000
Cell Signaling Technology	14814	BRAF	Rabbit	Western blot	1:1000
Santa Cruz Biotechnology	sc-5284	BRAF	Mouse	Western blot, Immunoprecipitation	1:200, 1 µg/IP
Cell Signaling Technology	53745	CRAF	Rabbit	Western blot	1:1000
Millipore Sigma	07-396	CRAF	Rabbit	Immunoprecipitation	1 µg
Cell Signaling Technology	12552	CRAF	Mouse	Western blot	1:1000
Cell Signaling Technology	4695	ERK1/2	Rabbit	Western blot	1:1000
Cell Signaling Technology	4696	ERK1/2	Mouse	Western blot	1:1000
Cell Signaling Technology	5415	Isotype control	Rabbit	Immunoprecipitation	1 µg/IP
Cell Signaling Technology	3900	Isotype control	Mouse	Immunoprecipitation	1 µg/IP
Millipore Sigma	07-641	MEK1	Rabbit	Immunoprecipitation	1 µg/IP
Cell Signaling Technology	9122	MEK1/2	Rabbit	Western blot	1:1000
Cell Signaling Technology	4694	MEK1/2	Mouse	Western blot	1:1000
Cell Signaling Technology	3169	PDGFRβ	Rabbit	Western blot	1:500
Cell Signaling Technology	3175	PDGFRβ	Mouse	Western blot	1:500
Cell Signaling Technology	4370	phospho-ERK1/2	Rabbit	Western blot	1:1000
Cell Signaling Technology	9421	phospho-CRAF-S259	Rabbit	Western blot	1:1000

Cell Signaling Technology	9431	phospho-CRAF-S289, S296, S301	Rabbit	Western blot	1:1000
Cell Signaling Technology	9427	phospho-CRAF-S338	Rabbit	Western blot	1:1000
Cell Signaling Technology	9154	phospho-MEK1/2	Rabbit	Western blot	1:1000
Cell Signaling Technology	53600	SHOC2	Rabbit	Western blot	1:1000
Cell Signaling Technology	13901	Vinculin	Rabbit	Western blot	1:1000
Cell Signaling Technology	7074	Anti-rabbit IgG, HRP-linked	2ry Antibody	Western blot	1:2000
Cell Signaling Technology	7076	Anti-mouse IgG, HRP-linked	2ry Antibody	Western blot	1:2000
LI-COR	926-32211	IRDye® 800CW Goat anti-Rabbit IgG	2ry Antibody	Western blot	1:10,000
LI-COR	926-68070	IRDye 680RD Goat anti-Mouse IgG	2ry Antibody	Western blot	1:20,000

CHAPTER 2.2 – METHODS

CHAPTER 2.2.1 – CELL VIABILITY ASSAY

MPNST cells (1–3 x 10^3 cells/well) were seeded in clear bottom 96-well white or black plates, allowed to attach overnight, and treated the next day with serial dilutions of a single drug, a combination of drugs, or vehicle (1% DMSO). Cell viability was assayed five days post-treatment using the ATP CellTiter-Glo 2.0 cell viability assays (Promega) or Resazurin/Alamar Blue (R&D Systems) according to the manufacturer's protocol. IC_{50} values were calculated by nonlinear regression analysis using the GraphPad Prism 9.0 software. All the data were normalized to vehicle treatment. The BLISS synergy scores were calculated using the Combenefit platform as previously described [103].

CHAPTER 2.2.2 – DRUGS AND CHEMICALS

See Table 1 and Table 2 for information on all the drugs, chemicals, and reagents used in this study.

CHAPTER 2.2.3 – GENERATION OF DRUG-RESISTANT CELL LINES

MEKi-resistant cell lines resistant were generated by exposing the NF1-associated MPNST cell lines M3 and ST88-14 to increasing concentrations of trametinib for at least months of continuous drug exposure. The cell culture medium was changed twice per week, and fresh drug was added each time.

CHAPTER 2.2.4 – PROTEIN EXTRACTION AND WESTERN BLOTTING

After the indicated treatment time, cells were lysed using RIPA buffer (Thermo Fisher) supplemented with phosphatase and protease inhibitors (Thermo Fisher Scientific or Millipore Sigma), followed by boiling for 5 min at 95°C, sonicating 5-10 min, and protein quantification by BCA protein assay kit (Thermo Fisher). Protein samples were prepared by mixing with NuPAGE LDS sample buffer (Thermo Fisher) and 1 M DTT (Thermo Fisher), followed by boiling for 10 min at 70°C. Proteins samples were then separated by SDS-PAGE on 4-12% Bis-Tris Gel (Thermo Fisher) with MOPS/SDS running buffer (Teknova), and followed by protein transfer to nitrocellulose membranes (BioRad) by wet electroblotting. Membranes were blocked for 1 hr at room temperature with StartingBlock TBS buffer (Thermo Fisher) or Intercept (TBS) Blocking buffer (LI-COR), and incubated with primary antibodies of interest overnight at 4°C under soft rotations. Then membranes were washed thrice with 1x TBS-T, and incubated with HRP-conjugated secondary antibody (for ECL detection) or fluorescent dye-labeled secondary antibody (for fluorescence detection with LI-COR) for 1 hr at room temperature. Then membranes were washed thrice with 1x TBS-T. Membranes for ECL detection were visualized with chemiluminescence using HRP substrates (Millipore, or Thermo Fisher), and chemiluminescence scanning with ImageQuant LAS4000 (GE Healthcare). Membranes for fluorescence detection were imaged

with the Odyssey Infrared Imaging System (LI-COR Biosciences). The list of antibodies used can be found in Table 5.

CHAPTER 2.2.5 – PHOSPHO-RTK ARRAY ASSAY

MPNST cells were seeded in 15-cm dishes, allowed cell attachment overnight, treated the next day with the desired drug concentrations, harvested at the experiment endpoint, and lysed using the lysis buffer provided by the Human Phospho-RTK Array Kit (R&D). For tumor samples, the tumor tissue collected at the experiment endpoint was homogenized and then lysed using the same lysis buffer and kit. Cell lysates were centrifuged for 5min at 14,000 x g, and the supernatant was then processed following the kit manufacturer's instructions, and ECL western blotting was performed as described above. Band intensity quantifications were done using the Image Studio Lite Software.

CHAPTER 2.2.6 – IMMUNOPRECIPITATION ASSAY

After the indicated treatment time, cells in 10-cm or 15-cm plates were washed once with cold PBS, then harvested by scraping in PBS, pelleted at 600 x g for 5min, and then lysed using a 1% Triton lysis buffer (Cell Signaling) supplemented with phosphatase and protease inhibitors (Thermo Fisher Scientific or Millipore Sigma). Samples were sonicated for 5min, the protein was isolated by centrifuging for 10min at 14,000 x g, and quantified. 1µg of the antibodies of interest was added, and samples were incubated overnight under gentle rocking. Next, Protein A/G

Magnetic Beads (Thermo Fisher) were added to the samples, and immunoprecipitates were purified using a magnetic separation rack, washed three times with 1% Triton lysis buffer, and then pelleted for 5min at 1,000rpm in 4°C. The sample was resuspended in 3X SDS sample buffer (Cell Signaling), boiled for 5min, centrifuged for 1min at 14,000 x g, and then the protein supernatant was collected for subsequent studies using the western blotting procedures described above. See Table 5 for the list of antibodies used.

CHAPTER 2.2.7 – ACTIVE RAS PULL-DOWN ASSAY

MPNST cells were seeded in 10-cm dishes, allowed cell attachment overnight, and treated the next day with the desired drug concentrations. The cells were then collected 2hr, 24hr, or 48hr after treatment and GTP-bound RAS was quantified using an active RAS detection kit (Cell Signaling Technology, #8821) according to the manufacturer's instructions.

CHAPTER 2.2.8 – RNA ISOLATION AND QRT-PCR

Total RNA was isolated from cells using the E.Z.N.A total RNA Kit (Omega), and homogenizer columns (Omega). The RNA quality and quantity were determined using the NanoDrop 8000 Spectrophotometer (Thermo Scientific). RNA was then reverse transcribed using the High-Capacity cDNA Reverse Transcription kit (Thermo Fisher). qPCR was performed following the manufacturer instructions of the PowerUp SYBR Green Master Mix (Thermo Fisher), with a ViiA 7 Real-Time

PCR system (Applied Biosystems). The specificity of the amplified DNA was confirmed by performing melting curves after each qPCR, and PCR contaminations that could affect the results were determined by also running a no template control in the RT-qPCR reactions. The housekeeping gene RPL27 was used as the reference gene for normalization, and the ΔΔCT method was used to calculate the relative fold change gene expression. Each RT-qPCR was performed in at least triplicates. Primers were designed using the online NCBI Primer-BLAST tool, and then purchased from Eurofins Genomics. The sequences of all the primers used for qPCR are listed in Table 4.

CHAPTER 2.2.9 – GENE KNOCKOUT BY CRISPR/CAS9

The LentiCRISPR-v2, LentiGuide-Puro and LentiCas9-Blast vectors were purchased from Addgene. The sgRNA oligos (as listed in Table 3) were annealed, digested using BsmBI (New England BioLabs), and cloned into the vectors. The plasmid was co-transfected into HEK-293T cells with the packaging plasmids psPAX2 (Addgene)and pVSVg (Addgene), and the resulting lentivirus was collected. MPNST cells were then transduced with respective plasmids with the sgRNA of interest and then were selected with 2 - 5 μg/ml Puromycin dihydrochloride (Thermo Fisher) or Blasticidin S HCl (Thermo Fisher) until all negative control cells were dead. All the relevant reagents are listed in Table 1.

CHAPTER 2.2.10 – *IN VIVO* MOUSE STUDIES

For MPNST M3 cells and PDXs xenograft studies, 2 x 10^6 and 3 x 10^6 cells, respectively, were resuspended in 100mL of 1:1 mix of DMEM media and Matrigel (Corning, #356237), and subcutaneously injected into both flanks of 6- to 8-week-old CB17 SCID mice (Taconic). When tumors reached 100-150 mm^3 on average, the mice were assigned to different treatment groups to ensure similar distribution of tumor sizes and mouse weights. Tumors size was measured twice a week with a caliper, and tumor volume was calculated with the formula Vol=(4/3)π x (length/2) x (width/2) x (depth/2). Binimetinib and Trametinib were administered by oral gavage, and Ripretinib was administered in a mouse diet formulated to achieve approximate levels of 25 or 100 mg/kg/day in mouse efficacy studies [94]. Control treatments involve a control chow provided by Deciphera Pharmaceuticals, and the drug vehicle for oral gavage (1% carboxymethyl cellulose + 0.5% Tween 80 in ddH_2O). The body weight of the mice was monitored during the whole experiment. Mice were euthanized once the experiment endpoint was reached, or humane endpoints were required. All the relevant reagents are listed in Table 1 and Table 2. All data was plotted and analyzed with the GraphPad Prism 7-9 software.

CHAPTER 2.2.11 – QUANTIFICATION AND STATISTICAL ANALYSIS

All statistical analyses and plots were generated using GraphPad Prism 7–9 software. All data are presented as the mean ± SEM (unless otherwise noted). Statistical comparisons between two groups were performed using a two-tailed

unpaired t-test, and for more than two groups were performed using one-way ANOVA. Significant differences between groups are defined by ns $P>0.05$; * $P<0.05$; ** $P<0.005$; *** $P<0.0005$; **** $P<0.0001$.

CHAPTER 3 – MEK INHIBITION LEADS TO AN INCREASE OF PDGFRB AND REACTIVATION OF MAPK SIGNALING IN NF1-DEFICIENT MPNST

CHAPTER 3.1 – ACUTE EXPOSURE TO MEKI TREATMENT LEADS TO THE INCREASE OF PHOSPHORYLATED PDGFRB

To determine the potential contribution of upstream signaling in the ability of MPNST to develop resistance to MEK inhibition, we evaluated the levels of active RAS upon treatment with a MEK inhibitor (MEKi). Interestingly, although MEKi treatment led to the inhibition of the ERK signaling, there was an increase in the RAS-GTP and pMEK levels in a dose and time-dependent manner, suggesting that MEKi treatment over time leads to an increase in the MAPK pathway activity in MPNST cells (Figure 7 A). Previous studies have shown that loss of ERK-mediated negative regulation of RAS and different MAPK pathway proteins as well as upregulation of RTK activity, are two adaptive mechanisms that could lead MPNST cells to present this behavior [76,88,89,101,102]. We decided to first focus on assessing the role of the latter, as RTK upregulation has been characterized as a mechanism of drug resistance in many different cancers.

A phospho-RTK array performed after MEKi treatment of MPNST M3 cells revealed that the PDGFRβ and MET receptors are activated following MEKi treatment (Figure 7 B). The activity of both PDGFRβ and MET receptors has been previously shown to increase following MEKi treatment in MPNST [90]. However, only phospho-PDGFRβ levels, but not those of MET, were also increased in a second MPNST cell line as well as in an MPNST cell xenograft upon MEKi treatment (Figure 7 C-D). Furthermore, in the ST88-14 cell line, the levels of

phospho-PDGFRβ didn’t change after MEKi treatment, but PDGFRβ was the RTK with the highest detected levels which could suggest that it plays an important role in RTK signaling in this cell line (Figure 7 E). Hence, we decided to further study the role of PDGFRβ in the response of MPNST cells to MEKi treatment.

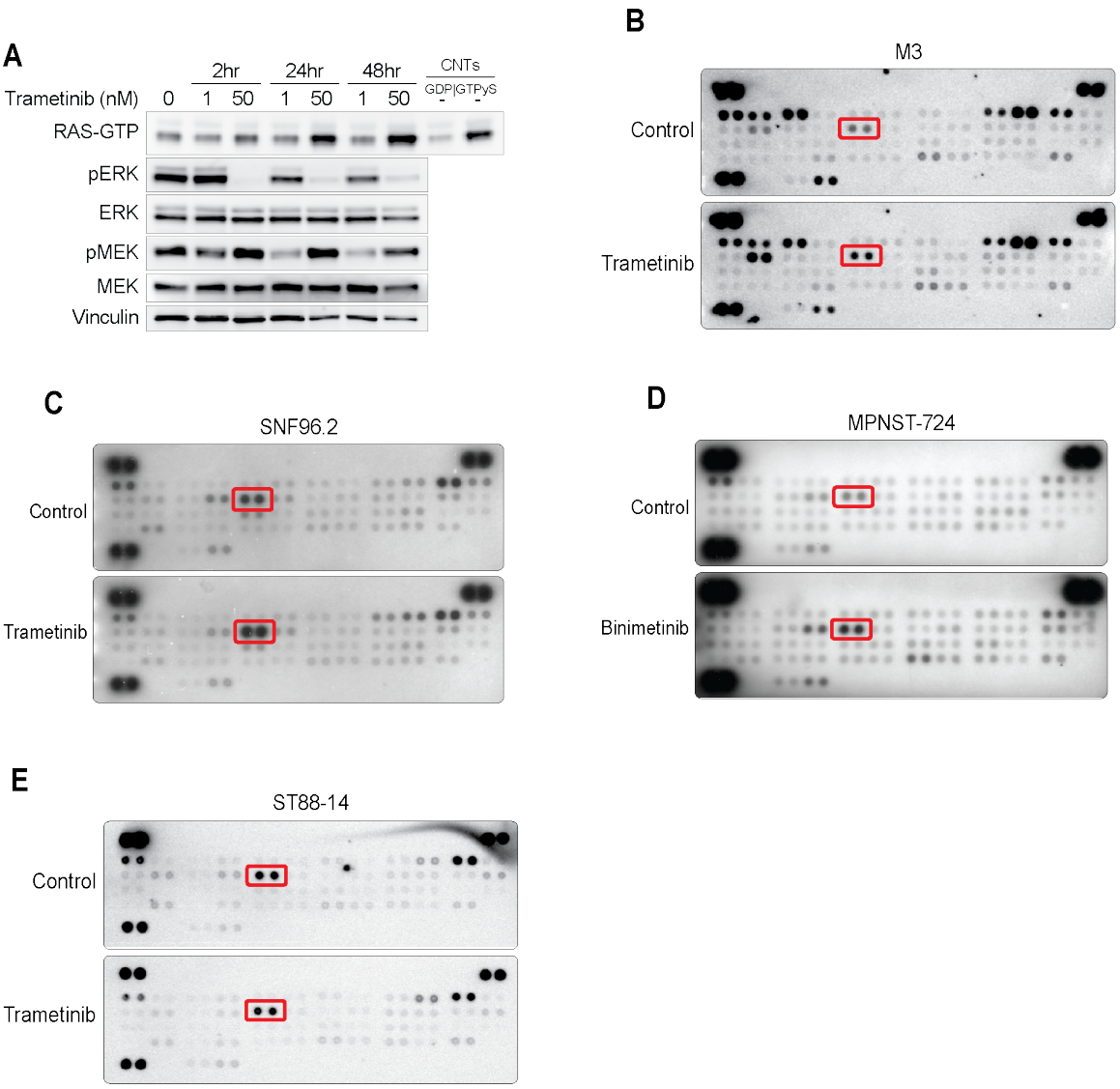

Figure 7. Acute exposure to MEKi treatment leads to the increase of phosphorylated PDGFRβ

A) Western blot analysis of M3 cells were treated with 1 nM or 50 nM Trametinib for 2hr, 24hr, or 48hr.

B-E) Phospho-RTK arrays of M3 (B) and ST88-14 (E) cells treated with DMSO or 50 nM Trametinib for 48hr, or SNF96.2 cells treated with DMSO or 500 nM Binimetinib for 2hr (C), or M724 cells treated *in vivo* with vehicle or oral Binimetinib (30mg/kg BID) for 48hr (D). PDGFRβ is identified by red squares.

CHAPTER 3.2 – ACUTE EXPOSURE TO MEKI TREATMENT LEADS TO AN INCREASE IN TOTAL PDGFRB

To further evaluate the role of PDGFRβ in MPNST, total levels of this protein were assessed in a panel of cell lines. Results indicate that PDGFRβ levels increased in the M3 cells following MEKi treatment (Figure 8 B), but did not increase in the ST88-14 cell line, the cell lines whose phospho-PDGFRβ levels didn't change in response to MEKi treatment (Figure 8 C). Nevertheless, the increase in PDGFRβ levels was observed in the majority of MPNST cells tested (Figure 8 A-I), further supporting the observation that PDGFRβ is a key RTK involved in MPNST response to MEKi treatment.

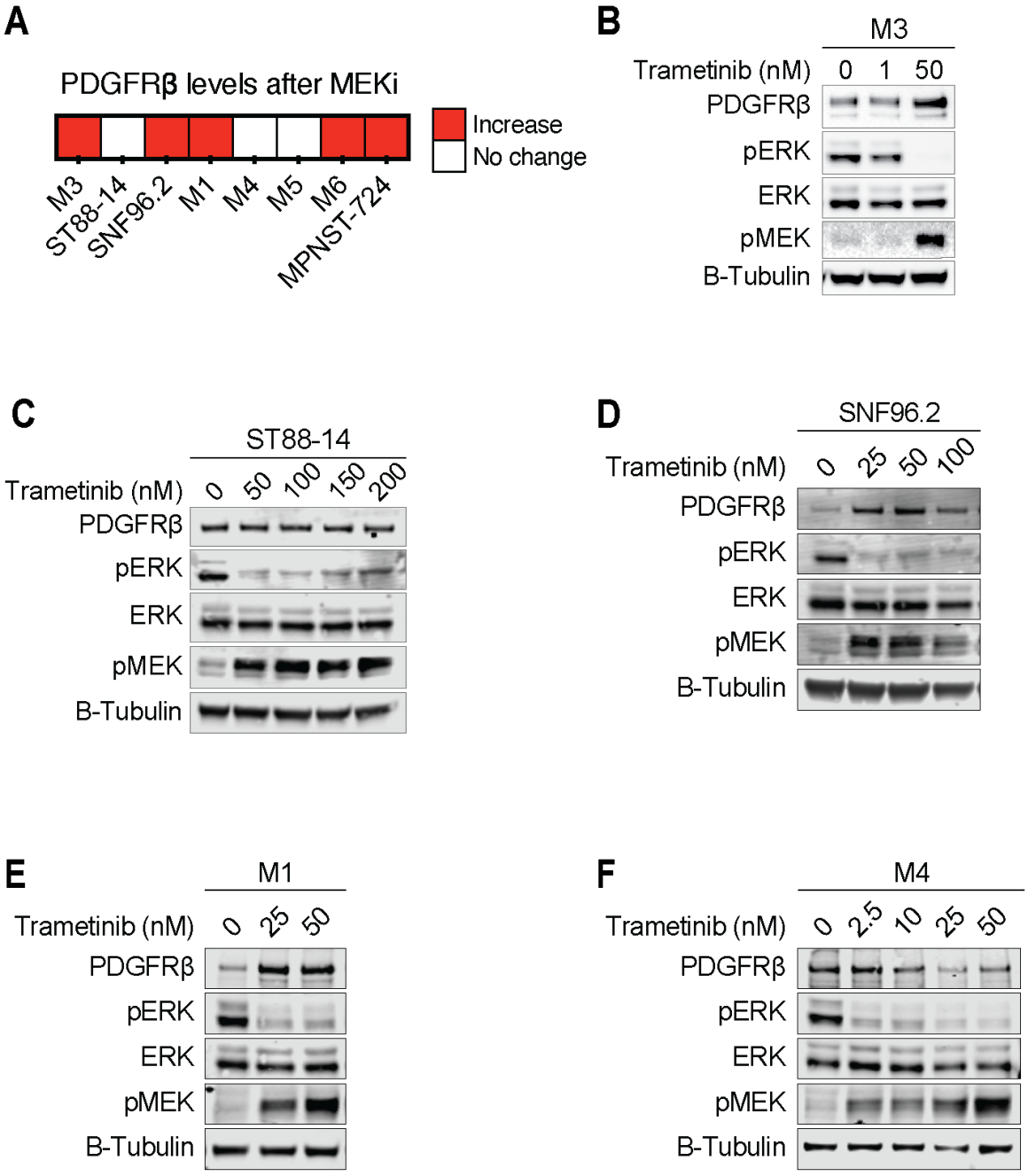
A
PDGFRβ levels after MEKi
Increase
No change
M3
ST88-14
SNF96.2
M1
M4
M5
M6
MPNST-724
B
M3
Trametinib (nM) 0 1 50
PDGFRβ
pERK
ERK
pMEK
B-Tubulin
C
ST88-14
Trametinib (nM) 0 50 100 150 200
PDGFRβ
pERK
ERK
pMEK
B-Tubulin
D
SNF96.2
Trametinib (nM) 0 25 50 100
PDGFRβ
pERK
ERK
pMEK
B-Tubulin
E
M1
Trametinib (nM) 0 25 50
PDGFRβ
pERK
ERK
pMEK
B-Tubulin
F
M4
Trametinib (nM) 0 2.5 10 25 50
PDGFRβ
pERK
ERK
pMEK
B-Tubulin

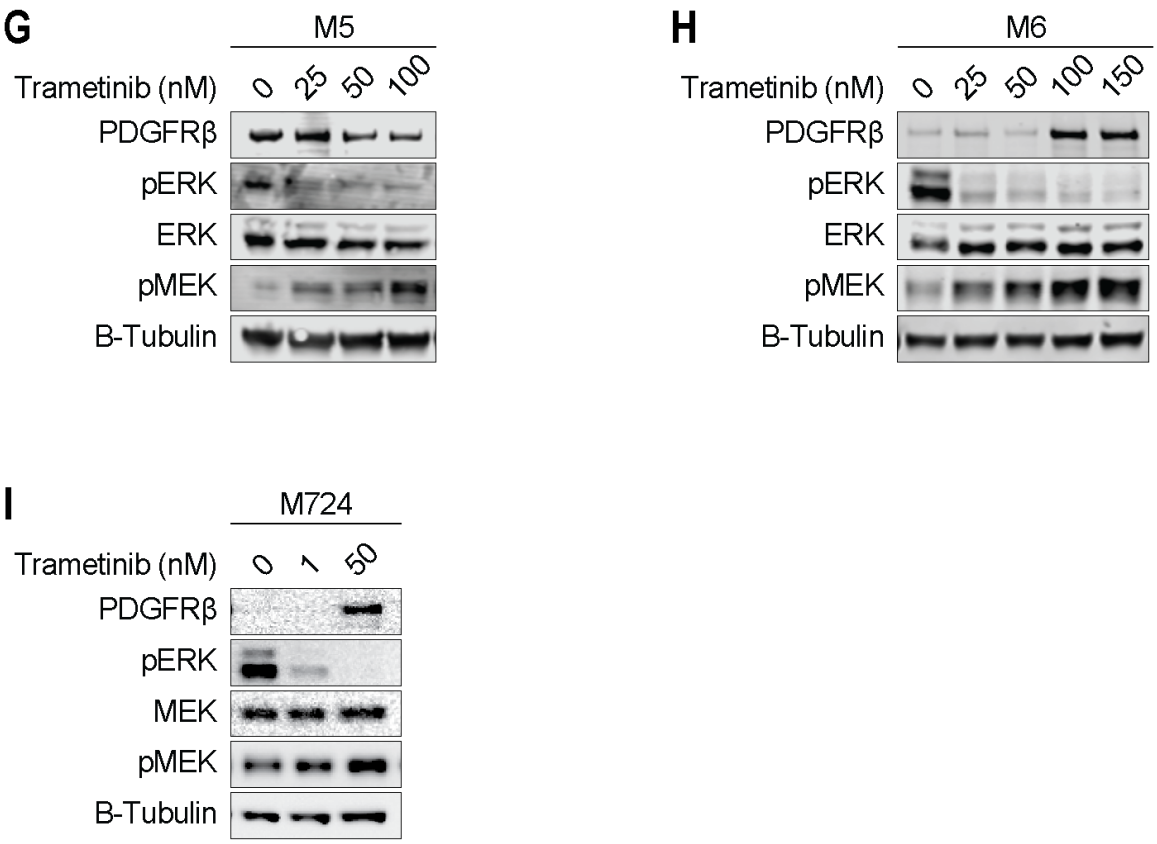

Figure 8. Acute exposure to MEKi treatment leads to an increase in total PDGFRβ

A) Summary heatmap highlighting the MPNST cell lines in which PDGFRβ protein levels increase as a response to 48hr *in vitro* Trametinib treatment.

B-I) Western blot analysis of M3 (B) and ST88-14 (C), SNF96.2 (D), M1 (E), M4 (F), M5 (G), M6 (H) or M724 (I) cells treated with increasing concentrations of Trametinib for 48hr.

CHAPTER 3.3 – CHRONIC EXPOSURE MEKI TREATMENT LEADS TO PDGFRB INCREASE

While acute exposure to MEKi treatment resulted in an increase of PDGFRβ in the majority of MPNST cell lines, we wondered whether chronic exposure to the MEKi would have similar effects. To assess this, we developed MEKi-resistant M3 cells (Figure 9 A-B) and ST88-14 cells (Figure 9 D-E), by culturing the cells under increasing concentrations of the MEKi Trametinib. Similar to the effects of acute MEKi treatment (Figure 9 F), PDGFRβ levels were increased in MEKi-resistant M3 cells (Figure 9 C). On the other hand, MEKi-resistant ST88-14 cells also showed increased PDGFRβ levels as they adapted to the constant exposure to MEKi treatment, and this increase was reversible as a 72-hours washout of the drug resulted in PDGFRβ returning to basal levels (Figure 9 F). Taken together, these results point to increasing PDGFRβ levels as a mechanism through which MPNST cells respond and develop resistance to MEKi treatment and highlight the importance of developing a drug combination strategy that takes this into account.

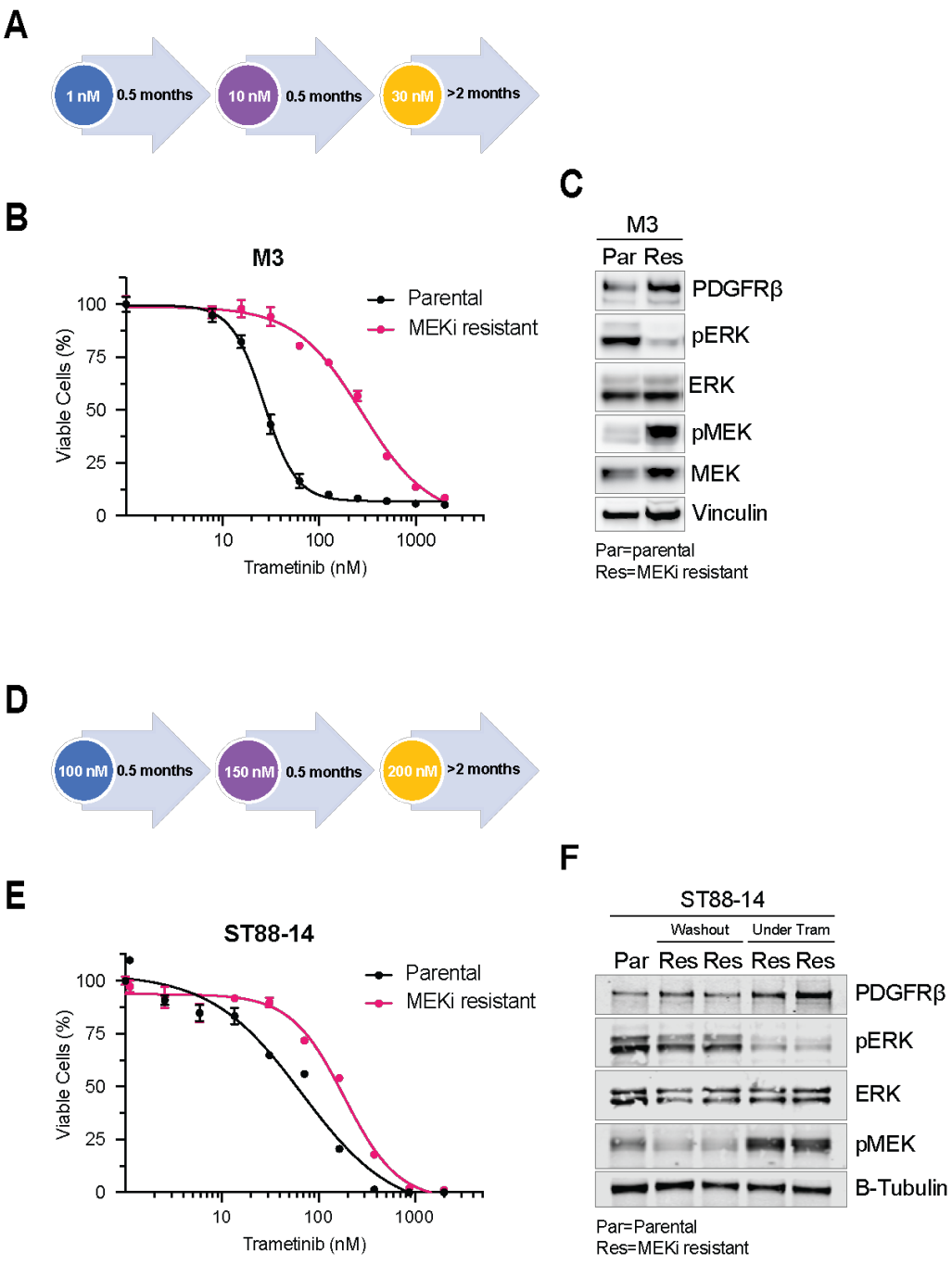

Figure 9. Chronic exposure MEKi treatment leads to PDGFRβ increase

A,D) Schematic of the strategy followed for developing Trametinib resistant M3 (A) and ST88-14 (D) cells.

B,E) Cell viability of parental and Trametinib resistant M3 (B) and ST88-14 (E) cells treated with increasing doses of Trametinib for 5 days. Error bars represent the mean of three measurements ± SEM.

C) Western blot analysis of M3 parental and Trametinib resistant cells.
F) Western blot analysis of ST88-14 parental and Trametinib resistant cells after a 72hr drug washout or under constant MEKi treatment.

CHAPTER 4 – RIPRETINIB SYNERGIZES WITH MEKI AT INHIBITING MAPK SIGNALING AND CELL VIABILITY PARTIALLY THROUGH TARGETING PDGFRB

CHAPTER 4.1 – PDGFRB INHIBITORS EFFICACY AGAINST MPNST

Considering that MPNST cells respond to acute or chronic MEKi treatment by increasing PDGFRβ levels, we decided to test the efficacy of combining the MEKi Trametinib with the type I inhibitor Avapritinib, the type II inhibitor AZD-3229, and the novel PDGFRα/β and KIT inhibitor Ripretinib [94]. *In vitro* cell viability assays carried out after treating ST88-14 or M3 cells with the different drug combinations showed that the RTK inhibitors by themselves had little to no effect at the selected doses (Figure 10. A,C,E,G,I,K)

When combined with the MEKi, Ripretinib was able to potentiate the effect of the drug as the concentration of Trametinib needed to reach IC_{50} was significantly reduced as demonstrated by the left shifting of the curves in the cell viability plots, suggesting that the combination has a high efficacy at decreasing ST88-14 cell viability (Figure 10 A), and Bliss synergy analysis demonstrated that this combination has a strong synergetic effect (Figure 10 B). Similar results were obtained with the M3 cells, which also showed a high drug synergy for the Trametinib and Ripretinib combination treatment (Figure 10 C,D). On the other hand, the MEKi and Avapritinib or AZD3229 combination treatment resulted in a greatly reduced synergy in the ST88-14 cells (Figure 10 E-F,I-J), and was completely lost in the M3 cells (Figure 10 G-H,K-L).

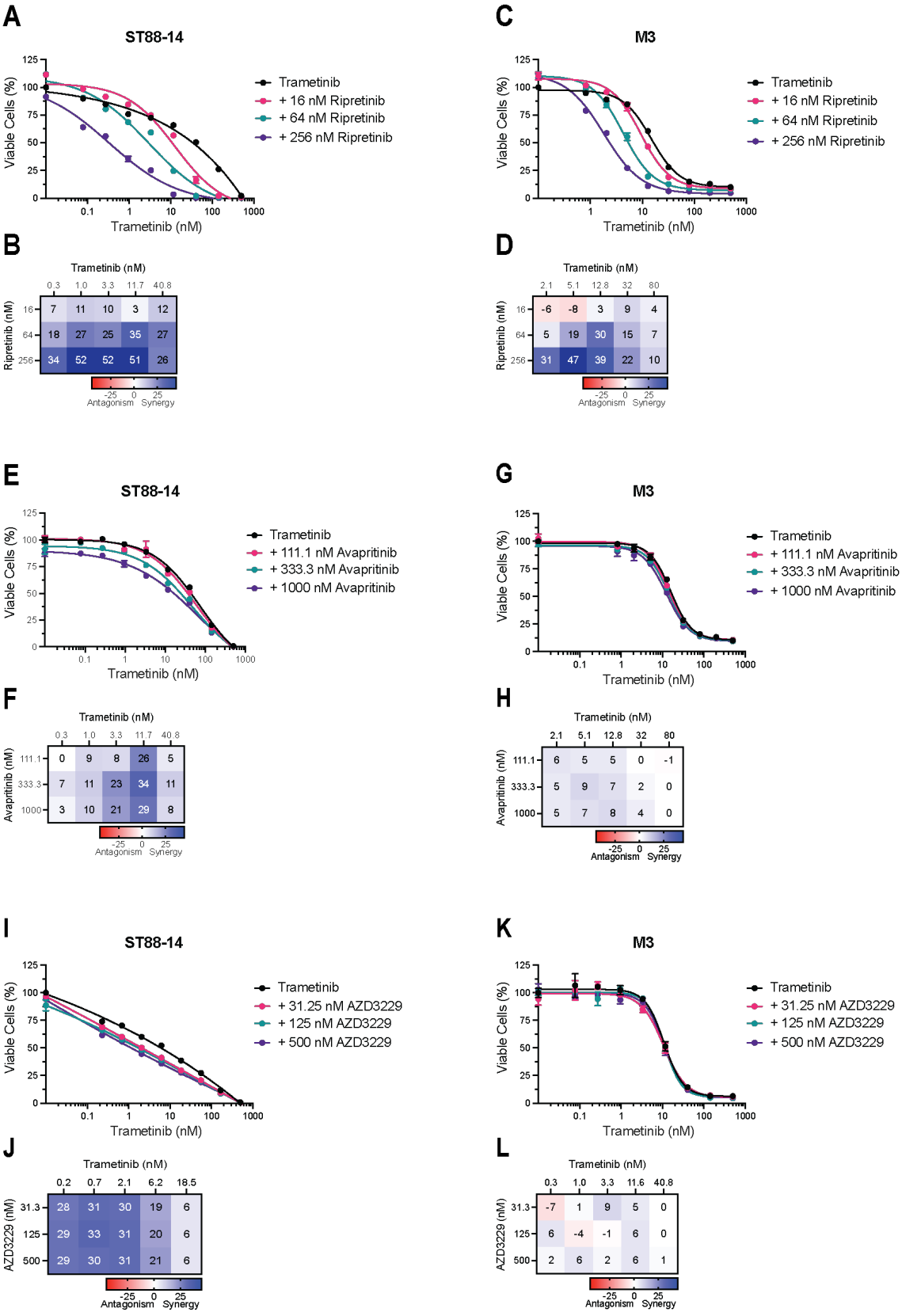
A
ST88-14
Viable Cells (%)
Trametinib (nM)
Trametinib
+ 16 nM Ripretinib
+ 64 nM Ripretinib
+ 256 nM Ripretinib
B
Trametinib (nM)
Ripretinib (nM)
0.3 1.0 3.3 11.7 40.8
16 7 11 10 3 12
64 18 27 25 35 27
256 34 52 52 51 26
Antagonism Synergy
C
M3
D
2.1 5.1 12.8 32 80
16 -6 -8 3 9 4
64 5 19 30 15 7
256 31 47 39 22 10
E
ST88-14
+ 111.1 nM Avapritinib
+ 333.3 nM Avapritinib
+ 1000 nM Avapritinib
F
Avapritinib (nM)
111.1 0 9 8 26 5
333.3 7 11 23 34 11
1000 3 10 21 29 8
G
M3
H
2.1 5.1 12.8 32 80
111.1 6 5 5 0 -1
333.3 5 9 7 2 0
1000 5 7 8 4 0
I
ST88-14
+ 31.25 nM AZD3229
+ 125 nM AZD3229
+ 500 nM AZD3229
J
AZD3229 (nM)
0.2 0.7 2.1 6.2 18.5
31.3 28 31 30 19 6
125 29 33 31 20 6
500 29 30 31 21 6
K
M3
L
0.3 1.0 3.3 11.6 40.8
31.3 -7 1 9 5 0
125 6 -4 -1 6 0
500 2 6 2 6 1

Figure 10. PDGFRβ inhibitors' efficacy against MPNST

A,C) Cell viability of ST88-14 (A) or M3 (C) cells treated with increasing doses of Trametinib and Ripretinib for 5 days. Error bars represent the mean of three measurements ± SEM.

B,D) Bliss synergy score heat map for the combination treatment of Trametinib and Ripretinib in ST88-14 (B) or M3 (D) cells. Data represent the mean from n = 3.

E,G) Cell viability of ST88-14 (E) or M3 (G) cells treated with increasing doses of Trametinib and Avapritinib for 5 days. Error bars represent the mean of three measurements ± SEM.

F,H) Bliss synergy score heat map for the combination treatment of Trametinib and Avapritinib in ST88-14 (F) or M3 (H) cells. Data represent the mean from n = 3.

I,K) Cell viability of ST88-14 (I) or M3 (K) cells treated with increasing doses of Trametinib and AZD3229 for 5 days. Error bars represent the mean of three measurements ± SEM.

J,L) Bliss synergy score heat map for the combination treatment of Trametinib and AZD3229 in ST88-14 (J) or M3 (L) cells. Data represent the mean from n = 3.

CHAPTER 4.2 – RIPRETINIB EFFECTS ON RTKS IN MPNST ARE SPECIFIC TO PDGFRB

To assess the specificity of Ripretinib at inhibiting PDGFRβ in MPNST, we carried out a phospho-RTK array, which demonstrated that PDGFRβ was the only RTK to be inhibited by Ripretinib in MPNST (Figure 11 A-B,D-E). Furthermore, Ripretinib was also able to inhibit the MEKi treatment mediated increase in phospho-PDGFRβ levels in M3 cells (Figure 11 D-E).

To determine if the drug combination was also effective at inhibiting the MAPK pathway activity, protein analyses were performed after treating ST88-14 and M3 cells with Trametinib and Ripretinib (Figure 11 C,F). Ripretinib treatment by itself had little to no effect on inhibiting pERK levels, but combining this with Trametinib resulted in a stronger pERK inhibition compared to either single agent alone, further supporting the previously observed drug synergy (Figure 10 A-B,C-D). Furthermore, the combination was also able to inhibit some of the Trametinib-treatment mediated increase of pMEK levels, in both cell lines (Figure 11 C,F). The MAPK pathway transcriptional output was also effectively inhibited by the combination as demonstrated by the reduction in DUSP6, SPRY2, and SPRED2 expression levels (Figure 12 B-D). Interestingly, the gene expression analysis also shows that the increase in PDGFRβ protein levels seen in M3 cells after MEKi treatment occurs because of an increase in its transcription levels (Figure 12 A).

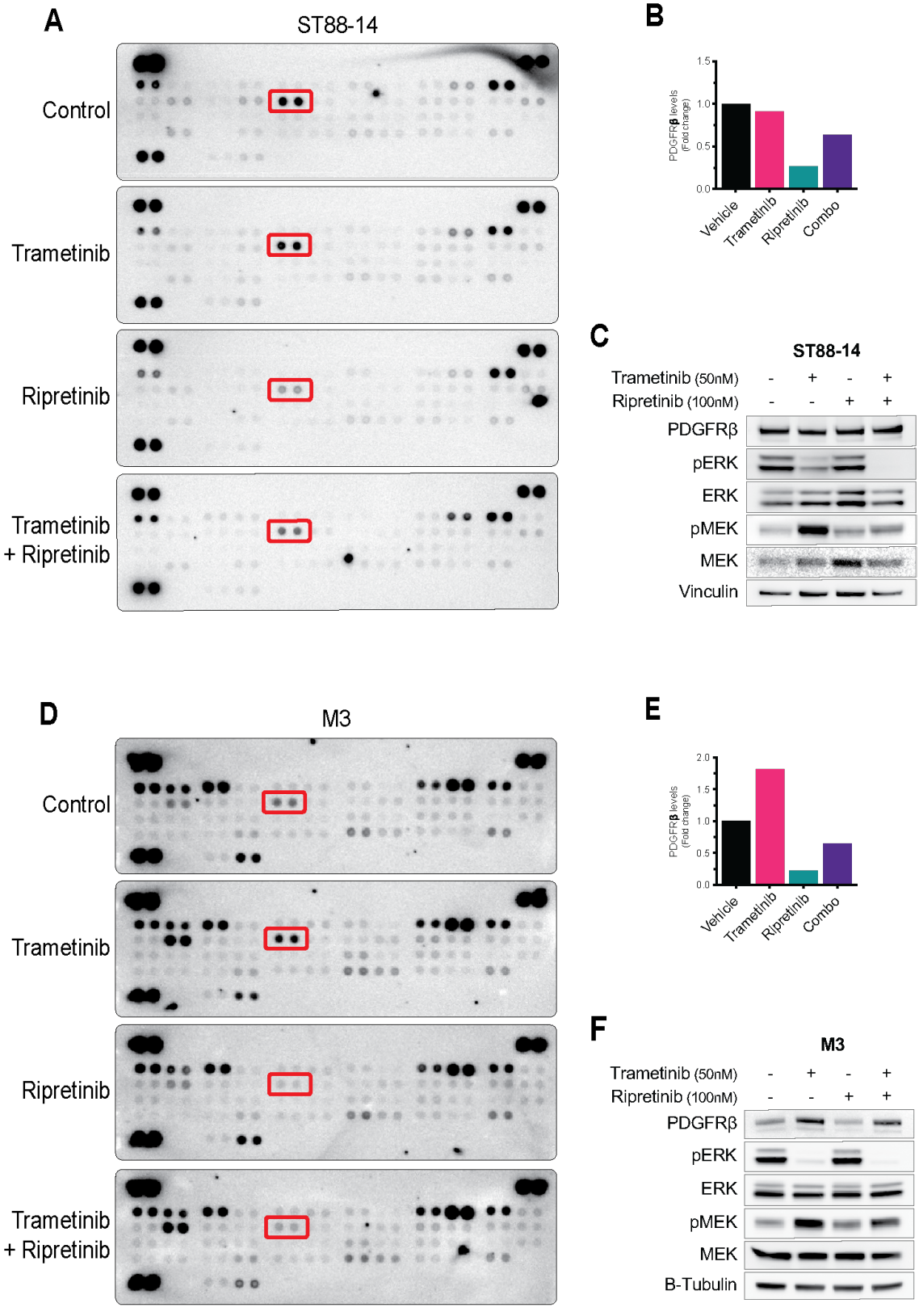
A
ST88-14
Control
Trametinib
Ripretinib
Trametinib
+ Ripretinib
B
PDGFRβ levels
(Fold change)
1.5
1.0
0.5
0.0
Vehicle
Trametinib
Ripretinib
Combo
C
ST88-14
Trametinib (50nM) - + - +
Ripretinib (100nM) - - + +
PDGFRβ
pERK
ERK
pMEK
MEK
Vinculin
D
M3
Control
Trametinib
Ripretinib
Trametinib
+ Ripretinib
E
PDGFRβ levels
(Fold change)
2.0
1.5
1.0
0.5
0.0
Vehicle
Trametinib
Ripretinib
Combo
F
M3
Trametinib (50nM) - + - +
Ripretinib (100nM) - - + +
PDGFRβ
pERK
ERK
pMEK
MEK
B-Tubulin

Figure 11. Ripretinib effects on RTKs in MPNST are specific to PDGFRβ

A,D) Phospho-RTK arrays of ST88-14 (A) and M3 (D) cells treated with DMSO, 50 nM Trametinib, 100 nM Ripretinib, or 50 nM Trametinib and 100 nM combination for 48hr. PDGFRβ is identified by red squares.

B,E) Normalized mean pixel intensity quantification of PDGFRβ levels in the Phospho-RTK arrays of ST88-14 (B) and M3 (E) cells.

C,F) Western blot analysis of ST88-14 (C) or M3 (F) cells treated with Trametinib and Ripretinib for 48hr.

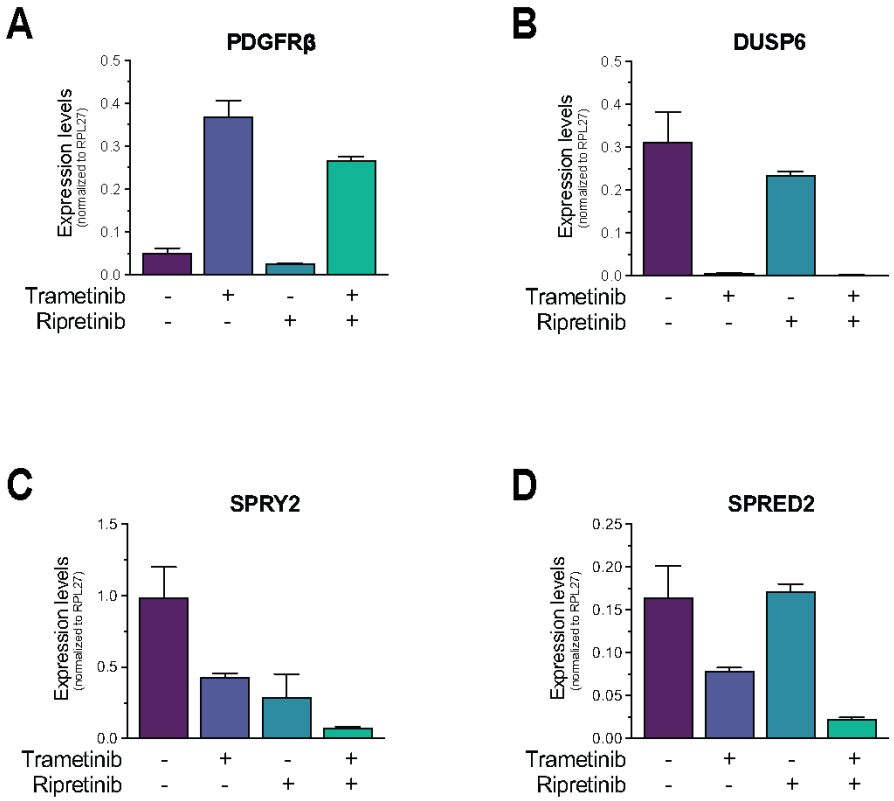

Figure 12. MPNST upregulates PDGFRβ in response to MEKi treatment
A-D) RT-qPCR analysis of the changes of PDGFRβ, DUSP6, SPRY2, or SPRED2 expression levels in M3 cells treated with 50 nM Trametinib and 100 nM Ripretinib for 48hr.

CHAPTER 4.3 – RIPRETINIB AND MEKI COMBINATION IS HIGHLY SYNERGETIC AGAINST A PANEL OF MPNST CELL LINES

Because of the high effectiveness and synergy observed for the Ripretinib and MEKi treatment, we decided to focus on this combination and test its effectiveness against a panel of MPNST cell lines with different genetic characteristics commonly found in MPNST (Figure 13 A) [104]

While all MPNST cell lines tested had different sensitivities to MEKi treatment (Figure 13 B), as seen with ST88-14 and M3 cell lines, Ripretinib treatment by itself had little to no effect at the selected doses (Figure 13 C), but the combination with Trametinib had similar high efficacy and synergy across all tested MPNST cell lines as demonstrated by the left shifting of the curves in the cell viability plots and the high scores obtained for the Bliss synergy analysis (Figure 14 A-H). This suggests that the combination of Trametinib and Ripretinib could be highly effective for the treatment of MPNST.

A

Cell Line	MPNST Clinical Sub-Type	NF1	CDKN2A	PRC2
M3	NF1	Y2485 (Frame Shift Del) X2624 (Splice)	Homozygous Loss *	WT
ST88-14	NF1	Homozygous Loss *	Homozygous Loss *	Homozygous Loss *
SNF96.2	NF1	Homozygous Loss *	Homozygous Loss *	Homozygous missense mutation
M1	NF1	X1870 (Splice)	Homozygous Loss *	Homozygous Loss *
M4	NF1	X1870 (Splice)	Homozygous Loss *	Homozygous Loss *
M5	NF1	X1870 (Splice)	Homozygous Loss *	Homozygous Loss *
M6	NF1	Q950 (Truncating)	Homozygous Loss *	Homozygous Loss *
M724	Sporadic	WT	Homozygous Loss *	WT

* = Confirmed by western blot

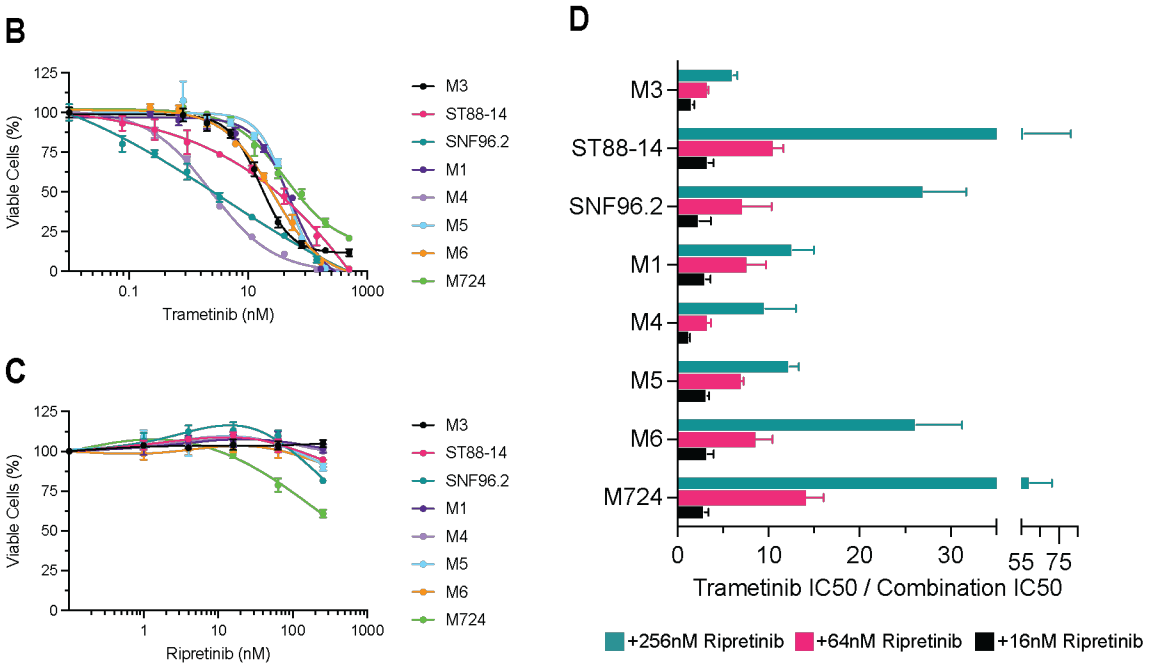

Figure 13. Ripretinib and MEKi combination is highly synergetic against a panel of MPNST cell lines

A) Genetic characteristics of the panel of MPNST cell lines used in the different experiments.

B-C) Cell viability of MPNST cell lines treated with increasing doses of Trametinib (B) or Ripretinib (C) for 5 days. Error bars represent the mean of three measurements ± SEM.

D) Bar graph plot of the cell viability IC_{50} (nM) fold change of MPNST cells treated for 5 days with Trametinib in combination with Ripretinib.

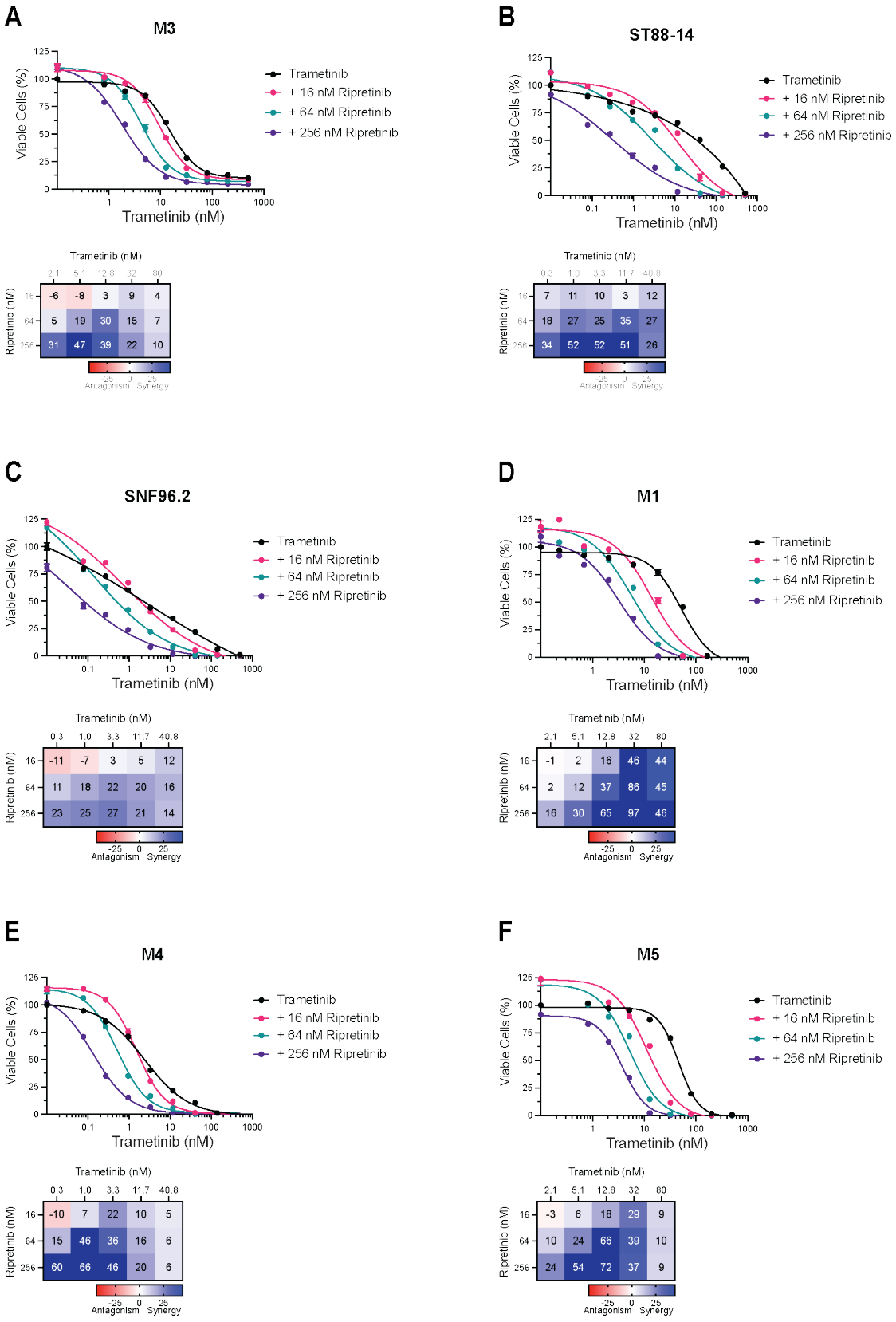
A
M3
Viable Cells (%)
Trametinib (nM)
Trametinib
+ 16 nM Ripretinib
+ 64 nM Ripretinib
+ 256 nM Ripretinib
Trametinib (nM)
Ripretinib (nM)
2.1 5.1 12.8 32 80
16 -6 -8 3 9 4
64 5 19 30 15 7
256 31 47 39 22 10
Antagonism Synergy
B
ST88-14
Viable Cells (%)
Trametinib (nM)
Trametinib
+ 16 nM Ripretinib
+ 64 nM Ripretinib
+ 256 nM Ripretinib
Trametinib (nM)
Ripretinib (nM)
0.3 1.0 3.3 11.7 40.8
16 7 11 10 3 12
64 18 27 25 35 27
256 34 52 52 51 26
Antagonism Synergy
C
SNF96.2
Viable Cells (%)
Trametinib (nM)
Trametinib
+ 16 nM Ripretinib
+ 64 nM Ripretinib
+ 256 nM Ripretinib
Trametinib (nM)
Ripretinib (nM)
0.3 1.0 3.3 11.7 40.8
16 -11 -7 3 5 12
64 11 18 22 20 16
256 23 25 27 21 14
Antagonism Synergy
D
M1
Viable Cells (%)
Trametinib (nM)
Trametinib
+ 16 nM Ripretinib
+ 64 nM Ripretinib
+ 256 nM Ripretinib
Trametinib (nM)
Ripretinib (nM)
2.1 5.1 12.8 32 80
16 -1 2 16 46 44
64 2 12 37 86 45
256 16 30 65 97 46
Antagonism Synergy
E
M4
Viable Cells (%)
Trametinib (nM)
Trametinib
+ 16 nM Ripretinib
+ 64 nM Ripretinib
+ 256 nM Ripretinib
Trametinib (nM)
Ripretinib (nM)
0.3 1.0 3.3 11.7 40.8
16 -10 7 22 10 5
64 15 46 36 16 6
256 60 66 46 20 6
Antagonism Synergy
F
M5
Viable Cells (%)
Trametinib (nM)
Trametinib
+ 16 nM Ripretinib
+ 64 nM Ripretinib
+ 256 nM Ripretinib
Trametinib (nM)
Ripretinib (nM)
2.1 5.1 12.8 32 80
16 -3 6 18 29 9
64 10 24 66 39 10
256 24 54 72 37 9
Antagonism Synergy

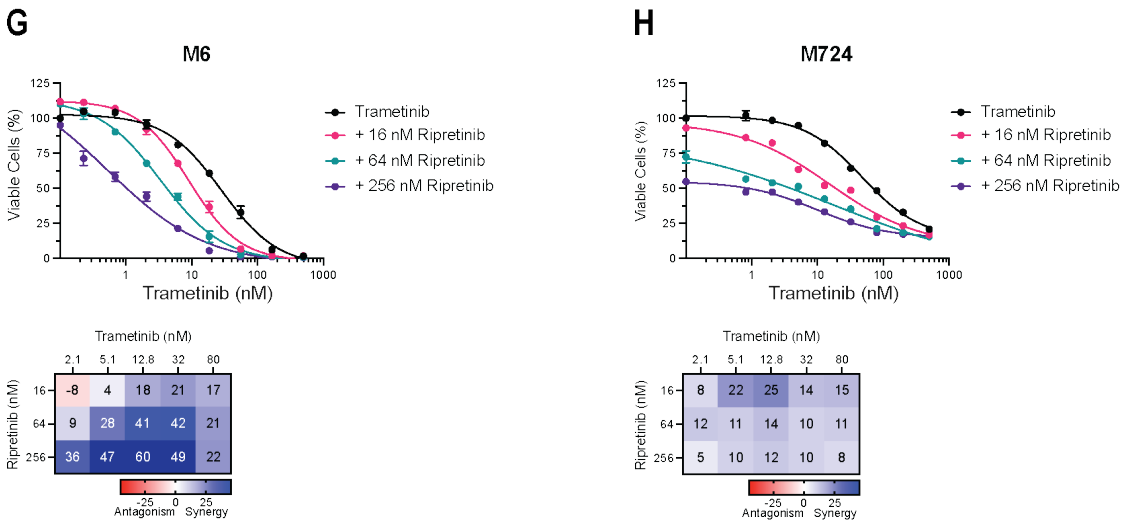

Figure 14. Cell Viability experiments for the Ripretinib and MEKi combination against a panel of MPNST cell lines

A-H) Cell viability and Bliss synergy score heat map for M3 (A), ST88-14 (B), SNF96.2 (C), M1 (D), M4 (E), M5 (F), M6 (G) or M724 (H) cells treated with increasing doses of Trametinib and Ripretinib for 5 days. Error bars represent the mean of three measurements ± SEM, and Bliss scores represent the mean from n = 3.

CHAPTER 4.3.1 – COMBINATION TREATMENT IS EFFECTIVE REGARDLESS OF MPNST PRC2 STATUS

Loss of PRC2 function by loss-of-function mutations in the SUZ12 or EED subunits is a common event in MPNST. Previous analysis of a panel of MPNST cells shows that both PRC2 WT and PRC2 loss cells are sensitive to the pharmacological combination of Trametinib and Ripretinib (Figure 13 A, Figure 14). However, to better assess if the presence or absence of PRC2 function has any effect on the sensitivity of MPNST cells to the combination, we repeated the drug treatment studies using PRC2 loss isogenic M3 cells (Figure 15 A) previously developed in the lab. Obtained results show that PRC2 loss isogenic M3 cells had similar sensitivity to Ripretinib single-agent treatment, as demonstrated by the similar downward shifting of the points in the y-axis of the graphs (Figure 15 B,E), and similar sensitivity to Trametinib single-agent treatment (Figure 15 B-C,E-F).

The combination also treatment had similar high efficacy and synergy in both cell lines tested as demonstrated by the left shifting of the curves in the cell viability plots (Figure 15 B,E), very similar Trametinib IC_{50} for the different combinations with Ripretinib (Figure 15 C,F) and similar high drug synergism (Figure 15 D,G). These results suggest that regardless of PRC2 status, the tested pharmacological combination is very effective and synergetic in MPNST.

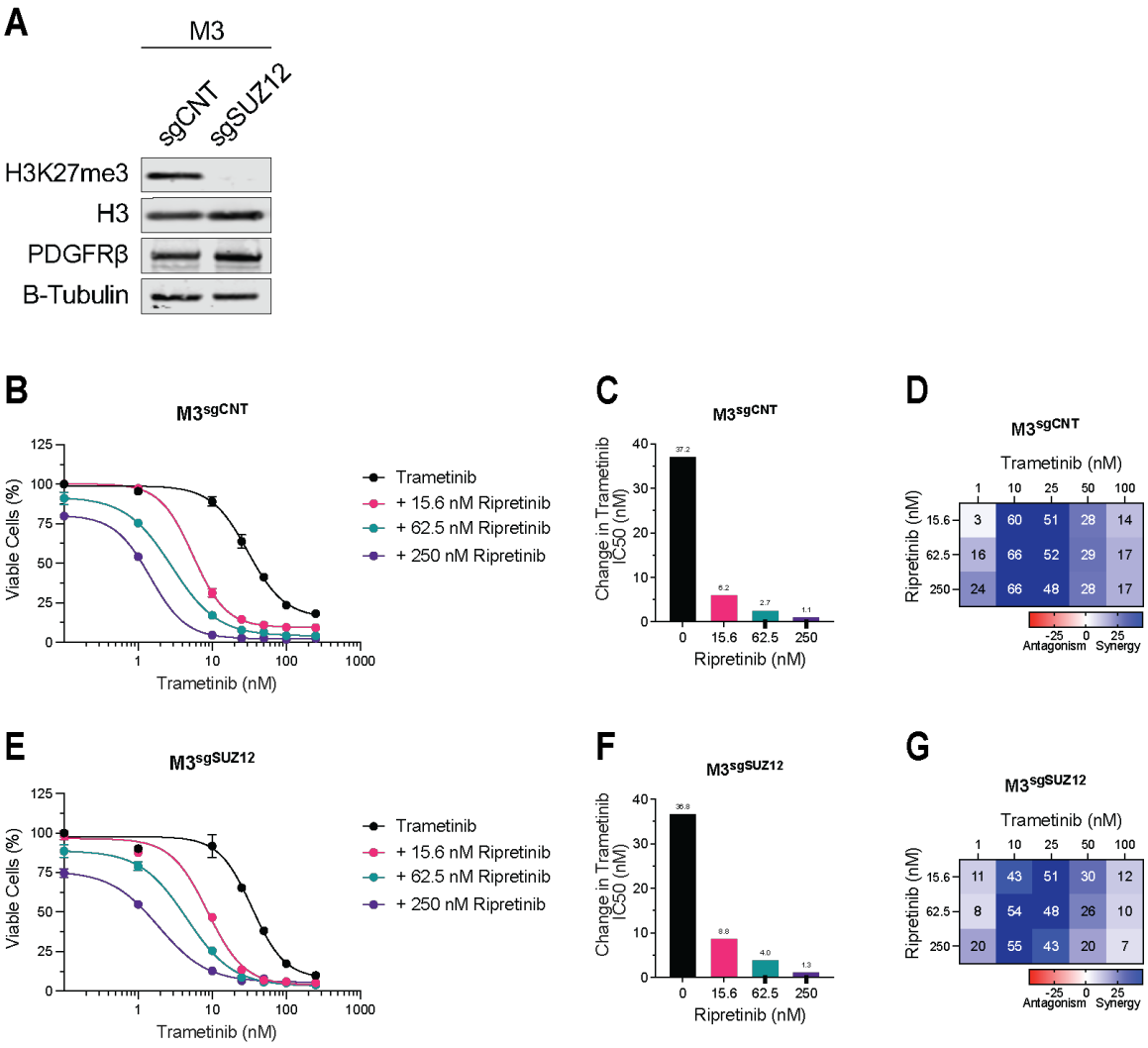

Figure 15. Combination treatment is effective regardless of MPNST PRC2 status

A) Western blot validation of SUZ12 KO in ST88-14 cells using CRISPR-Cas9.

B,E) Cell viability of $M3^{sgCNT}$ (B), and $M3^{sgSUZ12}$ (E) cells treated with increasing doses of Trametinib and Ripretinib for 5 days. Error bars represent the mean of three measurements ± SEM.

C,F) Bar graph plot of the change in Trametinib IC_{50} (nM) in $M3^{sgCNT}$ (C), and $M3^{sgSUZ12}$ (F) cells when combined with increasing doses of Ripretinib.

D,G) Bliss synergy score heat map from combination treatment of Trametinib and Ripretinib in $M3^{sgCNT}$ (D), and $M3^{sgSUZ12}$ (G) cells. Data represent the mean from n = 3.

CHAPTER 4.3.2 – COMBINATION TREATMENT IS EFFECTIVE AGAINST MEKI-RESISTANT MPNST CELLS

The ability of MPNST to develop MEKi treatment resistance has greatly affected the effectiveness of these small molecule inhibitors in the clinic. To assess the ability of Ripretinib and Trametinib combination treatment to overcome this drug resistance, we studied the efficacy of the combination treatment against the MEKi-resistant M3 and ST88-14 cells developed in Chapter 3.3. In both models tested the combination treatment was able to synergistically decrease the cell viability of both parental and resistant cells (Figure 16). This data suggests that even in models in which MEK inhibition is not enough to effectively lower cell viability, dual targeting with Trametinib and Ripretinib is able to overcome this.

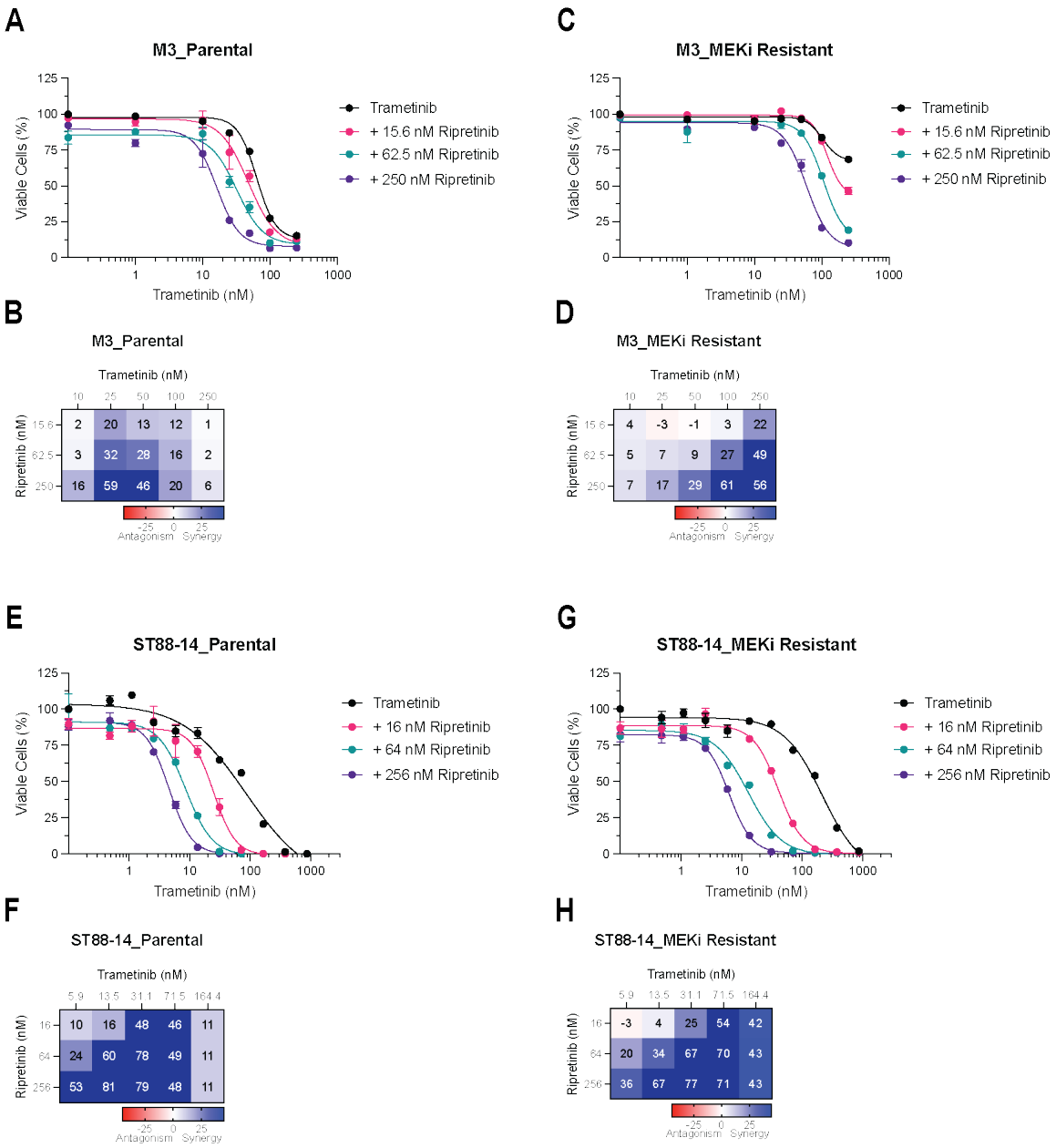

Figure 16. Combination treatment is effective against MEKi-resistant MPNST cells

A,C,E,G) Cell viability of M3 parental (A), M3 MEKi-Resistant (C), ST88-14 parental (E), and ST88-14 MEKi-Resistant (G) cells treated with increasing doses of Trametinib and Ripretinib for 5 days. Error bars represent the mean of three measurements ± SEM.

B,D,F,H) Bliss synergy score heat map from combination treatment of Trametinib and Ripretinib in M3 parental (B), M3 MEKi-Resistant (D), ST88-14 parental (F), and ST88-14 MEKi-Resistant (H) cells. Data represent the mean from n = 3.

CHAPTER 4.4 – EFFICACY OF RIPRETINIB AND MEKI IS PARTIALLY THROUGH TARGETING PDGFRB

Interestingly, while PDGFRβ knockout did make the cells more sensitive to MEKi treatment, as shown by the significant reduction in the trametinib IC_{50} (Figure 17 A,C-D), the absence of PDGFRβ did not affect the sensitivity of the cells to Ripretinib treatment (Figure 17 B) or the ability of the drug combination to synergize and be effective at reducing MPNST cell viability (Figure 17 E-H), suggesting that other targets of the drug might be also important for mediating this effect.

To identify important differences that could be leading Ripretinib but not Avapritinib to synergize more potently with MEKi, we carried out an immunoblot assay after the combination treatments, which showed that while both PDGFRβ inhibitors have very similar effects on PDGFRβ, RAS-GTP and pERK levels, there are key differences in the total and active BRAF and CRAF levels. Results showed that RAF levels are decreased with Ripretinib and MEKi combination but are not significantly affected by Avapritinib treatment (Figure 18). Interestingly, published literature on Ripretinib identifies BRAF and CRAF as secondary targets for this molecule [94]. Taken together, the results highlight that while PDGFRβ is an important player in the MPNST response to MEKi treatment, other proteins may be also playing a key role in mediating MPNST resistance to MEK inhibition.

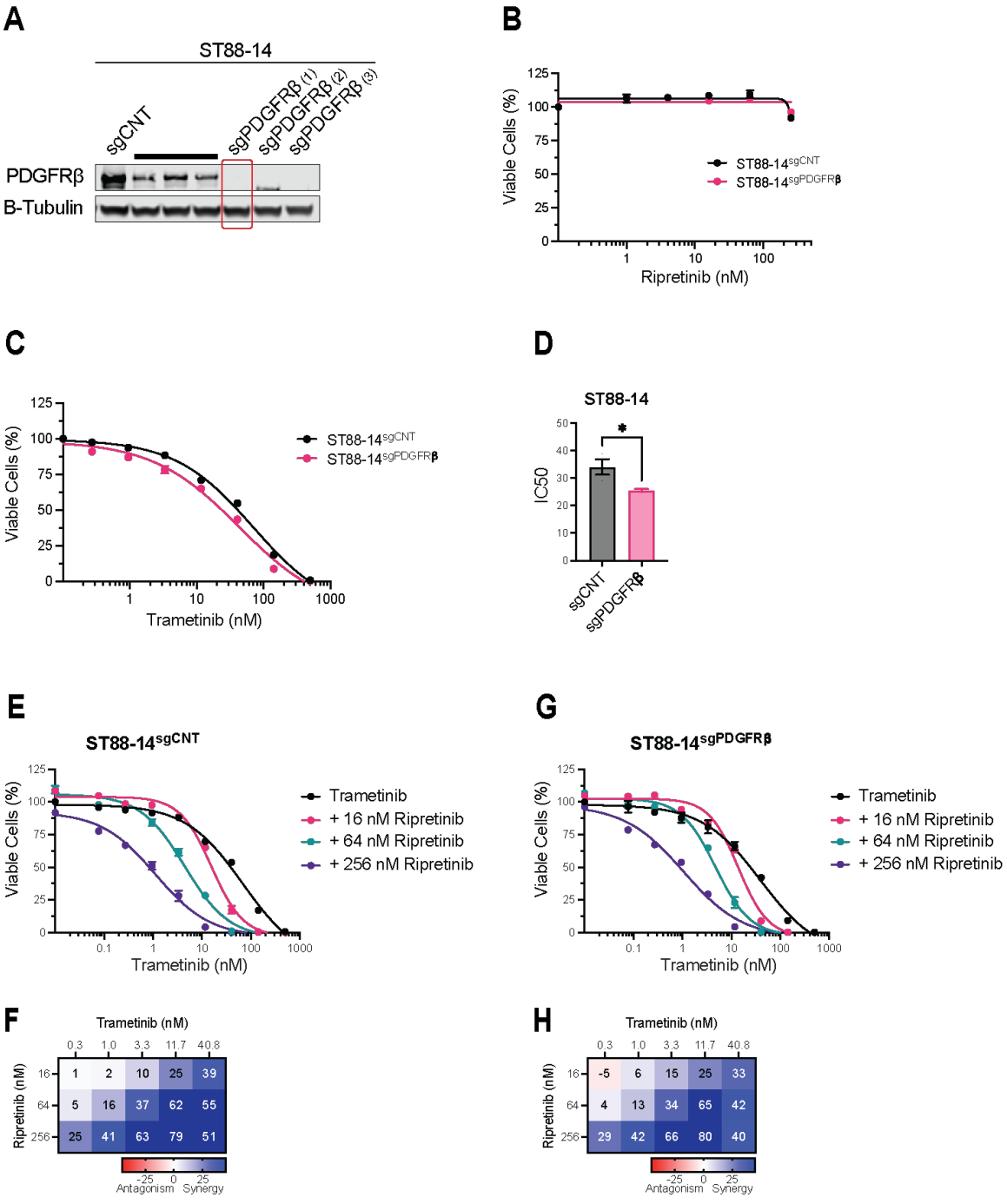

Figure 17. Efficacy of Ripretinib and MEKi is partially through PDGFRβ

A) Western blot validation of PDGFRβ KO in ST88-14 cells using CRISPR-Cas9 and three different single guide RNAs.

A-B) Cell viability of ST88-14^{sgCNT} and ST88-14^{sgPDGFRβ} cells treated with increasing doses of Ripretinib (B) or Trametinib (C) for 5 days. Error bars represent the mean of three measurements ± SEM.

D) Bar graph plot of the cell viability IC50 (nM) of ST88-14^{sgCNT} and ST88-14$^{sgPDGFR\beta}$ cells treated with increasing doses of Trametinib (C). Error bars represent the mean of triplicate experiments, with internal triplicates, ± SD.
E,G) Cell viability of ST88-14^{sgCNT} (E) or ST88-14$^{sgPDGFR\beta}$ (G) cells treated with increasing doses of Trametinib and Ripretinib for 5 days. Error bars represent the mean of three measurements ± SEM.
F,H) Bliss synergy score heat map for the combination treatment of Trametinib and Ripretinib in ST88-14^{sgCNT} (F) or ST88-14$^{sgPDGFR\beta}$ (H) cells. Data represent the mean from n = 3.
I) Western blot analysis of M3 cells treated with Trametinib, Ripretinib and Avapritinib for 48hr.

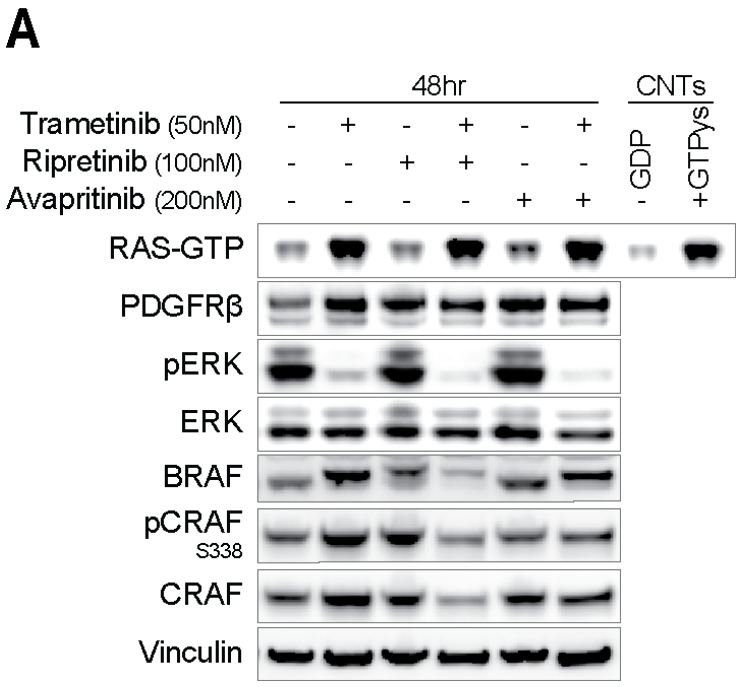

Figure 18. Effects of the Trametinib and Ripretinib or Avapritinib combination treatment on MAPK pathway-associated proteins

Western blot analysis of M3 cells treated with Trametinib, Ripretinib and Avapritinib for 48hr.

CHAPTER 5 – MEKI TREATMENT-INDUCED RAF DIMERIZATION MEDIATES SYNERGISM WITH RAF INHIBITORS IN MPNST

CHAPTER 5.1 – RAF PROTEINS PLAY A KEY ROLE IN MPNST RESPONSE TO MEKI TREATMENT

Based on the importance of the MAPK pathway in MPNST, and the role of BRAF and CRAF as key mediators of this signaling pathway, we decided to test the role of these kinases on the ability of MPNST cells to respond to MEKi treatment. Knocking out BRAF or CRAF resulted in the cells being more sensitive to MEKi treatment, with the greater reduction of Trametinib IC_{50} seen after the CRAF KO (Figure 19 A-B, Figure 20 A-B), which suggests that in MPNST CRAF could be a more important player than BRAF in the response to MEKi treatment.

While the KOs didn't influence the overall sensitivity of the cells to Ripretinib single drug treatment, lower concentrations of Ripretinib did cause an initial increase in cell proliferation, which was reversed as drug concentrations increased (Figure 19 C, Figure 20 C). Considering that RAF proteins are secondary targets of Ripretinib, the increase of cell proliferation seen with lower drug concentrations points to Ripretinib causing a paradoxical activation of the MAPK pathway, which RAF inhibitors are known of being capable of promoting in situations in which drug concentrations are not high enough to inhibit both units of the RAF dimers [81,82]. Interestingly, CRAF KO in ST88-14, and not BRAF KO, reduced the Ripretinib treatment mediated increase of cell proliferation, further supporting the previous observation that CRAF appears to play a more essential role than BRAF in MPNST cells (Figure 19 C).

To determine if the absence of BRAF or CRAF affected the effectiveness of the drug combination, we performed cell viability experiments. Results show that while BRAF KO did have some effect in reducing the synergy for the drug combination, it was the CRAF KO that resulted in a nearly complete loss of the high drug synergy observed for Trametinib and Ripretinib combination in the control ST88-14 and M3 cells (Figure 19 D-I, Figure 20 D-I). This suggests that CRAF plays an important role in the ability of Trametinib and Ripretinib to synergize in MPNST.

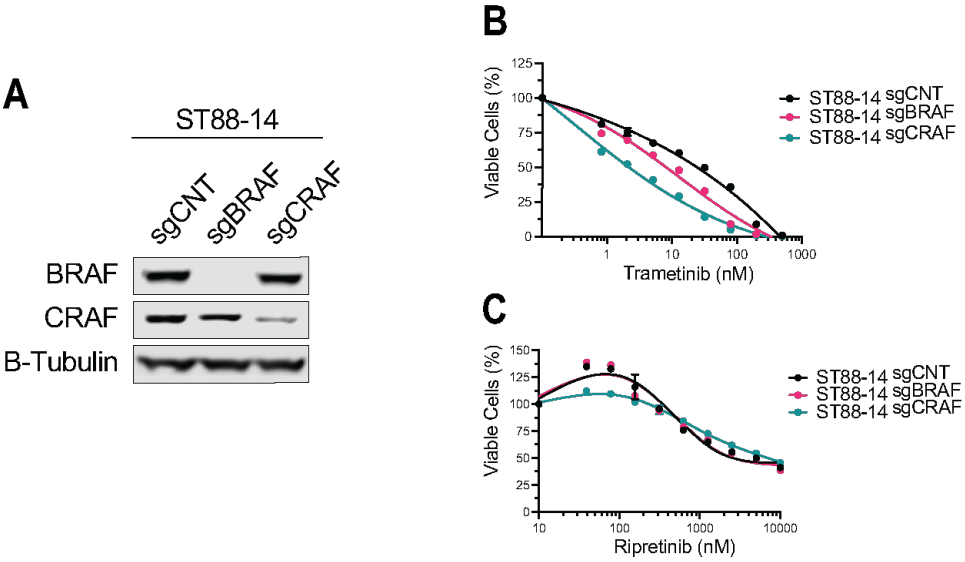
A
ST88-14
sgCNT
sgBRAF
sgCRAF
BRAF
CRAF
B-Tubulin
B
Viable Cells (%)
Trametinib (nM)
ST88-14 sgCNT
ST88-14 sgBRAF
ST88-14 sgCRAF
C
Viable Cells (%)
Ripretinib (nM)
ST88-14 sgCNT
ST88-14 sgBRAF
ST88-14 sgCRAF

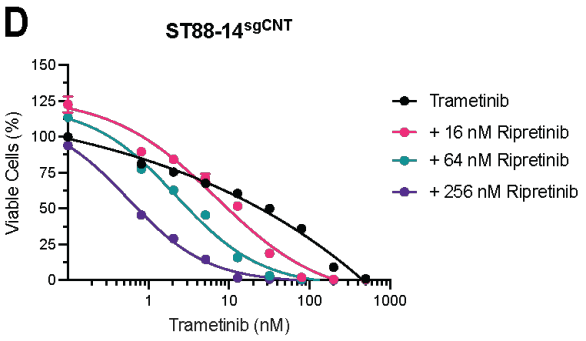
D
ST88-14sgCNT
Viable Cells (%)
Trametinib (nM)
Trametinib
+ 16 nM Ripretinib
+ 64 nM Ripretinib
+ 256 nM Ripretinib

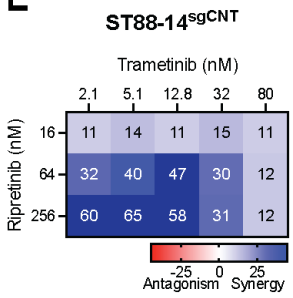
E
ST88-14sgCNT
Trametinib (nM)
2.1 5.1 12.8 32 80
Ripretinib (nM)
16 11 14 11 15 11
64 32 40 47 30 12
256 60 65 58 31 12
-25 0 25
Antagonism Synergy

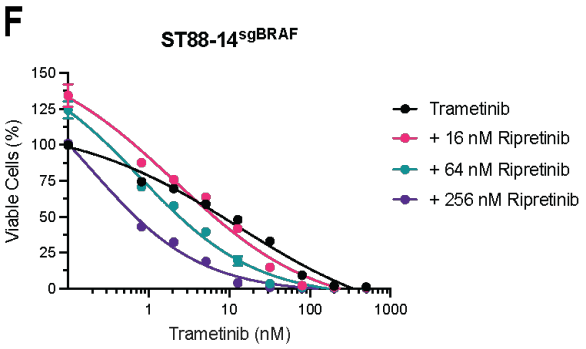
F
ST88-14sgBRAF
Viable Cells (%)
Trametinib (nM)
Trametinib
+ 16 nM Ripretinib
+ 64 nM Ripretinib
+ 256 nM Ripretinib

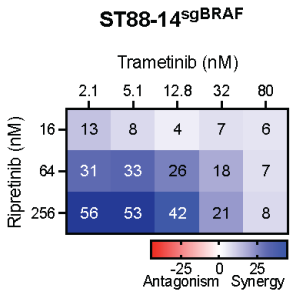
G
ST88-14sgBRAF
Trametinib (nM)
2.1 5.1 12.8 32 80
Ripretinib (nM)
16 13 8 4 7 6
64 31 33 26 18 7
256 56 53 42 21 8
-25 0 25
Antagonism Synergy

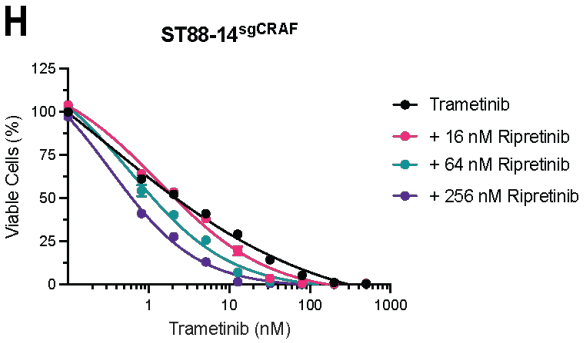
H
ST88-14sgCRAF
Viable Cells (%)
Trametinib (nM)
Trametinib
+ 16 nM Ripretinib
+ 64 nM Ripretinib
+ 256 nM Ripretinib

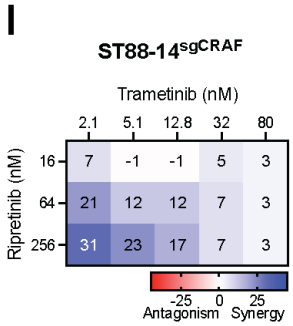
I
ST88-14sgCRAF
Trametinib (nM)
2.1 5.1 12.8 32 80
Ripretinib (nM)
16 7 -1 -1 5 3
64 21 12 12 7 3
256 31 23 17 7 3
-25 0 25
Antagonism Synergy

Figure 19. Assessing the role of RAF proteins in ST88-14 MPNST cells
A) Western blot validation of BRAF and CRAF KO in ST88-14 cells using CRISPR-Cas9.
B-C) Cell viability of ST88-14^{sgCNT}, ST88-14^{sgBRAF} and ST88-14^{sgCRAF} cells treated with increasing doses of Trametinib (B) or Ripretinib (C) for 5 days. Error bars represent the mean of three measurements ± SEM.
D,F,H) Cell viability of ST88-14^{sgCNT} (D), ST88-14^{sgBRAF} (F) and ST88-14^{sgCRAF} (H) cells treated with increasing doses of Trametinib and Ripretinib for 5 days. Error bars represent the mean of three measurements ± SEM.
E,G,I) Bliss synergy score heat map from combination treatment of Trametinib and Ripretinib in ST88-14^{sgCNT} (E), ST88-14^{sgBRAF} (G) and ST88-14^{sgCRAF} (I) cells. Data represent the mean from n = 3.

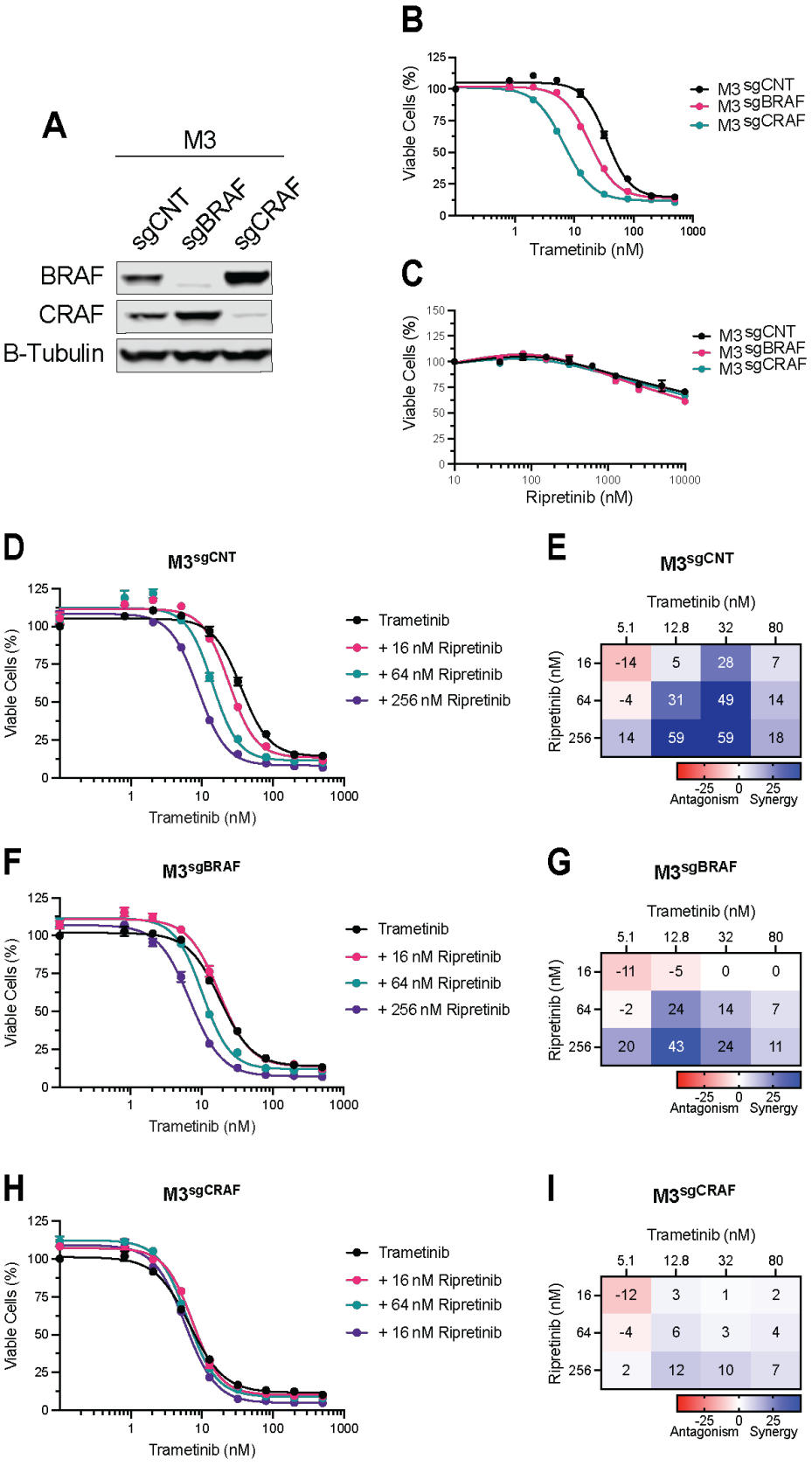
A
M3
sgCNT
sgBRAF
sgCRAF
BRAF
CRAF
B-Tubulin
B
Viable Cells (%)
Trametinib (nM)
M3 sgCNT
M3 sgBRAF
M3 sgCRAF
C
Viable Cells (%)
Ripretinib (nM)
M3 sgCNT
M3 sgBRAF
M3 sgCRAF
D
M3sgCNT
Viable Cells (%)
Trametinib (nM)
Trametinib
+ 16 nM Ripretinib
+ 64 nM Ripretinib
+ 256 nM Ripretinib
E
M3sgCNT
Trametinib (nM)
5.1 12.8 32 80
Ripretinib (nM)
16 -14 5 28 7
64 -4 31 49 14
256 14 59 59 18
-25 0 25
Antagonism Synergy
F
M3sgBRAF
Viable Cells (%)
Trametinib (nM)
Trametinib
+ 16 nM Ripretinib
+ 64 nM Ripretinib
+ 256 nM Ripretinib
G
M3sgBRAF
Trametinib (nM)
5.1 12.8 32 80
Ripretinib (nM)
16 -11 -5 0 0
64 -2 24 14 7
256 20 43 24 11
-25 0 25
Antagonism Synergy
H
M3sgCRAF
Viable Cells (%)
Trametinib (nM)
Trametinib
+ 16 nM Ripretinib
+ 64 nM Ripretinib
+ 16 nM Ripretinib
I
M3sgCRAF
Trametinib (nM)
5.1 12.8 32 80
Ripretinib (nM)
16 -12 3 1 2
64 -4 6 3 4
256 2 12 10 7
-25 0 25
Antagonism Synergy

Figure 20. Assessing the role of RAF proteins in M3 MPNST cells

A) Western blot validation of BRAF and CRAF KO in M3 cells using CRISPR-Cas9.

B-C) Cell viability of $M3^{sgCNT}$, $M3^{sgBRAF}$ and $M3^{sgCRAF}$ cells treated with increasing doses of Trametinib (B) or Ripretinib (C) for 5 days. Error bars represent the mean of three measurements ± SEM.

D,F,H) Cell viability of $M3^{sgCNT}$ (D), $M3^{sgBRAF}$ (F) and $M3^{sgCRAF}$ (H) cells treated with increasing doses of Trametinib and Ripretinib for 5 days. Error bars represent the mean of three measurements ± SEM.

E,G,I) Bliss synergy score heat map from combination treatment of Trametinib and Ripretinib in $M3^{sgCNT}$ (E), $M3^{sgBRAF}$ (G) and $M3^{sgCRAF}$ (I) cells. Data represent the mean from n = 3.

CHAPTER 5.2 – MEKI AND RAFI TREATMENT INDUCES RAF DIMERIZATION IN MPNST

Next, we decided to test the role of these kinases and their ability to dimerize on the capacity of MPNST cells to respond to MEKi treatment. MEKi treatment resulted not only in a reduction of phospho-ERK levels and an increase in phospho-MEK levels, but it also resulted in an activation of the upstream RAF proteins as demonstrated by the upwards shifting of the BRAF band, the increase of active S338 phospho-CRAF, and the decrease of the inhibitory CRAF phosphorylations in S289, S296, and S301 (Figure 21 A). Ripretinib treatment had minimal effects on phospho-ERK and phospho-MEK levels but did cause some minor increases in active BRAF and CRAF levels. This increase was further induced by the Trametinib and Ripretinib combination treatment, all while the drug combination was still effective at inhibiting downstream MAPK pathway activity as shown by diminished levels of phospho-ERK (Figure 21 A). We then performed co-immunoprecipitation assays to assess how RAF dimer formation was affected by the combination treatment. While MEKi treatments by themselves promoted the increase of BRAF and CRAF interaction and even BRAF/CRAF interaction with MEK, the combination treatment resulted in a further induction of the RAF dimerization and their interaction with MEK (Figure 21 B). Interestingly, this combination treatment mediated an increase in RAF dimerization and interaction with MEK occurs at drug concentrations that synergize at decreasing both MPNST cell viability and phospho-ERK levels (Figure 21 A, Figure 10 A).

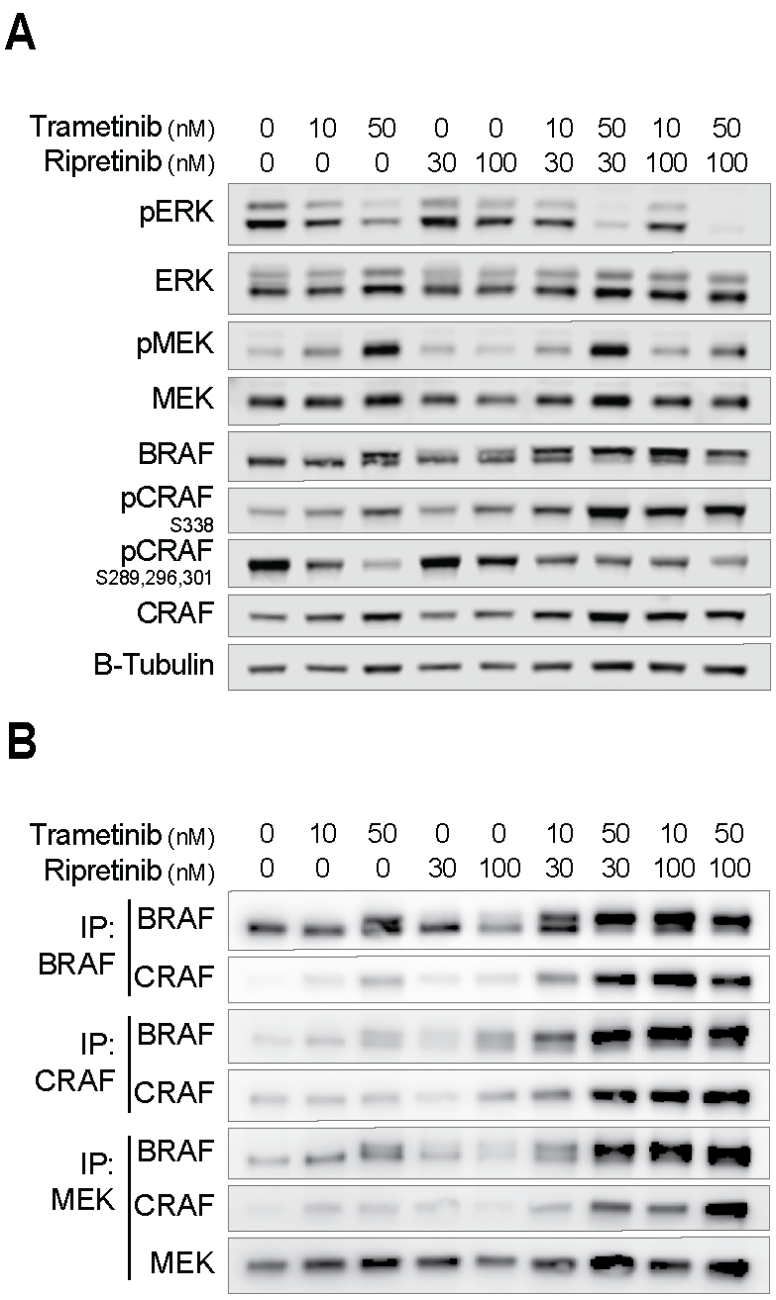

Figure 21. MEKi and RAFi treatment induces RAF dimerization in MPNST
A-B) Western blot analysis of ST88-14 cells whole-cell lysate (A) or lysate subjected to immunoprecipitation (B) after 24hr treatment with Trametinib and Ripretinib.

CHAPTER 5.3 – RAF DIMERIZATION IS REQUIRED FOR THE SYNERGISM OF MEKI AND RAFI TREATMENT IN MPNST

Studies have shown that SHOC2-mediated de-phosphorylation of a conserved phosphorylation site in RAF proteins provides a key input that facilitates RAF dimerization [55,57,58]. Thus, to further study how the MEKi treatment mediated RAF dimerization plays a role in the effectiveness of the combination treatment, we knocked out SHOC2 to develop RAF dimerization deficient MPNST cells (Figure 23 A). As expected, SHOC2 KO cells were more sensitive to MEKi treatment, as shown by the reduction in Trametinib IC_{50} compared to the sgCNT cells (Figure 22 A,C), as the cells are not able to effectively respond to MEK inhibition when they lack the ability to increase MAPK pathway activity through RAF dimer formation [105].

Knocking out SHOC2 in MPNST also resulted in a meaningful reduction of the synergism for the Trametinib and Ripretinib combination, and even some drug concentrations now had an antagonistic effect as highlighted by the decrease in the Bliss synergy score (Figure 22 A-D). This decrease in drug synergy coincides with the decrease in both RAF dimer formation and BRAF/CRAF interaction with MEK following the SHOC2 KO (Figure 23 B). Interestingly, regardless of the KO, the combination treatment still resulted in the increase of active BRAF and CRAF levels and RAF dimerization, albeit to a lesser extent in SHOC2 KO cells (Figure 23 A-B). At these same drug concentrations, Trametinib and Ripretinib still

synergized at inhibiting MAPK pathway downstream activity, as shown by the decrease of pERK levels (Figure 23 A). Taken together, decreased RAF dimer formation and BRAF/CRAF interaction with MEK did not affect the ability of the combination treatment to decrease pERK levels, but it did result in a significant reduction in the ability of the combination treatment to synergistically inhibit MPNST cell viability, suggesting that RAF dimerization in response to MEKi treatment is an important event required for RAF targeting drugs to be able to potentiate MEKi treatment.

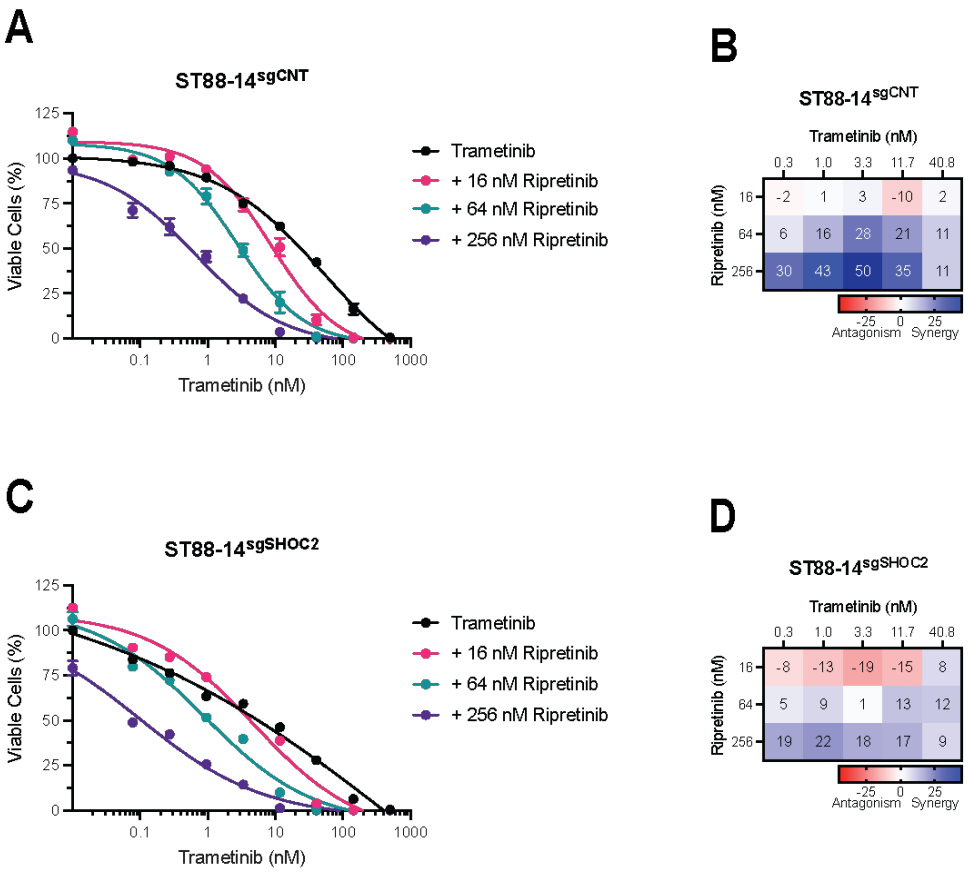

Figure 22. RAF dimerization is required for the synergism of MEKi and RAFi treatment in MPNST

A,C) Cell viability of ST88-14^{sgCNT} (A) and ST88-14^{sgSHOC2} (C) cells treated with increasing doses of Trametinib and Ripretinib for 5 days. Error bars represent the mean of three measurements ± SEM.

B,D) Bliss synergy score heat map for the combination treatment of Trametinib and Ripretinib in ST88-14^{sgCNT} (B) and ST88-14^{sgSHOC2} (D) cells. Data represent the mean from n = 3.

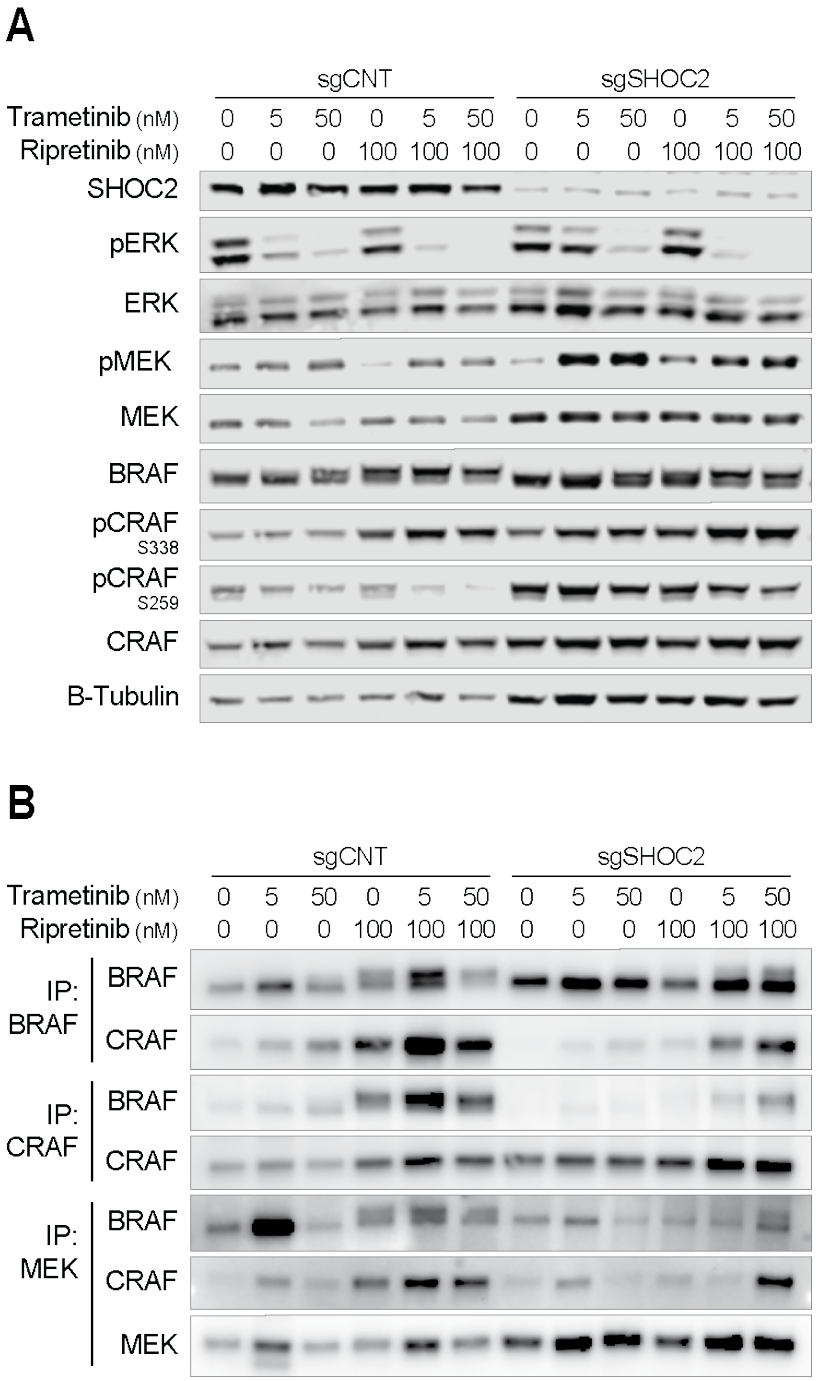

Figure 23. SHOC2 KO leads to a reduction of RAF dimer formation and RAF–MEK interactions

A-B) Western blot analysis of ST88-14^{sgCNT} and ST88-14^{sgSHOC2} cells whole-cell lysate (A) or lysate subjected to immunoprecipitation (B) after 24hr treatment with Trametinib and Ripretinib.

CHAPTER 6 – MEKI TREATMENT SENSITIZES TUMOR CELLS TO RAF DIMER INHIBITORS IN NF1-DEFICIENT MPNST

CHAPTER 6.1 – RAF DIMER INHIBITORS SYNERGIZE WITH MEKI TREATMENT IN MPNST

Considering that Ripretinib synergizes with MEKi due to its ability to target RAF proteins in the presence of MEKi treatment-induced RAF dimerization, we wondered whether other RAF inhibitors (RAFi) were also able to effectively synergize with MEKi treatment in MPNST. Currently, three main types of RAF inhibitors (RAFi) exist: equipotent RAFi that target both monomeric and dimeric RAF, those selective against monomeric RAF, and those selective against dimeric RAF [68]. Combination treatment with Trametinib and either LY3009120, an equipotent pan-RAF inhibitor [83,106], or Naporafenib, a dimer-selective pan-RAF inhibitor [68,107], resulted in a high drug synergism at decreasing cell viability (Figure 24 C-F). Thus, both LY3009120 and Naporafenib showed a high ability to potentiate MEKi treatment (Figure 24 I), like what is observed with Ripretinib and Trametinib treatment (Figure 24 A-B,I). On the other hand, Encorafenib, a monomer-selective pan-RAF inhibitor [68], did not present any synergism when combined with Trametinib treatment (Figure 24 G-I), highlighting the importance of inhibiting RAF dimers in order to synergize with MEKi treatment in MPNST.

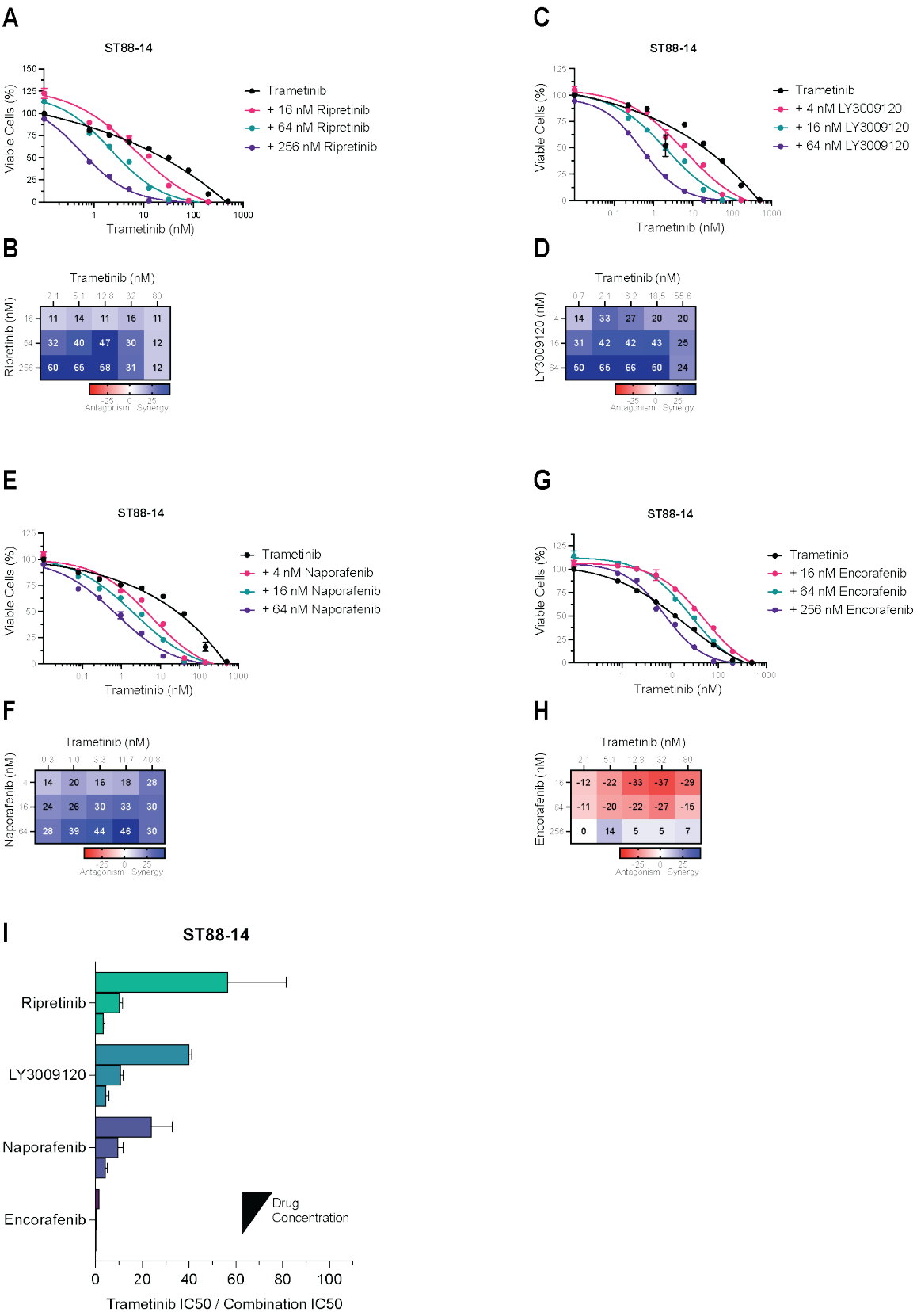
A
ST88-14
Viable Cells (%)
Trametinib (nM)
Trametinib
+ 16 nM Ripretinib
+ 64 nM Ripretinib
+ 256 nM Ripretinib
B
Trametinib (nM)
Ripretinib (nM)
11 14 11 15 11
32 40 47 30 12
60 65 58 31 12
Antagonism
Synergy
C
ST88-14
Viable Cells (%)
Trametinib (nM)
Trametinib
+ 4 nM LY3009120
+ 16 nM LY3009120
+ 64 nM LY3009120
D
Trametinib (nM)
LY3009120 (nM)
14 33 27 20 20
31 42 42 43 25
50 65 66 50 24
Antagonism
Synergy
E
ST88-14
Viable Cells (%)
Trametinib (nM)
Trametinib
+ 4 nM Naporafenib
+ 16 nM Naporafenib
+ 64 nM Naporafenib
F
Trametinib (nM)
Naporafenib (nM)
14 20 16 18 28
24 26 30 33 30
28 39 44 46 30
Antagonism
Synergy
G
ST88-14
Viable Cells (%)
Trametinib (nM)
Trametinib
+ 16 nM Encorafenib
+ 64 nM Encorafenib
+ 256 nM Encorafenib
H
Trametinib (nM)
Encorafenib (nM)
-12 -22 -33 -37 -29
-11 -20 -22 -27 -15
0 14 5 5 7
Antagonism
Synergy
I
ST88-14
Ripretinib
LY3009120
Naporafenib
Encorafenib
Drug Concentration
Trametinib IC50 / Combination IC50

Figure 24. RAF dimer inhibitors synergize with MEKi treatment in MPNST
A,C,E,G) Cell viability of ST88-14 cells treated with increasing doses of Trametinib and Ripretinib (A), LY3009120 (C), Naporafenib (E), or Encorafenib (G) for 5 days. Error bars represent the mean of three measurements ± SEM.
B,D,F,H) Bliss synergy score heat map for the combination treatment of Trametinib and Ripretinib (B), LY3009120 (D), Naporafenib (F), or Encorafenib (H) in ST88-14 cells. Data represent the mean from n = 3.
I) Bar graph plot of the cell viability IC50 (nM) fold change of ST88-14 cells treated for 5 days with Trametinib and Ripretinib (16, 64 or 256 nM), LY3009120 (4, 16 or 64 nM), Naporafenib (4, 16 or 64 nM), or Encorafenib (16, 64 or 256 nM).

CHAPTER 6.2 – DIFFERENT TYPES OF MEKI CAN SYNERGIZE WITH RAFI IN MPNST

Different MEKi have different properties that can affect their effectiveness at inhibiting both MEK and ERK phosphorylations, and even disrupting RAF–MEK complexes [68,73–75]. However, combinations of other MEKi, like Binimetinib and Selumetinib, with dimer-specific RAFi proved to be equally effective and highly synergistic, like the effects seen in combinations with Trametinib (Figure 25 A-H), which highlights the important role of MEK inhibition in mediating the increased cell sensitivity to the RAFi.

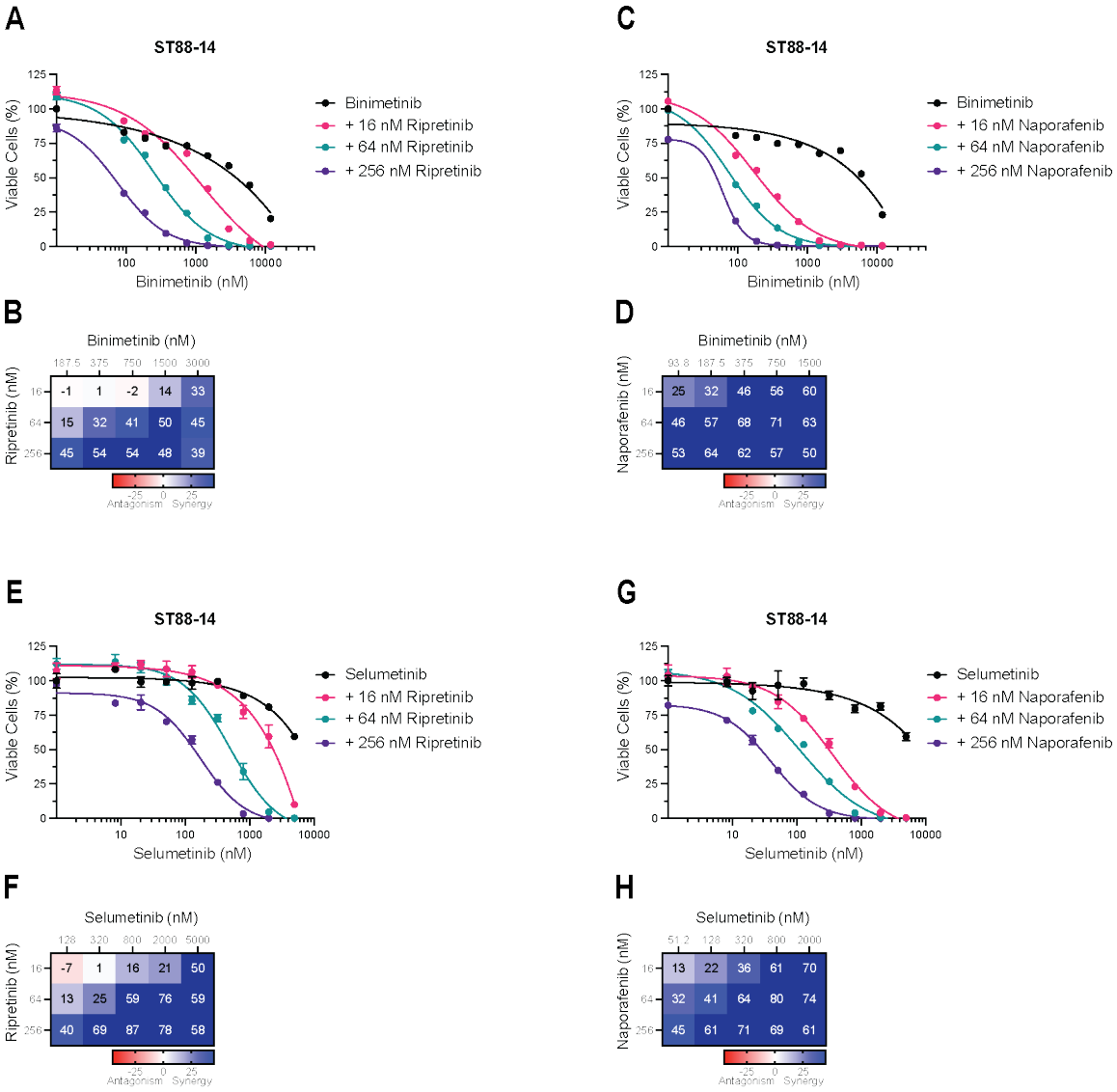

Figure 25. Different types of MEKi can synergize with RAFi in MPNST

A-D) Cell viability and Bliss synergy score heat map for ST88-14 cells treated with increasing doses of Binimetinib and Ripretinib (A-B) or Naporafenib (C-D) for 5 days. Error bars represent the mean of three measurements ± SEM, and Bliss scores represent the mean from n = 3.

E-H) Cell viability and Bliss synergy score heat map for ST88-14 cells treated with increasing doses of Selumetinib and Ripretinib (E-F) or Naporafenib (G-H) for 5 days. Error bars represent the mean of three measurements ± SEM, and Bliss scores represent the mean from n = 3.

CHAPTER 6.3 – RAF DIMER INHIBITORS INDUCE RAF DIMERIZATION AND RAF/MEK INTERACTION IN MPNST

Next, we characterized through immunoblot assays the response of MPNST cells to RAFi-mediated perturbations in the MAPK pathway. Treatments with Ripretinib and Encorafenib had no noticeable effects on pERK levels, while LY3009120 and Naporafenib started to cause minor reductions in pERK levels (Figure 26 A). However, Treatment with LY3009120 and Naporafenib resulted in a similar increase of active BRAF and CRAF levels as seen with Ripretinib treatment (Figure 26 A). This increase was less prominent in the cells treated with Encorafenib. Similar to Ripretinib, LY3009120 and Naporafenib treatment also resulted in an increase in RAF dimer formation and BRAF/CRAF interaction with MEK, whereas Encorafenib had a significantly decreased ability to promote dimer formation (Figure 26 B). Collectively, these data suggest that MEKi treatment of MPNST is an important step needed to potentiate the effects of RAF dimer-targeted inhibitors.

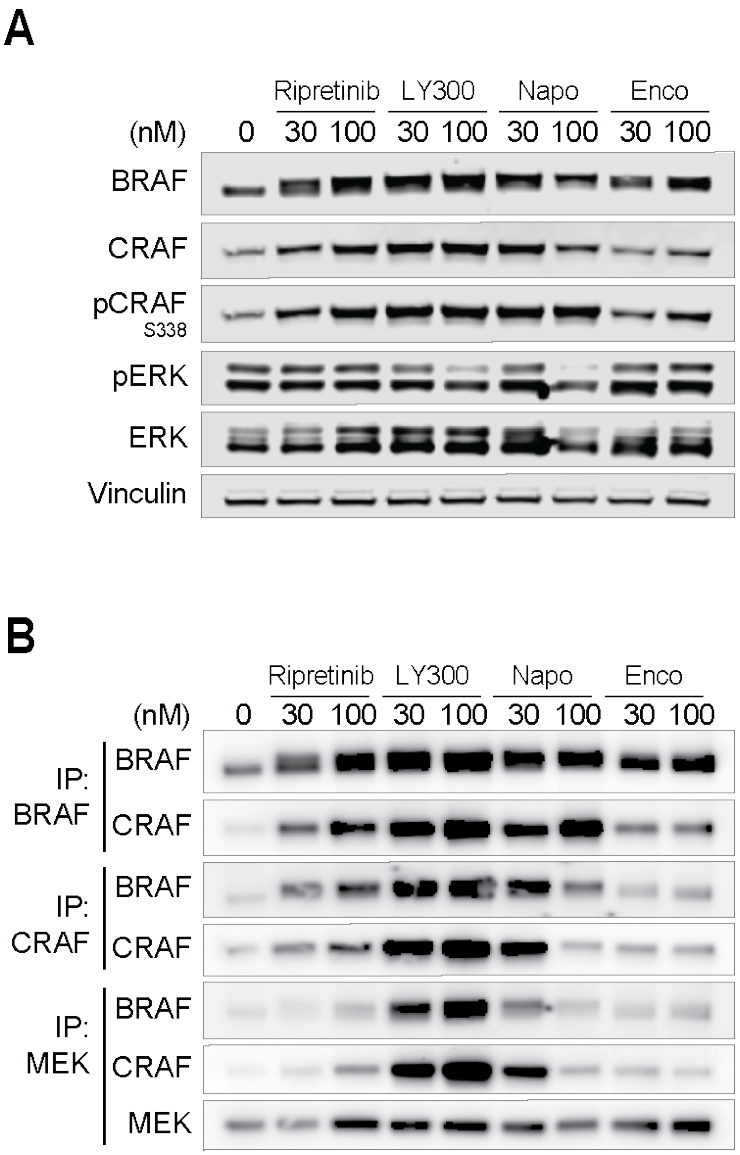

Figure 26. RAF dimer inhibitors induce RAF dimerization and RAF/MEK interaction in MPNST

A-B) Western blot analysis of ST88-14 cells whole-cell lysate (A) or lysate subjected to immunoprecipitation (B) after 24hr treatment with Ripretinib, LY3009120, Naporafenib or Encorafenib.

CHAPTER 7 – COMBINED INHIBITION OF PDGFRB AND RAF DIMERS ENHANCES THE SENSITIVITY OF MPNST TUMORS TO MEKI

CHAPTER 7.1 – ASSESSING THE PHARMACODYNAMICS OF THE MEKI AND RAFI COMBINATION STRATEGY

To study the *in vivo* pharmacodynamics of the combination strategy, we grafted an MPNST PDX into SCID mice and treated them with Ripretinib and Trametinib once the tumor volume reached 100-150 mm^3 (Figure 27 A). Immunoblot analysis of the sample shows that *in vivo* MEKi treatment resulted in an increase in PDGFRβ levels and a slight reduction of pERK levels (Figure 27 B), like what is also seen in the *in vitro* studies (Figure 8 A-I). On the other hand, Ripretinib treatment did not affect PDGFRβ but showed a marked increase in pERK levels possibly through a treatment-induced paradoxical activation of RAF proteins as not enough drug has accumulated in the tumor to fully inhibit their activity, which could lead to an increase cancer cell proliferation like the one observed *in vitro* (Figure 13 C). Finally, while the drug combination strategy did lead to an increase in PDGFRβ levels in some samples, the combination treatment was more effective than either single agent at inhibiting pERK levels (Figure 27 B).

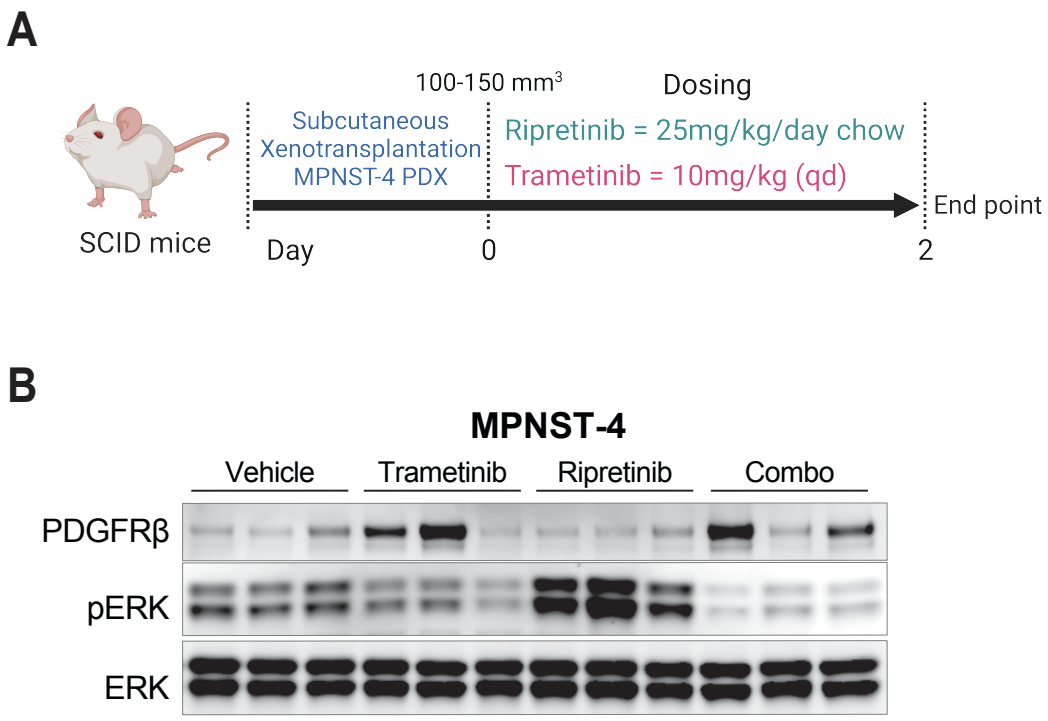

Figure 27. Assessing the pharmacodynamics of the MEKi and RAFi combination strategy

A) Schematic of the MPNST-4 PDX pharmacodynamic study.

B) Western blot analysis of MPNST-4 PDX tumors after treatment for 48hr.

CHAPTER 7.2 – ASSESSING THE EFFICACY OF THE MEKI AND RAFI COMBINATION STRATEGY

To study the *in vivo* efficacy of the drug combination, an MPNST PDX was grafted into SCID mice, and treatment was started once tumors reached the appropriate size (Figure 28 A). While Trametinib treatment by itself was capable of controlling tumor growth, there was no significant difference between the vehicle-treated and the Ripretinib-treated groups. Nevertheless, Ripretinib treatment was able to potentiate the effects of Trametinib as the combination treatment was more effective at controlling the tumor growth than either single agent (Figure 28 B-C). Immunoblot analysis of the samples collected at the endpoint of the study showed that while *in vivo* MEKi treatment did result in a decrease in pERK levels, the treatment also led to an increase in PDGFRβ levels (Figure 28 D), like the one observed in the previous *in vitro* studies (Figure 8 A-I). On the other hand, an increase in PDGFRβ levels was only detected in one sample of the combination group and was not observed in the Ripretinib treatment group. Nevertheless, the combination treatment was more effective than MEKi single treatment at inhibiting pERK levels in the tumors (Figure 28 D).

Considering that the pharmacodynamics study showed that Ripretinib treatment with a 25 mg/kg/day dose led to an increase in pERK levels (Figure 27 B) and that this drug dose was not capable of controlling tumor growth (Figure 28 B-C), we wanted to determine if a higher dose of Ripretinib was more effective as a single

agent and in combination with a MEKi. To study this, we grafted MPNST M3 cells into SCID mice and started treatment with a 100 mg/kg/day dose of Ripretinib and MEKi once the tumor volume reached the appropriate size (Figure 29 A). Both single agents decreased tumor growth compared to the vehicle-treated group, but the combination treatment was more effective than either treatment by itself as demonstrated by the further reduction in tumor growth (Figure 29 B-C). Furthermore, treatments were also well tolerated as there was no significant loss of mice weight following treatment administration (Figure 29 D).

Taken together, the *in vivo* studies show that Ripretinib and MEKi combination is more effective than either drug by themselves at leading to a reduction in MAPK pathway activity and MPNST tumor growth, which supports its use as a therapeutic strategy for the treatment of MPNST patients.

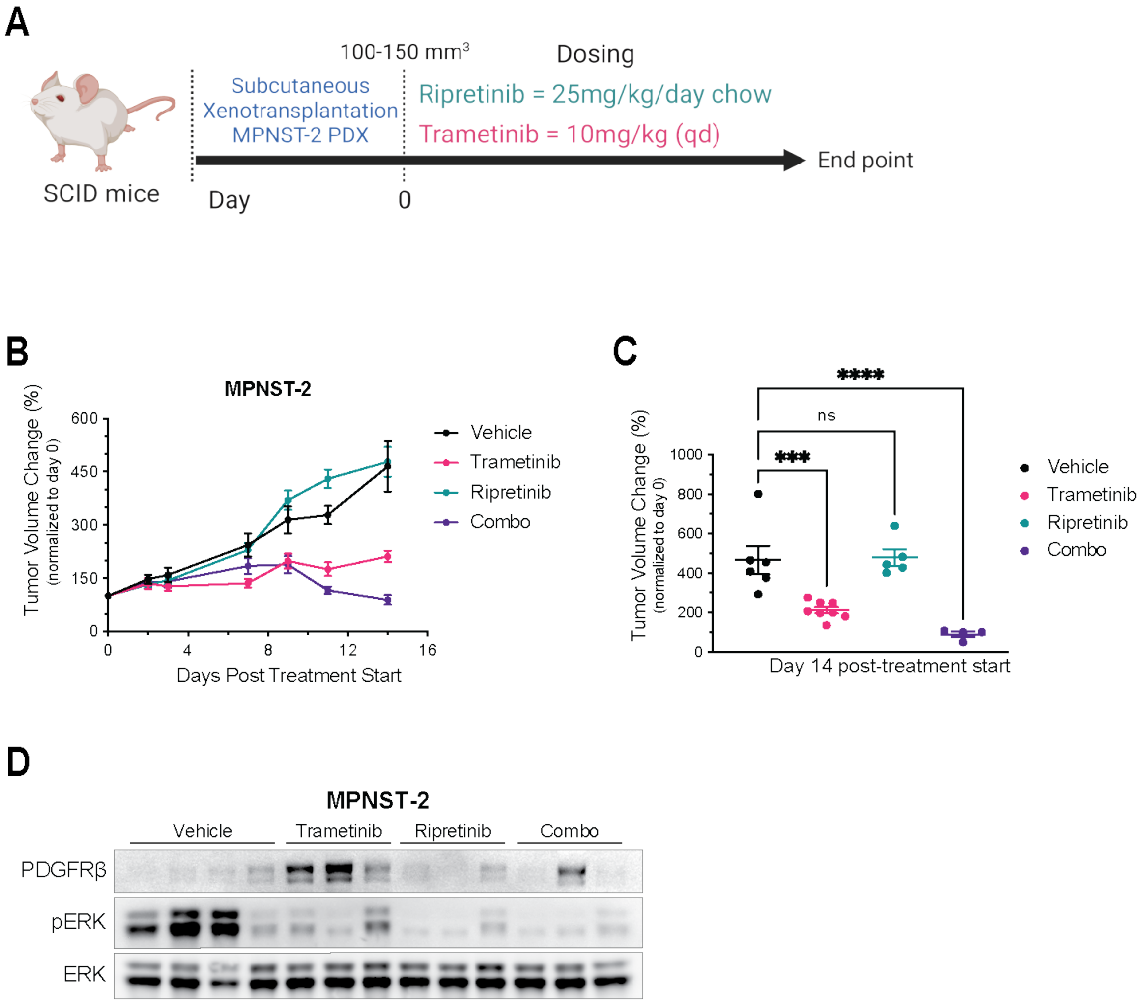

Figure 28. Assessing the efficacy of the MEKi and RAFi combination strategy against an MPNST PDX

A) Schematic of the MPNST-2 PDX efficacy study.

B) MPNST-2 PDX tumor volume curves of vehicle, Trametinib, Ripretinib, or the combination cohorts.

C) MPNST-2 PDX tumor volume distribution at the experiment endpoint.

D) Western blot analysis of MPNST-4 PDX tumors collected and the experiment endpoint.

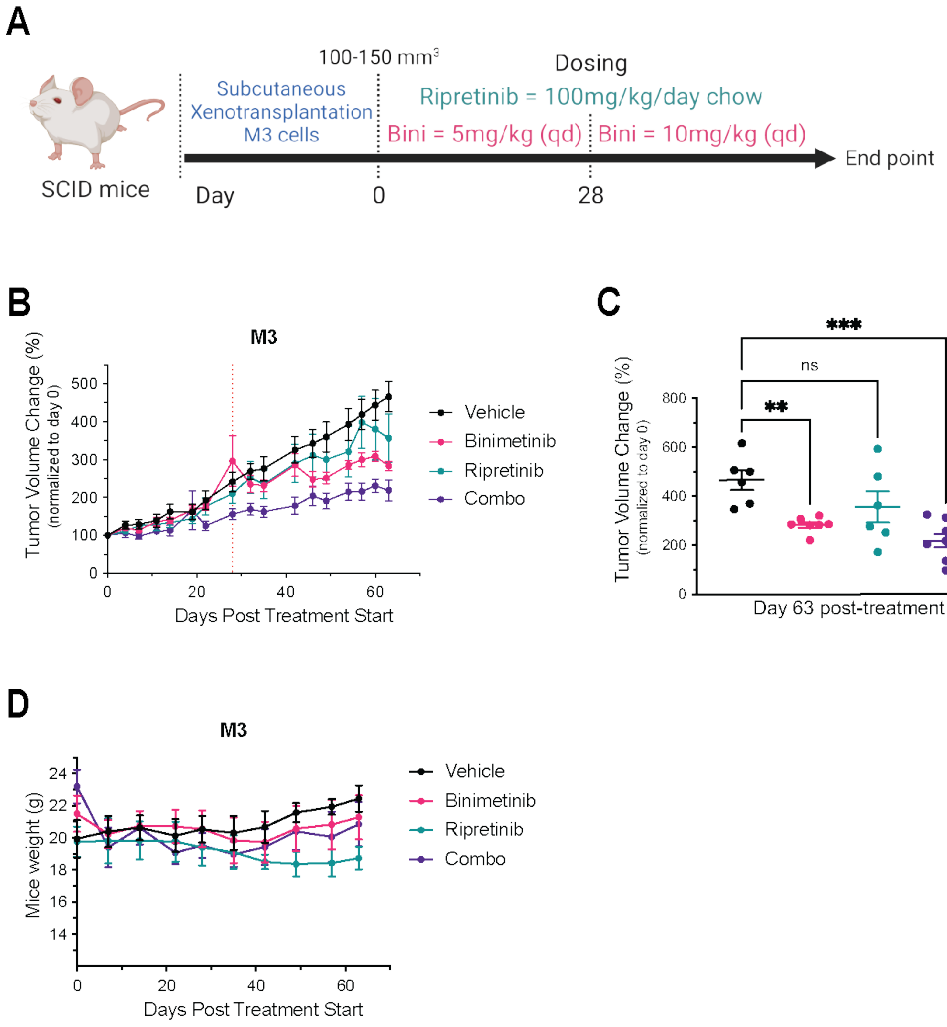

Figure 29. Assessing the efficacy of the MEKi and RAFi combination strategy against a xenograft of MPNST cells

A) Schematic of the M3 cells xenograft efficacy study.

B) M3 xenograft tumor volume curves of vehicle, Binimetinib, Ripretinib, or the combination cohorts.

C) M3 xenograft tumor volume distribution at the experiment endpoint.

D) Body weight measurements of SCID mice treated with vehicle, Binimetinib, Ripretinib, or the combination.

CHAPTER 8 – DISCUSSION

CHAPTER 8.1 – MEKI TREATMENT RESISTANCE BY DIRECT TRANSCRIPTIONAL UPREGULATION OF THE RECEPTOR TYROSINE KINASE PDGFRB

While targeted cancer treatment has brought significant improvements in the field of cancer therapeutics, the ability of tumors to develop resistance to these therapies has been a limiting factor in the treatment of cancer. Studies all over the world have focused on the development of novel therapeutic strategies to overcome this problem. One of the most proposed ways to overcome the development of resistance is the use of combination strategies that take into account the rewiring mechanisms of cancer cells to target them rationally with novel therapeutic strategies. While there has been a lot of progress in some cancer types, no targeted treatments have been effectively developed for MPNST, cancer that is very aggressive and that has a high propensity to metastasize, all while often being resistant to chemotherapy and radiotherapy [1–3]. For this reason, the present study focused on the study and development of novel therapeutic strategies for the treatment of MPNST patients.

MPNST is characterized by the loss-of-function of NF1, a tumor suppressor and negative regulator of the MAPK pathway [47]. Loss of NF1 function can drive the formation of different tumors by leading to sustained ERK activation. Recently, preclinical studies have evaluated the use of single-agent MEKi for the treatment of MPNST [95–97]. However, despite studies showing that MEKi treatment is effective

against the MPNST precursor NF1-associated plexiform neurofibroma [98–100], this therapeutic strategy has failed to be effective and produce a good and sustained inhibition of ERK activity in MPNST as these tumors have been found to develop resistance to single-agent MEK inhibition.

In addition to the loss of NF1 function, MPNSTs also present frequent co-occurring loss-of-function mutations of the Polycomb repressive complex 2 (PRC2), on the EED or SUZ12 subunits [12,14]. Interestingly, this loss of PRC2 function can also indirectly potentiate the effects of NF1 loss-of-function by amplifying Ras-driven transcription [13], which highlights the importance of developing novel therapeutic strategies to improve MEKi efficacy in MPNST and overcome the ability of the tumor to develop resistance.

The activation of RTKs or the development of adaptive resistance after the release of the ERK-mediated feedback regulation of the MAPK pathway, are two mechanisms of resistance previously identified in other cancers that may also be involved in MPNST [76,88,89,101,102]. To better assess the involvement of RTKs in MPNST's ability to develop MEKi resistance, we carried out *in vitro* drug treatments followed by immunoblots or phospho-RTK array assays. The results identify several RTKs that are dysregulated in response to MEKi treatment. These RTKs include PDGFRβ, PDGFRα, c-MET, HER kinases, among others, many of which have also been reported before to increase their activation in response to MEK inhibition in MPNST [90]. However, in this study, we identified that PDGFRβ is the

RTK whose total and active levels most consistently increase in MPNST in response to acute MEKi treatment (Figure 7 and Figure 8), and that this increase occurs as a result of its direct transcriptional upregulation in response to MEKi treatment (Figure 12 A). Moreover, even in the ST88-14 cell line, in which PDGFRβ levels do not change in response to acute treatment, we identified that PDGFRβ is the RTK with higher detectable phosphorylated levels, suggesting that it also plays an important role in RTK signaling in this cell line (Figure 7 E).

Considering that all the initial observations of PDGFRβ increase were in response to acute MEKi treatment, we wondered whether MPNST cells that develop resistance to single-agent MEK inhibitors would similarly increase the levels of PDGFRβ. To assess this, we developed MEKi resistance MPNST cells by culturing them for several months under increasing concentrations of Trametinib. Obtained results demonstrate that PDGFRβ levels were still increased in MEKi-resistant M3, a cell line that also increased PDGFRβ levels after acute exposure to the inhibitor. However, the ST88-14 cells that adapted to the constant exposure to MEKi treatment now showed an increase in PDGFRβ levels (Figure 9).

Therefore, the observed increase in PDGFRβ levels can occur both as a response to acute MEKi exposure or as an adaptation to chronic exposure. Thus, our results identify PDGFRβ as a key RTK involved in MPNST's ability to develop resistance to MEKi treatment and an important target for the development of combinatorial treatments.

Different types of PDGFRβ inhibitors have been developed and subjected to preclinical and clinical studies. These small molecule inhibitors can be divided into type I inhibitors that bind to the active conformation of a kinase in the ATP pocket (e.g., Avapritinib), type II inhibitors that bind to an inactive conformation of the kinase (e.g., AZD-3229), and type III inhibitors that are allosteric ligands that bind to a site different from the active site like (e.g., Ripretinib) [93,94].

In this study, we identified that combination treatments with Trametinib and Ripretinib have a strong synergetic effect and are very effective at decreasing MPNST cell viability, regardless of the different common genetic alterations found in MPNST (Figure 10, Figure 13, and Figure 14). The obtained results for this combination treatment are also very promising because doses of Ripretinib that had little to no effect on MPNST cell viability were capable of greatly potentiating the effects of MEKi treatment. Additionally, the levels of no other RTKs were affected by Ripretinib treatment in MPNST (Figure 11).

Interestingly, not only do the expression levels of PDGFRβ increase in response to MEKi treatment in M3 cells, but the expression levels of the PDGFRβ ligands PDGFA, PDGFB, and PDGFC also increase in response to MEK inhibition (Figure 30). The obtained results also show that single-agent treatment with Ripretinib or Avapritinib had no effect and that these PDGFRβ inhibitors were not able to either promote or completely inhibit the MEKi treatment mediated increase of PDGFA,

PDGFB, and PDGFC expression levels. PDGFB was the PDGFRβ ligand whose expression levels were more significantly upregulated in response to the MEKi treatment, which suggests it may be playing a more important role in mediating the activation of the PDGFRβ signaling compared to the other ligands. Further studies would need to be carried out in order to determine how universal this event is in MPNST and what role it could be playing in the response of MPNST cells to MEKi treatment.

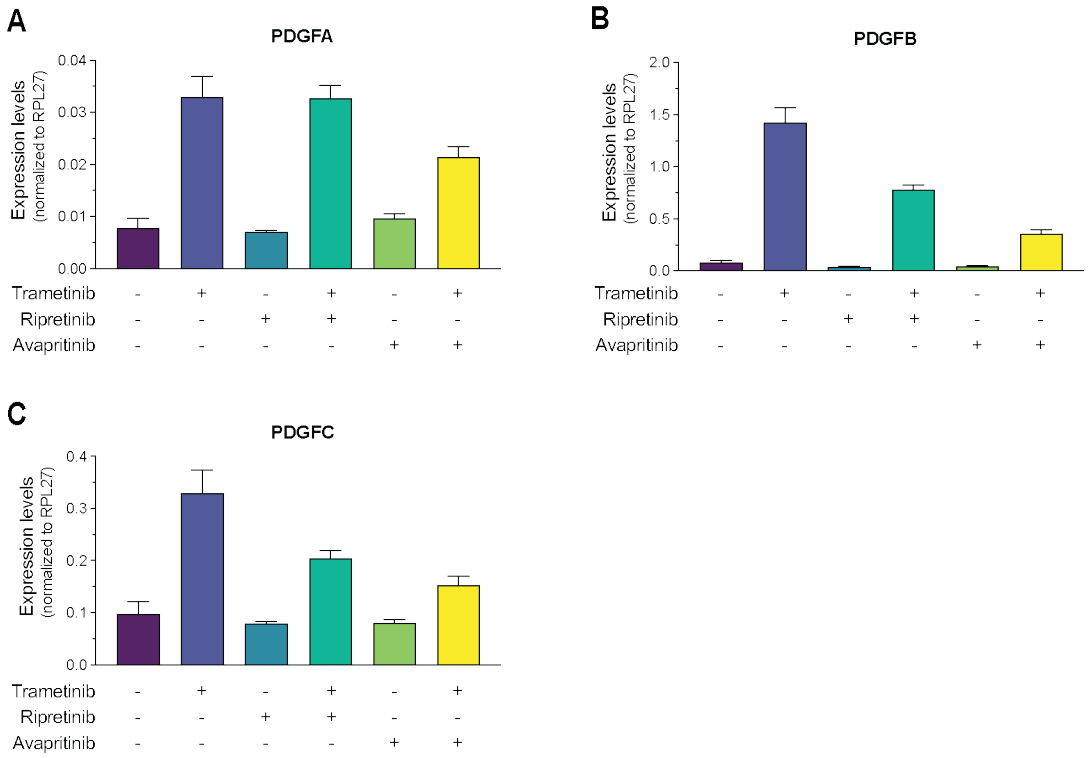

Figure 30. Changes in expression levels of PDGFRβ ligands in response to combination treatments

A-C) RT-qPCR analysis of the changes of PDGFA, PDGFB, or PDGFC expression levels in M3 cells treated with DMSO, 50 nM Trametinib, 100 nM Ripretinib, or 200 nM Avapritinib for 48hr.

Since the loss of PRC2 function has been found to indirectly promote Ras-driven transcription [13], we decided to study whether the absence or presence of PRC2 activity in MPNST might have some role in the sensitivity of the cells to the combination treatment. For this study, we treated PRC2 loss isogenic M3 cells, which had been previously developed in the lab, with the Trametinib and Ripretinib combination. The obtained results show that the combination treatment is effective and synergetic regardless of MPNST PRC2 status (Figure 15). Nevertheless, more detailed studies could help to better identify smaller changes in the sensitivity of MPNST cells to the different drugs tested that could be occurring because of losing PRC2 function.

CHAPTER 8.2 – MEKI RESISTANCE BY MEKI-TREATMENT-INDUCED INCREASE IN RAF DIMER FORMATION AND ACTIVATION OF DOWNSTREAM SIGNALING

On the other hand, while pharmacological combinations of MEKi with Ripretinib were found to be very effective, combinations of MEKi with the PDGFRβ specific inhibitors Avapritinib and AZD3229 proved to have limited effects as these drugs had a reduced ability to potentiate the effects and synergize with MEKi (Figure 10). Additionally, while knocking out PDGFRβ did make the cells more sensitive to MEKi treatment, its absence did not diminish the ability of the MEKi and Ripretinib combination to synergize and be effective at reducing MPNST cell viability (Figure 17). This result suggests that other targets of Ripretinib might also be important for mediating this effect. Interestingly, BRAF and CRAF, important players of the MAPK pathway, have been described as secondary targets for this molecule [94].

Additionally, immunoblot assays performed in the present study show that RAF levels are decreased with Ripretinib and MEKi combination but are not significantly affected by Avapritinib treatment (Figure 18), further supporting the role of BRAF and CRAF as important targets of Ripretinib in MPNST, and potential key players in mediating the high drug synergy observed for the MEKi and Ripretinib combination treatment. Furthermore, our studies identify CRAF as the key RAF kinase involved in the response of MPNST cells to the MEKi and RAFi treatment (Figure 19 and Figure 20).

In this study, we also identified that NF1-deficient MPNST can adapt and overcome MEKi treatment through the stimulation of RAF dimer formation and RAF/MEK complex formation, which in turn can lead to an increase in the downstream MAPK signaling (Figure 21), in a similar manner to what has been previously described in KRAS mutant cancers [74]. Interestingly, doses of the drug combination that cause an increase in RAF dimer formation, RAF interaction with MEK, and active phosphorylated BRAF and CRAF, are the doses that also present high drug synergy in reducing MPNST cell viability, which goes in hand with the completely diminished pERK levels (Figure 21).

To determine the role that RAF dimer formation could have in the synergy observed for the MEKi and Ripretinib mediated RAF inhibition, we developed RAF dimerization deficient cells by knocking out SHOC2. This protein is a key phosphatase involved in the dephosphorylation of an inhibitory site in RAF, an event that promotes the eventual dimerization and activation of RAF kinases [57,58,105]. These cells were then subjected to drug treatment studies as part of cell viability or co-immunoprecipitation and immunoblot experiments. The obtained results demonstrate that the decrease in RAF dimer formation and BRAF/CRAF interaction with MEK, as a result of loss of SHOC2 function, resulted in a significant reduction in the drug synergy observed for the MEKi and RAFi combination treatment (Figure 22 and Figure 23). This observation suggests that RAF

dimerization in response to MEKi treatment is an important event required for RAF-targeting drugs to potentiate MEKi treatment.

Taken together, this study demonstrates that MEKi treatment resistance in MPNST involves two pathways: direct transcriptional upregulation of the receptor tyrosine kinase (RTK) PDGFRβ and MEKi-induced increase in RAF dimer formation and activation of downstream signaling. While these two pathways for the development of MEKi resistance in MPNST may not be completely independent, our studies show that the induction of RAF dimer formation is the main pathway that needs to be inhibited.

CHAPTER 8.3 – THERAPEUTIC STRATEGIES FOR THE TREATMENT OF MPNST

Current clinical RAF inhibitors have different affinities towards RAF monomers and dimers, and can be classified as inhibitors with an increased affinity towards either RAF monomers, RAF dimers, or those that are equipotent against both RAF monomers and dimers [68]. As expected, monomer-specific RAF inhibitors (Encorafenib) were not able to potentiate the effect of MEKi treatment in MPNST as RAF dimer formation overcomes the effect of the inhibitors. On the other hand, pharmacological combinations of the RAF dimer selective (Naporafenib) or the equipotent (LY3009120) inhibitors with MEKi resulted in a robust drug synergy at inhibiting both the MAPK pathway signaling and viability of MPNST cells (Figure 24). However, while very effective at inhibiting RAF dimers, equipotent RAF inhibitors have failed to be successful in the clinic, and they are predicted to cause on-target toxicities at the doses required for a strong antitumor effect [68,83,84]. Because of this, RAF-dimer selective inhibitors like Naporafenib, Regorafenib, Sorafenib, and others [68,107], may prove to be more tolerable and effective as a combination treatment with MEKi.

Another therapeutic strategy that could prove to be very effective for MPNST is the combination of MEKi with a drug capable of targeting the two mechanisms of resistance to MEKi described in our study. As we show here, Ripretinib, a “switch-control” kinase inhibitor with high affinities against both PDGFRβ, and B-RAF and

C-RAF dimers [94], is an example of a molecule that not only fits the targeting requirement, but that presents a very robust ability to synergize and potentiate MEKi treatment in MPNST. The pharmacological combination of the MEKi Trametinib and Ripretinib was not only able to be highly effective and synergetic in naïve MPNST cells, but it was similarly effective against the MEKi resistance cell lines developed in the study (Figure 16).

This combination strategy was also found to be effective and well tolerated in the *in vivo* experiments, with studies showing that Ripretinib and MEKi combination is more effective than either drug by themselves at leading to a reduction in MAPK pathway activity and MPNST tumor growth (Figure 27, Figure 28, and Figure 29). Results also show that low Ripretinib doses (25 mg/kg/day chow) not only had no noticeable effect in reducing tumor growth, but this low dose may even be leading to some increased tumor growth compared to the vehicle-treated group (Figure 28). This event may be provoked by the RAF inhibitor properties of Ripretinib that are leading to a paradoxical activation of the MAPK pathway signaling and an increase in tumor growth when it is exposed to drug doses that are incapable of successfully inhibiting both units of the RAF dimers. Treatment with a high dose of Ripretinib (100 mg/kg/day chow) not only diminished this increase in tumor growth but also resulted in single-agent Ripretinib now being able to decrease tumor growth compared to the vehicle-treated group (Figure 29). Taken together, the obtained results support its use as a therapeutic strategy for the treatment of NF1-deficient MPNST patients.

Additionally, preliminary experiments done in this study demonstrate that the MEKi and Ripretinib combination treatment is also effective and synergetic at decreasing the cell viability of a panel of NF1-mutant melanoma cell lines (Figure 31). The results suggest that the proposed combination strategy might also be highly effective for the treatment of this and other NF1-deficient cancer. These observations go in hand with results from recent studies that show that loss of NF1 makes melanoma and lung cancer more sensitive to inhibitions of the RAS-ERK signaling by the use of SHP2 inhibitors [108]. However, further experiments are needed in order to completely determine the specific role that the absence of NF1 has in mediating the synergy and effectiveness of the proposed therapeutic strategy and to determine if the loss of NF1 is a sufficient marker to identify cancers susceptible to this pharmacological combination.

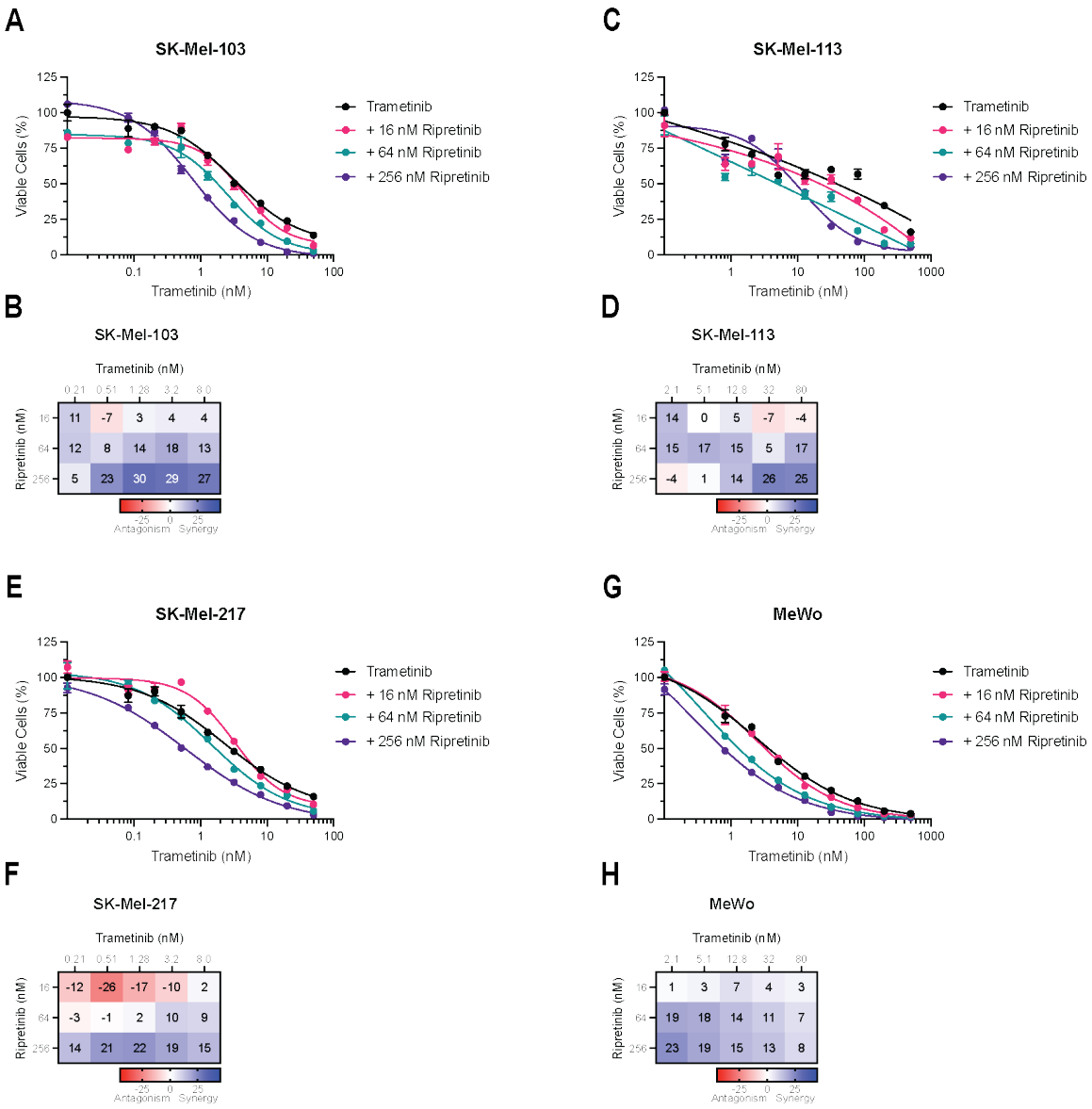

Figure 31. Assessing the efficacy of the MEKi and Ripretinib combination against a panel of NF1-mutant melanoma cell lines

A,C,E,G) Cell viability of SK-Mel-103 (A), SK-Mel-113 (C), SK-Mel-217 (E), and MeWo (G) cells treated with increasing doses of Trametinib and Ripretinib for 5 days. Error bars represent the mean of three measurements ± SEM.

B,D,F,H) Bliss synergy score heat map for the combination treatment of Trametinib and Ripretinib in SK-Mel-103 (B), SK-Mel-113 (D), SK-Mel-217 (F), and MeWo (H) cells. Data represent the mean from n = 3.

In addition to the proposed therapeutic strategy of this study, as mentioned before, PDGFRβ is not the only RTK whose levels change in MPNST following MEKi treatment. This suggests that other RTKs may also have a role in the development of resistance to MEK inhibition. The increased signaling coming from these RTKs would converge on RAS activation. However, no good pan-RAS inhibitors are available at the moment and, for this reason, other studies have looked into the possibility of inhibiting SHP2, a key mediator of RAS signal transduction downstream of RTKs, in combination with MEKi [90]. Results from this study showed that the combined MEKi and SHP2 inhibition with SHP099 was more effective than MEKi alone and that the combination was effective against both naïve and MEKi resistant MPNST. While this is a potential therapeutic strategy capable of overcoming MPNST's ability to develop resistance to MEKi treatment, further studies would also be needed to determine its efficacy in the clinic.

On the other hand, for all the pharmacological combinations tested in the present study, the act of inhibiting MEK was more important than the specific MEKi used, as combinations with either Trametinib, Binimetinib, or Selumetinib were all able to robustly synergize with both Ripretinib and Naporafenib (Figure 25). This is of particular interest as MEKi have different biochemical properties and abilities to inhibit MEK and ERK phosphorylation or disrupt RAF-MEK complexes. Trametinib, in particular, has been found to be a more potent inhibitor and disruptor of these cellular processes than Binimetinib or Selumetinib [68,74,75,109]; still, combinations of either MEKi with RAF dimer inhibitors were all very effective in MPNST.

CHAPTER 8.4 – STUDY IMPLICATIONS AND FUTURE DIRECTIONS

Currently, there is an unmet clinical need for the development of novel effective therapeutic strategies for NF1-deficient MPNST patients. This study demonstrates that NF1-deficient MPNST develops resistance to MEKi treatment by upregulating PDGFRβ transcription and increasing RAF dimer formation. Furthermore, the present findings provide the scientific rationale and support for the clinical evaluation of MEKi and PDGFRβ / RAF-dimer inhibitors for the treatment of MPNST, findings that could impact the development of future clinical trials for this patient population.

Further studies will determine the efficacy of other PDGFRβ / RAF-dimer inhibitors in combination with MEKi for the treatment of MPNST. One combination strategy we are particularly interested in testing for MPNST is the triple combination treatment of MEKi (e.g., Trametinib, Binimetinib, etc.), RAF monomer-specific (e.g., Dabrafenib, Encorafenib, etc.), and RAF dimer-specific (e.g., Regorafenib, Sorafenib, etc.) inhibitors. This therapeutic strategy has already been studied for other cancers and, interestingly, while it has not been found to be necessarily more effective at reducing tumor growth when compared to the dual treatment with MEKi and RAF-dimer-inhibitors, as both have similar effectiveness, the triple drug combination treatment was found to be more tolerable [68]. This observation is very significant as improving the well-being of the patients under cancer treatment should also be a major focus for the scientific community.

On the other hand, results from the present studies highlight the importance of further studying and identifying potential differences in how RAF dimers and RAF-MEK complexes are formed in response to either upstream activation of the MAPK pathway or because of direct induction of the compounds interacting with either RAF or MEK proteins. Something that we will want to address is determining how important is the contribution of upstream signaling in promoting RAF dimer formation compared to the role that the relief of ERK feedback inhibition has in this process in response to MEKi and RAFi treatment. To address this, we could inhibit upstream signaling with SHP2i like SHP099 and determine if the MEKi and RAFi treatments are still able to efficiently induce the formation of the RAF dimers and RAF-MEK complexes. Other questions that would need to be addressed include: Are the complexes formed by upstream activation the same that are formed in response to RAFi or MEKi treatment? Does RAFi or MEKi interact with different pools of RAF dimers and RAF-MEK complexes? How is the cellular localization or size of the complexes affected by the different drug treatments?

Additionally, to elucidate the specific role that the absence of NF1 has in mediating the synergy observed for the proposed combination strategy, we could perform NF1 KO, rescue, and over-expression experiments to determine how this affects the efficacy and synergy of the combination treatment and the cell sensitivity to single-agent treatments. We could also determine how NF1 might be involved in regulating the formation of RAS-RAF-MEK complexes in basal conditions and in

response to drug treatments, which might provide novel insights into NF1 role in regulating the MAPK pathway signaling, in addition to its direct RAS-GAP activity. One limitation that we could encounter in this study is that knocking out NF1 in a cell line does not necessarily create a cell line dependency in the MAPK pathway. To overcome this, we could develop TPA-independent NF1 KO melan-a cells, which are immortalized mouse melanocytic cell line that requires 12-O-tetradecanoylphorbol-13-acetate (TPA) for normal growth [110]. This might prove to be a good model to study how NF1 absence affects the pathway and drug effectiveness since the growth of these cells would be expected to be dependent on the NF1 absence and the subsequent increased activation of the MAPK pathway signaling.

Further studies would also help to determine ways to improve the *in vivo* administration of the combination strategy to obtain a better synergy and improved antitumor efficacy. One potential strategy that has been proposed before is the implementation of sequential administration of drugs that takes into account sequence-dependent effects of the drug treatment in order to improve its efficacy [111].

In the case of the present study, PDGFRβ levels were found to increase in response to MEKi treatment, which led to the testing of a combination strategy that inhibited both MEK and PDGFRβ in MPNST. However, considering that the observed increase in PDGFRβ levels in response to MEKi treatment was not

immediate and depended on the increase of its transcription, it would be interesting to test if a therapeutic strategy that involved an initial single-agent MEKi treatment, followed by treatment with the combination of MEKi and PDGFRβi will lead to an increase in drug synergy and treatment efficacy.

MEKi treatment was also found to increase RAF dimer formation in MPNST, and combinations of MEKi and RAF dimer inhibitors were highly effective and synergetic. Therefore, further studies will determine if an initial induction of RAF dimer formation by single-agent treatment with MEKi will lead to a subsequent increase in both the drug synergy of MEKi and RAFi combination and of the treatment efficacy. Initial single-agent treatment with RAFi might not have the same benefit and could be even detrimental as low concentrations of RAFi may lead to an increase of both RAF dimerization and RAF downstream signaling, leading to an increase in tumor growth until enough RAFi accumulates in the tumor to successfully inhibits the RAF proteins.

Future studies could also study potential mechanisms of resistance that MPNST could use to overcome the different proposed pharmacological combination treatments. To identify these mechanisms, we could develop combination-treatment-resistant cell lines and initially determine if an increase of different specific RTKs is involved. It would also be important to carry out RNA-seq experiments to identify different cellular processes and signaling pathways that are dysregulated following both acute and chronic exposure to combination

treatments. Careful studies of these dysregulated pathways could lead to the identification of potential mechanisms of resistance to the combination strategy and would inform future studies that focus on developing novel more effective therapeutic strategies for MPNST.

Finally, considering that the proposed combination strategy leads to an increase in RAF dimer formation and RAF interaction with MEK, we could determine if MPNST is able to take advantage of this and increase MAPK pathway signaling to a level that can by itself overcome the combination treatment. If this is the mechanism in play, then an increase in drug doses may be enough to overcome the resistance unless the dose needed is not safely achievable and has many associated toxicities. In this case, changing drugs with other more potent and tolerable MEK or RAF inhibitors could be enough to overcome this problem and develop novel therapeutics for MPNST that are highly effective and able to avoid MPNST's ability to develop resistance to drug treatments.

APPENDIXES

APPENDIX I: RESEARCH MANUSCRIPT

Miranda-Román MA et. al. “MEK inhibitors lead to PDGFR pathway upregulation and sensitize tumors to RAF dimer inhibitors in NF1-deficient malignant peripheral nerve sheath tumor (MPNST)”

MEK inhibitors lead to PDGFR pathway upregulation and sensitize tumors to RAF dimer inhibitors in NF1-deficient malignant peripheral nerve sheath tumor (MPNST)

Miguel A. Miranda-Román[1,2], Cindy J. Lee[1], Eve Fishinevich[1], Leili Ran[1], Amish J. Patel[1], Juan Yan[1], Makhzuna N. Khudoynazarova[1], Sarah Warda[1], Mohini R. Pachai[1], Yu Chen[1,2,3,4,5] & Ping Chi[1,2,3,4,5]

[1]Human Oncology and Pathogenesis Program, Memorial Sloan Kettering Cancer Center, New York, NY, USA.
[2]Louis V. Gerstner, Jr., Graduate School of Biomedical Sciences, Memorial Sloan Kettering Cancer Center, New York, NY, USA.
[3]Weill Cornell Graduate School of Medical Sciences, Cornell University, New York, NY, USA.
[4]Department of Medicine, Memorial Sloan Kettering Cancer Center, New York, NY, USA.
[5]Department of Medicine, Weill Cornell Medical College, New York, NY, USA.

Running title: Overcoming MEKi resistance in NF1-deficient MPNST

Keywords: MEK inhibition, RAF dimers, combination treatment, drug resistance, PDGFRβ

Financial support: This work was supported in part by the Office of the Assistant Secretary of Defense for Health Affairs through the Department of Defense Horizon (W81XWH-19-1-0268) to M.M.R.; and by grants from the National Institute of Health (NIH) and National Cancer Institute (NCI) grants (R01 CA228216, DP2 CA174499), Department of Defense (DOD) grants (W81XWH-15-1-0124, W81XWH-22-1-0326), Francis Collins Scholar NTAP, Cycle for Survival and Linn Family Discovery Fund to P.C.; the NIH/NCI grants (5R01CA208100-04, 5U54CA224079-03, 5P50CA092629-20) to Y.C.; Geoffrey Beene Cancer Research Fund to P.C.; and the NIH grant P30 CA 008748 to Memorial Sloan Kettering Cancer Center (Core Grant).

Corresponding authors: Dr. Ping Chi, Memorial Sloan Kettering Cancer Center, 1275 York Avenue, New York, NY 10065. Phone: 646-888-3338; Email: chip@mskcc.org; and Dr. Yu Chen Memorial Sloan Kettering Cancer Center, 1275 York Avenue, New York, NY 10065. Phone: 646-888-3356; Email: cheny1@mskcc.org;

Conflicts of interest: Ping Chi has received personal honoraria/advisory boards/consulting fees from Deciphera, Exelixis, Zai Lab, Novartis, Ningbo NewBay Medical Technology; Ping Chi has received institutional research funding

from Pfizer/Array, Novartis, Deciphera, Ningbo NewBay Medical Technology. Deciphera Pharmaceuticals provided the Ripretinib used for both the *in vitro* and *in vivo* studies of this paper. The remaining authors declare no competing interests.

Abstract

Malignant peripheral nerve sheath tumor (MPNST) is a highly aggressive type of soft tissue sarcoma with high propensity to metastasize and very limited treatment options. Loss of the RAS-GAP NF1 leads to sustained RAF/MEK/ERK signaling in MPNST. However, single-agent MEK inhibitors (MEKi) have failed to elicit a good and sustained inhibition of the pathway in MPNST. Here, we report that MEKi treatment resistance in MPNST involves two pathways: direct transcriptional upregulation of the receptor tyrosine kinase (RTK) PDGFRβ, and MEKi-induced increase in RAF dimer formation and activation of downstream signaling. While the pharmacological combination of MEKi with a PDGFRβ specific inhibitors was more effective than treatment with MEKi alone, the combination of MEKi and RAF-dimer inhibitors led to a robust inhibition of the MAPK pathway signaling. This combination treatment was effective in vitro and in vivo as demonstrated by the significant increase in drug synergism and its high effectiveness at decreasing MPNST viability. Our findings support the use of this combination strategy to overcome MEKi resistance, and as a novel targeted therapeutic strategy for NF1-deficient MPNST patients, which in turn could impact future clinical trials for this patient population.

Significance

This study demonstrates that NF1-deficient MPNST develops resistance to MEKi treatment by upregulating PDGFRβ transcription and increasing RAF dimer formation, and a combination of MEKi and RAF-dimer inhibitors can overcome this resistance.

Introduction

Malignant peripheral nerve sheath tumors (MPNST) originate in the cellular component of the peripheral nerves and account for 5-10% of all soft tissue sarcomas (1). It is a highly aggressive disease with a high propensity to metastasize and poor sensitivity to systemic chemotherapy and radiotherapy. Complete surgical resection with wide margins remains the best treatment option for MPNST patients, which makes the disease outcome particularly detrimental in cases with unresectable or metastatic disease (1–4). Therefore, the discovery of novel targeted therapeutic strategies for MPNST is an urgent clinical need.

MPNST arises through three distinct clinical settings. Around 45% of MPNSTs arise in the setting of Neurofibromatosis type I (NF1-associated), another 45% arise sporadically, and 10% are associated with previous radiotherapy treatment. Interestingly, regardless of the clinical setting through which it arises, most MPNSTs share a frequent biallelic genetic inactivation of three major tumor suppressor pathways including the NF1, CDKN2A, and PRC2 (EED or SUZ12) (5–7). NF1 functions as a RAS-GAP, and its absence can lead to uncontrolled activation of RAS and subsequent sustained activation of the RAF/MEK/ERK signaling (8,9), which identifies this signaling pathway as an important target for MPNST treatment.

Recently, preclinical studies have evaluated the use of single-agent MEK inhibitors (MEKi) as a treatment for MPNST (10–12). While this strategy has been effective for plexiform neurofibromas (13–15), an MPNST precursor, it has failed to show a good and sustained inhibition of ERK activity in MPNST. As with other cancers, activation of the receptor tyrosine kinases (RTKs) or the development of adaptive resistance after the release of ERK feedback inhibition of the MAPK pathway signaling could play a major role in the development of this resistance (16–20). Additionally, MEKi has also been found able to reactivate C-RAF and induce RAF/MEK complex formation, which in turn could also lead to the development of resistance (21).

Here we identified that MEKi treatment resistance in MPNST involves two pathways, PDGFRβ upregulation through direct transcriptional upregulation, and MEKi treatment induced RAF dimer formation which leads to an increased MAPK pathway signaling. These resistance mechanisms can be overcome by the pharmacological combination of MEK inhibition and RAF-dimer inhibitors. Our findings support the use of this combination strategy to overcome MEKi resistance, and as a novel targeted therapeutic strategy for MPNST patients.

Materials and Methods

Cell lines, cultures, and reagents

The ST88-14 (RRID:CVCL_8916) and the M724 (MPNST724, RRID:CVCL_AU20) human MPNST cell lines were obtained as gifts provided by Jonathan A. Fletcher (Brigham and Women's Hospital, Harvard Medical School). The SNF96.2 (CRL-2884, RRID:CVCL_K281) human MPNST cell line and the HEK-293T (CRL-3216, RRID:CVCL_0063) cell line were purchased from ATCC. The M1, M3, M4, M5 and M6 Human NF1 associated MPNST cell lines were gifts developed by William L. Gerald and Xiaoliang L. Xu at the Memorial Sloan Kettering Cancer Center. The ST88-14 and M724 cell lines were grown in RPMI supplemented with 10% FBS, the SNF96.2 cell line was grown in DME HG supplemented with 10% FBS and 1mM Sodium Pyruvate at 1.5 g/L-Sodium Bicarbonate, and the M1, M3, M4, M5,

M6, and HEK-293T cell lines were grown in DMEM HG supplemented with 10% FBS. All these culture media were also supplemented with penicillin (100 U/ml), streptomycin (100 µg/ml), and L-glutamine (2 mM), and cells were cultured in 5% CO2 incubator at 37°C. All cell lines were tested negative for mycoplasma by the ABM Mycoplasma PCR Detection Kit (catalog # G238). Other relevant reagents used in this study are listed in Supplementary Table 1.

Cell viability assay

MPNST cells (1–3 x 10^3 cells/well) were seeded in clear bottom 96-well white or black plates, allowed to attach overnight, and treated the next day with serial dilutions of a single drug, a combination of drugs, or vehicle (1% DMSO). Cell viability was assayed five days post-treatment using the ATP CellTiter-Glo 2.0 cell viability assays (Promega) or Resazurin/Alamar Blue (R&D Systems) according to the manufacturer's protocol. IC_{50} values were calculated by nonlinear regression analysis using the GraphPad Prism 9.0 software. All the data were normalized to vehicle treatment. The BLISS synergy scores were calculated using the Combenefit platform as previously described (22).

Drugs and chemicals

See Supplementary Table 1 for information on all the drugs, chemicals, and reagents used in this study.

Generation of drug-resistant cell lines

MEKi-resistant cell lines resistant were generated by exposing the NF1-associated MPNST cell lines M3 and ST88-14 to increasing concentrations of trametinib for at least months of continuous drug exposure. The cell culture medium was changed twice per week, and fresh drug was added each time.

Protein extraction and western blotting

After the indicated treatment time, cells were lysed using RIPA buffer (Thermo Fisher) supplemented with phosphatase and protease inhibitors (Thermo Fisher Scientific or Millipore Sigma), followed by boiling for 5 min at 95°C, sonicating 5-10 min, and protein quantification by BCA protein assay kit (Thermo Fisher). Protein samples were prepared by mixing with NuPAGE LDS sample buffer (Thermo Fisher) and 1 M DTT (Thermo Fisher), followed by boiling for 10 min at 70°C. Proteins samples were then separated by SDS-PAGE on 4-12% Bis-Tris Gel (Thermo Fisher) with MOPS/SDS running buffer (Teknova), and followed by protein transfer to nitrocellulose membranes (BioRad) by wet electroblotting. Membranes were blocked for 1 hr at room temperature with StartingBlock TBS buffer (Thermo Fisher) or Intercept (TBS) Blocking buffer (LI-COR), and incubated with primary antibodies of interest overnight at 4°C under soft rotations. Then membranes were washed thrice with 1x TBS-T, and incubated with HRP-conjugated secondary antibody (for ECL detection) or fluorescent dye-labeled secondary antibody (for fluorescence detection with LI-COR) for 1 hr at room temperature. Then membranes were washed thrice with 1x TBS-T. Membranes for

ECL detection were visualized with chemiluminescence using HRP substrates (Millipore, or Thermo Fisher), and chemiluminescence scanning with ImageQuant LAS4000 (GE Healthcare). Membranes for fluorescence detection were imaged with the Odyssey Infrared Imaging System (LI-COR Biosciences). The list of antibodies used can be found in Supplementary Table 4.

Phospho-RTK array assay

MPNST cells were seeded in 15-cm dishes, allowed cell attachment overnight, treated the next day with the desired drug concentrations, harvested at the experiment endpoint, and lysed using the lysis buffer provided by the Human Phospho-RTK Array Kit (R&D). For tumor samples, the tumor tissue collected at the experiment endpoint was homogenized and then lysed using the same lysis buffer and kit. Cell lysates were centrifuged for 5min at 14,000 x g, and the supernatant was then processed following the kit manufacturer's instructions, and ECL western blotting was performed as described above. Band intensity quantifications were done using the Image Studio Lite Software.

Immunoprecipitation assay

After the indicated treatment time, cells in 10-cm or 15-cm plates were washed once with cold PBS, then harvested by scraping in PBS, pelleted at 600 x g for 5min, and then lysed using a 1% Triton lysis buffer (Cell Signaling) supplemented with phosphatase and protease inhibitors (Thermo Fisher Scientific or Millipore Sigma). Samples were sonicated for 5min, the protein was isolated by centrifuging for 10min at 14,000 x g, and quantified. 1µg of the antibodies of interest was added, and samples were incubated overnight under gentle rocking. Next, Protein A/G Magnetic Beads (Thermo Fisher) were added to the samples, and immunoprecipitates were purified using a magnetic separation rack, washed three times with 1% Triton lysis buffer, and then pelleted for 5min at 1,000rpm in 4°C. The sample was resuspended in 3X SDS sample buffer (Cell Signaling), boiled for 5min, centrifuged for 1min at 14,000 x g, and then the protein supernatant was collected for subsequent studies using the western blotting procedures described above. See Supplementary Table 4 for the list of antibodies used.

Active RAS pull-down assay

MPNST cells were seeded in 10-cm dishes, allowed cell attachment overnight, and treated the next day with the desired drug concentrations. The cells were then collected 2hr, 24hr, or 48hr after treatment and GTP-bound RAS was quantified using an active RAS detection kit (Cell Signaling Technology, #8821) according to the manufacturer's instructions.

RNA isolation and qRT-PCR

Total RNA was isolated from cells using the E.Z.N.A total RNA Kit (Omega), and homogenizer columns (Omega). The RNA quality and quantity were determined using the NanoDrop 8000 Spectrophotometer (Thermo Scientific). RNA was then reverse transcribed using the High-Capacity cDNA Reverse Transcription kit

(Thermo Fisher). qPCR was performed following the manufacturer instructions of the PowerUp SYBR Green Master Mix (Thermo Fisher), with a ViiA 7 Real-Time PCR system (Applied Biosystems). The specificity of the amplified DNA was confirmed by performing melting curves after each qPCR, and PCR contaminations that could affect the results were determined by also running a no template control in the RT-qPCR reactions. The housekeeping gene RPL27 was used as the reference gene for normalization, and the ΔΔCT method was used to calculate the relative fold change gene expression. Each RT-qPCR was performed in at least triplicates. Primers were designed using the online NCBI Primer-BLAST tool, and then purchased from Eurofins Genomics. The sequences of all the primers used for qPCR are listed in Supplementary Table 3.

Gene knockout by CRISPR/Cas9

The LentiCRISPR-v2, LentiGuide-Puro and LentiCas9-Blast vectors were purchased from Addgene. The sgRNA oligos (as listed in Supplementary Table 2) were annealed, digested using BsmBI (New England BioLabs), and cloned into the vectors. The plasmid was co-transfected into HEK-293T cells with the packaging plasmids psPAX2 (Addgene)and pVSVg (Addgene), and the resulting lentivirus was collected. MPNST cells were then transduced with respective plasmids with the sgRNA of interest and then were selected with 2 - 5 μg/ml Puromycin dihydrochloride (Thermo Fisher) or Blasticidin S HCl (Thermo Fisher) until all negative control cells were dead. All the relevant reagents are listed in Supplementary Table 1.

***In vivo* mouse studies**

For MPNST M3 cells and PDXs xenograft studies, 2 x 10^6 and 3 x 10^6 cells, respectively, were resuspended in 100mL of 1:1 mix of DMEM media and Matrigel (Corning, #356237), and subcutaneously injected into both flanks of 6- to 8-week-old CB17 SCID mice (Taconic). When tumors reached 100-150 mm^3 on average, the mice were assigned to different treatment groups to ensure similar distribution of tumor sizes and mouse weights. Tumors size was measured twice a week with a caliper, and tumor volume was calculated with the formula Vol=(4/3)π x (length/2) x (width/2) x (depth/2). Binimetinib and Trametinib were administered by oral gavage, and Ripretinib was administered in a mouse diet formulated to achieve approximate levels of 25 or 100 mg/kg/day in mouse efficacy studies (23). Control treatments involve a control chow provided by Deciphera Pharmaceuticals, and the drug vehicle for oral gavage (1% carboxymethyl cellulose + 0.5% Tween 80 in ddH_2O). The body weight of the mice was monitored during the whole experiment. Mice were euthanized once the experiment endpoint was reached, or humane endpoints were required. All data was plotted and analyzed with the GraphPad Prism 7-9 software.

Quantification and Statistical analysis

All statistical analyses and plots were generated using GraphPad Prism 7–9 software. All data are presented as the mean ± SEM (unless otherwise noted).

Statistical comparisons between two groups were performed using a two-tailed unpaired t-test, and for more than two groups were performed using one-way ANOVA. Significant differences between groups are defined by ns $P>0.05$; * $P<0.05$; ** $P<0.005$; *** $P<0.0005$; **** $P<0.0001$.

Data availability

The authors confirm that the data supporting the findings of this study are available within the paper. Any additional information required to reanalyze the reported data is available from the corresponding authors upon request.

Results

MEK inhibition leads to an increase of PDGFRβ and reactivation of MAPK signaling in NF1-deficient MPNST

To determine the potential contribution of upstream signaling in the ability of MPNST to develop resistance to MEK inhibition, we evaluated the levels of active RAS upon treatment with a MEK inhibitor (MEKi). Interestingly, although MEKi treatment led to the inhibition of the ERK signaling, there was an increase in the RAS-GTP and pMEK levels in a dose and time-dependent manner, suggesting that MEKi treatment over time leads to an increase in the MAPK pathway activity in MPNST cells (FIG. 1 A). Previous studies have shown that loss of ERK-mediated negative regulation of RAS and different MAPK pathway proteins as well as upregulation of RTK activity, are two adaptive mechanisms that could lead MPNST cells to present this behavior (16–20). We decided to first focus on assessing the role of the latter, as RTK upregulation has been characterized as a mechanism of drug resistance in many different cancers.

A phospho-RTK array performed after MEKi treatment of MPNST M3 cells revealed that the PDGFRβ and MET receptors are activated following MEKi treatment (FIG. 1 B). The activity of both PDGFRβ and MET receptors has been previously shown to increase following MEKi treatment in MPNST (24). However, only phospho-PDGFRβ levels, but not those of MET, were also increased in a second MPNST cell line as well as in an MPNST cell xenograft upon MEKi treatment (SUPP FIG. 1 A-B). Hence, we decided to further study the role of PDGFRβ in the response of MPNST cells to MEKi treatment.

To further evaluate the role of PDGFRβ in MPNST, total levels of this protein were assessed in a panel of cell lines. Results indicate that PDGFRβ levels increased in the M3 cells following MEKi treatment (FIG. 1 C). This increase in PDGFRβ levels was observed in the majority of MPNST cells tested (FIG. 1 D, SUPP FIG. 1 C-H). Performing the same phospho-RTK array with the MPNST ST88-14 cell line, one of the cell lines where PDGFRβ total levels didn't change in response to MEKi treatment (FIG. 1 F), showed that the levels of activated PDGFRβ also didn’t

change after MEK inhibition (FIG. 1 E), but PDGFRβ was the RTK with the highest detected levels. This points to PDGFRβ having an important role in RTK signaling in this cell line.

While acute exposure to MEKi treatment resulted in an increase of PDGFRβ in the majority of MPNST cell lines, we wondered whether chronic exposure to the MEKi would have similar effects. To assess this, we developed MEKi-resistant M3 cells (FIG. 1 G-H) and ST88-14 cells (FIG. 1 J-K), by culturing the cells under increasing concentrations of the MEKi Trametinib. Similar to the effects of acute MEKi treatment (FIG. 1 C), PDGFRβ levels were increased in MEKi-resistant M3 cells (FIG. 1 I). On the other hand, MEKi-resistant ST88-14 cells also showed increased PDGFRβ levels as they adapted to the constant exposure to MEKi treatment, and this increase was reversible as a 72-hours washout of the drug resulted in PDGFRβ returning to basal levels (FIG. 1 L). Taken together, these results point to increasing PDGFRβ levels as a mechanism through which MPNST cells respond and develop resistance to MEKi treatment and highlights the importance of developing a drug combination strategy that takes this into account.

Ripretinib synergizes with MEKi at inhibiting MAPK signaling and cell viability partially through targeting PDGFRβ

Considering that MPNST cells respond to acute or chronic MEKi treatment by increasing PDGFRβ levels, we decided to test the efficacy of combining the MEKi Trametinib with the type I inhibitor Avapritinib, the type II inhibitor AZD-3229, and the novel PDGFRα/β and KIT inhibitor Ripretinib (23). *In vitro* cell viability assays carried out after treating ST88-14 cells with the different drug combinations showed that the RTK inhibitors by themselves had little to no effect at the selected doses (FIG. 2 A,C, SUPP FIG. 2 A). When combined with the MEKi, Ripretinib was able to potentiate the effect of the drug as the concentration of Trametinib needed to reach IC_{50} was significantly reduced as demonstrated by the left shifting of the curves in the cell viability plots, suggesting that the combination has a high efficacy at decreasing MPNST cell viability (FIG. 2 A), and Bliss synergy analysis demonstrated that this combination has a strong synergetic effect (FIG. 2 B). Similar results were obtained with the M3 cells, which also showed a high drug synergy for the Trametinib and Ripretinib combination treatment (FIG. 2 E-F).

On the other hand, the MEKi and Avapritinib or AZD3229 combination treatment resulted in a greatly reduced synergy in the ST88-14 cells (FIG. 2 C-D, SUPP FIG. 2 A-B), and was completely lost in the M3 cells (SUPP FIG. 2 C-F). To assess the specificity of Ripretinib at inhibiting PDGFRβ in MPNST, we carried out a phospho-RTK array, which demonstrated that PDGFRβ was the only RTK to be inhibited by Ripretinib in MPNST (SUPP FIG. 2 G,I). Furthermore, Ripretinib was also able to inhibit the MEKi treatment mediated increase in phospho-PDGFRβ levels in M3 cells (SUPP FIG. 2 G-H). For this reason, we decided to focus on the Ripretinib

and MEKi combination and test its effectiveness against a panel of MPNST cell lines with different genetic characteristics commonly found in MPNST (SUPP FIG. 3 A) (25). The obtained results demonstrated that this combination treatment has similar high efficacy and synergy across all tested MPNST cell lines (FIG. 2 G, SUPP FIG. 3 D-I). This suggests that the combination of Trametinib and Ripretinib could be highly effective for the treatment of MPNST.

To determine if the drug combination was also synergistic at inhibiting the MAPK pathway activity, protein analyses were performed after treating ST88-14 and M3 cells with Trametinib and Ripretinib (FIG. 2 H-I). Ripretinib treatment by itself had little to no effect on inhibiting pERK levels, but combining this with Trametinib resulted in a stronger pERK inhibition compared to either single agent alone, further supporting the previously observed drug synergy (FIG. 2 G). Furthermore, the combination was also able to inhibit some of the Trametinib-treatment mediated increase of pMEK levels, in both cell lines tested (FIG. 2 H-I). The MAPK pathway transcriptional output was also effectively inhibited by the combination strategy as demonstrated by the reduction in DUSP6, SPRY2, and SPRED2 expression levels (FIG. 2 K-M). Interestingly, the gene expression analysis also shows that the increase in PDGFRβ protein levels seen in M3 cells after MEKi treatment occurs as a result of an increase in its transcription levels (FIG. 2 J).

Interestingly, while PDGFRβ knockout did make the cells more sensitive to MEKi treatment, as shown by the significant reduction in the trametinib IC_{50} (SUPP FIG. 4 A-C), the absence of PDGFRβ did not affect the ability of the drug combination to synergize and be effective at reducing MPNST cell viability (SUPP FIG. 4 E-H), suggesting that other targets of the drug might be also important for mediating this effect.

To identify important differences that could be leading Ripretinib but not Avapritinib to synergize more potently with MEKi, we carried out an immunoblot assay after the combination treatments, which showed that while both PDGFRβ inhibitors have very similar effects on PDGFRβ, RAS-GTP and pERK levels, there are key differences in the total and active BRAF and CRAF levels. Results showed that RAF levels are decreased with Ripretinib and MEKi combination but are not significantly affected by Avapritinib treatment (FIG. 2 N). Interestingly, published literature on Ripretinib identifies BRAF and CRAF as secondary targets for this molecule (23). Taken together, the results highlight that while PDGFRβ is an important player in the MPNST response to MEKi treatment, other proteins may be also playing a key role in mediating MPNST resistance to MEK inhibition.

MEKi treatment-induced RAF dimerization mediates synergism with RAF inhibitors in MPNST

Based on the importance of the MAPK pathway in MPNST, and the role of BRAF and CRAF as key mediators of this signaling pathway, we decided to test the role of these kinases and their ability to dimerize on the capacity of MPNST cells to respond to MEKi treatment. Knocking out BRAF or CRAF resulted in the cells being more sensitive to MEKi treatment, with the greater reduction of Trametinib IC_{50} seen after the CRAF KO (FIG. 3 A-B), which suggests that in MPNST CRAF could be a more important player than BRAF in the response to MEKi treatment.

Next, we examined the effects of the drug combination on the BRAF and CRAF proteins and the dimer formation. MEKi treatment resulted not only in a reduction of phospho-ERK levels and an increase in phospho-MEK levels, but it also resulted in an activation of the upstream RAF proteins as demonstrated by the upwards shifting of the BRAF band, the increase of active S338 phospho-CRAF, and the decrease of the inhibitory CRAF phosphorylations in S289, S296, and S301 (FIG. 3 C). Ripretinib treatment had minimal effects on phospho-ERK and phospho-MEK levels but did cause some minor increases in active BRAF and CRAF levels. This increase was further induced by the Trametinib and Ripretinib combination treatment, all while the drug combination was still effective at inhibiting downstream MAPK pathway activity as shown by diminished levels of phospho-ERK (FIG. 3 C). We then performed co-immunoprecipitation assays to assess how RAF dimer formation was affected by the combination treatment. While MEKi treatments by themselves promoted the increase of BRAF and CRAF interaction and even BRAF/CRAF interaction with MEK, the combination treatment resulted in a further induction of the RAF dimerization and their interaction with MEK (FIG. 3 D). Interestingly, this combination treatment mediated an increase in RAF dimerization and interaction with MEK occurs at drug concentrations that synergize at decreasing both MPNST cell viability and phospho-ERK levels (FIG. 3 C, 2 A-B).

Studies have shown that SHOC2-mediated de-phosphorylation of a conserved phosphorylation site in RAF proteins provides a key input that facilitates RAF dimerization (26–28). Thus, to further study how the MEKi treatment mediated RAF dimerization plays a role in the effectiveness of the combination treatment, we knocked out SHOC2 to develop RAF dimerization deficient MPNST cells (FIG. 3 I). As expected, SHOC2 KO cells were more sensitive to MEKi treatment, as shown by the reduction in Trametinib IC_{50} compared to the sgCNT cells (FIG. 3 E,G), as the cells are not able to effectively respond to MEK inhibition when they lack the ability to increase MAPK pathway activity through RAF dimer formation (29).

Knocking out SHOC2 in MPNST also resulted in a meaningful reduction of the synergism for the Trametinib and Ripretinib combination, and even some drug concentrations now had an antagonistic effect as highlighted by the decrease in the Bliss synergy score (FIG. 3 E-H). This decrease in drug synergy coincides with the decrease in both RAF dimer formation and BRAF/CRAF interaction with MEK following the SHOC2 KO (FIG. 3 J). Interestingly, regardless of the KO, the

combination treatment still resulted in the increase of active BRAF and CRAF levels and RAF dimerization, albeit to a lesser extent in SHOC2 KO cells (FIG. 3 I-J). At these same drug concentrations, Trametinib and Ripretinib still synergized at inhibiting MAPK pathway downstream activity, as shown by the decrease of pERK levels (FIG. 3 I). Taken together, decreased RAF dimer formation and BRAF/CRAF interaction with MEK did not affect the ability of the combination treatment to decrease pERK levels, but it did result in a significant reduction in the ability of the combination treatment to synergistically inhibit MPNST cell viability, suggesting that RAF dimerization in response to MEKi treatment is an important event required for RAF targeting drugs to be able to potentiate MEKi treatment.

MEKi treatment sensitizes tumor cells to RAF dimer inhibitors in NF1-deficient MPNST

Considering that Ripretinib synergizes with MEKi due to its ability to target RAF proteins in the presence of MEKi treatment induced RAF dimerization, we wondered whether other RAF inhibitors (RAFi) were also able to effectively synergize with MEKi treatment in MPNST. Currently, three main types of RAF inhibitors (RAFi) exist: equipotent RAFi that target both monomeric and dimeric RAF, those selective against monomeric RAF, and those selective against dimeric RAF (30). Combination treatment with Trametinib and either LY3009120, an equipotent pan-RAF inhibitor (31,32), or Naporafenib, a dimer-selective pan-RAF inhibitor (30,33), resulted in a high drug synergism at decreasing cell viability (FIG. 4 C-F). Thus, both LY3009120 and Naporafenib showed a high ability to potentiate MEKi treatment (FIG. 4 I), like what is observed with Ripretinib and Trametinib treatment (FIG. 4 A-B, I). On the other hand, Encorafenib, a monomer-selective pan-RAF inhibitor (30), did not present any synergism when combined with Trametinib treatment (FIG. 4 G-H, I), highlighting the importance of inhibiting RAF dimers in order to synergize with MEKi treatment in MPNST.

In addition, combinations of other MEKi, like Binimetinib and Selumetinib, with dimer specific RAFi proved to be equally effective and highly synergistic, like the effects seen in combinations with Trametinib (SUPP FIG. 5), which highlights the important role of MEK inhibition in mediating the increased cell sensitivity to the RAFi.

Next, we characterized through immunoblot assays the response of MPNST cells to RAFi-mediated perturbations in the MAPK pathway. Treatments with Ripretinib and Encorafenib had no noticeable effects on pERK levels, while LY3009120 and Naporafenib started to cause minor reductions in pERK levels (FIG. 4 J). However, Treatment with LY3009120 and Naporafenib resulted in a similar increase of active BRAF and CRAF levels as seen with Ripretinib treatment (FIG. 4 J). This increase was less prominent in the cells treated with Encorafenib. Similar to Ripretinib, LY3009120 and Naporafenib treatment also resulted in an increase in RAF dimer

formation and BRAF/CRAF interaction with MEK, whereas Encorafenib had a significantly decreased ability to promote dimer formation (FIG. 4 K). Collectively, these data suggest that MEKi treatment of MPNST is an important step needed to potentiate the effects of RAF dimer-targeted inhibitors.

Combined inhibition of PDGFRβ and RAF dimers-enhances the sensitivity of MPNST tumors to MEKi

To study the *in vivo* pharmacodynamics of the combination strategy, we grafted an MPNST PDX into SCID mice and treated them with Ripretinib and Trametinib once the tumor volume reached 100-150 mm^3 (FIG. 5 A). Immunoblot analysis of the sample shows that *in vivo* MEKi treatment resulted in an increase in PDGFRβ levels and a slight reduction of pERK levels (FIG. 5 B), like what is also seen in the *in vitro* studies (FIG. 1 C-D). On the other hand, Ripretinib treatment did not affect PDGFRβ but showed a marked increase in pERK levels possibly through a treatment-induced paradoxical activation of RAF proteins as not enough drug has accumulated in the tumor to fully inhibit their activity, which could lead to an increase cancer cell proliferation like the one observed *in vitro* (SUPP FIG. 3 C). Finally, while the drug combination strategy did lead to an increase in PDGFRβ levels in some samples, the combination treatment was more effective than either single agent at inhibiting pERK levels (FIG. 5 B).

To study the *in vivo* efficacy of the drug combination, an MPNST PDX was grafted into SCID mice, and treatment was started once tumors reached the appropriate size (FIG. 5 C). While Trametinib treatment by itself was capable of controlling tumor growth, there was no significant difference between the vehicle-treated and the Ripretinib-treated groups. Nevertheless, Ripretinib treatment was able to potentiate the effects of Trametinib as the combination treatment was more effective at controlling the tumor growth than either single agent (FIG. 5 D-E). Immunoblot analysis of the samples collected at the endpoint of the study showed that while *in vivo* MEKi treatment did result in a decrease in pERK levels, the treatment also led to an increase in PDGFRβ levels (FIG. 5 F), like the one observed in the previous *in vitro* studies (FIG. 1 C-D). On the other hand, an increase in PDGFRβ levels was only detected in one sample of the combination group and was not observed in the Ripretinib treatment group. Nevertheless, the combination treatment was more effective than MEKi single treatment at inhibiting pERK levels in the tumors (FIG. 5 F).

Considering that the pharmacodynamics study showed that Ripretinib treatment with a 25 mg/kg/day dose led to an increase in pERK levels (FIG. 5 B) and that this drug dose was not capable of controlling tumor growth (FIG. 5 D-E), we wanted to determine if a higher dose of Ripretinib was more effective as a single agent and in combination with a MEKi. To study this, we grafted MPNST M3 cells into SCID mice and started treatment with a 100 mg/kg/day dose of Ripretinib and

MEKi once the tumor volume reached the appropriate size (FIG. 5 G). Both single agents decreased tumor growth compared to the vehicle-treated group, but the combination treatment was more effective than either treatment by itself as demonstrated by the further reduction in tumor growth (FIG. 5 H-I). Furthermore, treatments were also well tolerated as there was no significant loss of mice weight following treatment administration (FIG. 5 J).

Taken together, the *in vivo* studies show that Ripretinib and MEKi combination is more effective than either drug by themselves at leading to a reduction in MAPK pathway activity and MPNST tumor growth, which supports its use as a therapeutic strategy for the treatment of MPNST patients.

Discussion

Despite clinical studies showing that MEKi treatment is effective against the MPNST precursor NF1-associated plexiform neurofibroma (13–15), MPNST develop resistance to single-agent MEKi treatment. In addition to the loss of NF1 function, which can lead to a sustained activation of the RAS/ERK signaling, and the frequent somatic mutations in CDKN2A, MPNST also present frequent co-occurring loss-of-function mutations of the Polycomb repressive complex 2 (PRC2), on the EED or SUZ12 subunits (5,7). Interestingly, this loss of PRC2 function can also indirectly potentiate the effects of NF1 loss-of-function by amplifying Ras-driven transcription (6), which highlights the importance of developing novel therapeutic strategies to improve MEKi efficacy in MPNST and overcome the ability of the tumor to develop resistance.

We and others have revealed that MPNST in response to MEKi treatment upregulate different RTKs (24). In our present study we identify that the direct transcriptional upregulation of PDGFRβ in response to MEKi treatment serves as a mechanism of resistance in the majority of MPNST cell lines tested. This increase in PDGFRβ levels can occur both as a response to acute MEKi exposure or as an adaptation to chronic exposure. However, pharmacological combinations of MEKi with the PDGFRβ specific inhibitors Avapritinib and AZD3229 proved to have limited effects as these drugs had a reduced ability to potentiate the effects and synergize with MEKi.

In this study, we also identified that MPNST cells can adapt and overcome MEKi treatment through the stimulation of RAF dimer formation, which then leads to an increase in the downstream MAPK signaling. While these two pathways for the development of MEKi resistance in MPNST may not be completely independent, results from our studies show that the induction of RAF dimer formation is the main pathway that needs to be inhibited.

Current clinical RAF inhibitors have different affinities towards RAF monomers and dimers, and can be classified as inhibitors with increased affinity towards either RAF monomers, RAF dimers, or those that are equipotent against both RAF monomers and dimers (30). As expected, monomer-specific RAF inhibitors (Encorafenib) were not able to potentiate the effect of MEKi treatment in MPNST as RAF dimer formation overcomes the effect of the inhibitors. On the other hand, pharmacological combinations of the RAF dimer selective (Naporafenib) or the equipotent (LY3009120) inhibitors with MEKi resulted in a robust drug synergy at inhibiting both the MAPK pathway signaling and viability of MPNST cells. However, while very effective at inhibiting RAF dimers, equipotent RAF inhibitors have failed to be successful in the clinic and they are predicted to cause on-target toxicities at the doses required for strong antitumor effect (30,32,34). Because of this, RAF-dimer selective inhibitors like Naporafenib, Regorafenib, Sorafenib, and others (30,33), may prove to be more tolerable and effective as a combination treatment with MEKi.

Another therapeutic strategy that could prove to be very effective for MPNST is the combination of MEKi with a drug capable of targeting the two mechanisms of resistance to MEKi described in our study. As we show here, Ripretinib, a “switch-control” kinase inhibitor with high affinities against both PDGFRβ, and B-RAF and C-RAF dimers (23), is an example of a molecule that not only fits the targeting requirement, but that presented a be very robust ability to synergize and potentiate MEKi treatment in MPNST. This combination strategy was also found to be effective and well tolerated in the *in vivo* experiments.

For all these pharmacological combinations tested, the act of inhibiting MEK was more important than the specific MEKi used, as combinations with either Trametinib, Binimetinib, or Selumetinib were all able to robustly synergize with both Ripretinib and Naporafenib. This is of particular interest as MEKi have different biochemical properties and abilities to inhibit MEK and ERK phosphorylation or disrupt RAF-MEK complexes. Trametinib in particular has been found to be a more potent inhibitor and disruptor of these cellular processes than Binimetinib or Selumetinib (21,30,35,36), still combinations of either MEKi with RAF dimer inhibitors were all very effective in MPNST.

Currently there is an unmet clinical need for the development of novel effective therapeutics strategies for NF1-deficient MPNST patients. Our present findings provide the scientific rationale and support for the clinical evaluation of MEKi and PDGFRβ / RAF-dimer inhibitors for the treatment of MPNST, findings that could impact the development of future clinical trials for this patient population.

Ethics Statement: All animal experiments were performed following the protocols approved by the MSKCC Institutional Animal Care and Use Committee (IACUC),

and were in compliance with relevant ethical regulations regarding animal research.

Author's Contributions

Conceptualization: M.A. Miranda-Román, Y. Chen, P. Chi
Data curation: M.A. Miranda-Román
Formal Analysis: M.A. Miranda-Román
Funding Acquisition: M.A. Miranda-Román, Y. Chen, P. Chi
Investigation: M.A. Miranda-Román, C.J. Lee, E. Fishinevich, L. Ran, M.N. Khudoynazarova, S. Warda, M.R. Pachai
Methodology: M.A. Miranda-Román, C.J. Lee, L. Ran
Project Administration: M.A. Miranda-Román, Y. Chen, P. Chi
Resources: Y. Chen, P. Chi
Software: M.A. Miranda-Román, Y. Chen, P. Chi
Supervision: M.A. Miranda-Román, Y. Chen, P. Chi
Validation: M.A. Miranda-Román, C.J. Lee, E. Fishinevich, M.N. Khudoynazarova
Visualization: M.A. Miranda-Román, Y. Chen, P. Chi
Writing – original draft: M.A. Miranda-Román, P. Chi
Writing – reviewing and editing: all authors

Acknowledgments

We want to thank all members of the Ping Chi and Yu Chen laboratories at MSKCC for their support. We thank Drs. William L. Gerald and Xiaoliang L. Xu (MSKCC) for providing the patient derived M1, M3, M4, M5, and M6 MPNST cell lines. We thank Dr. Jonathan A. Fletcher for the patient-derived ST88-14 and M724 cell lines, and Daniel Flynn and Bryan Smith (Deciphera Pharmaceuticals) for providing Ripretinib and advice on its usage. This work was supported in part by the Office of the Assistant Secretary of Defense for Health Affairs through the Department of Defense Horizon (W81XWH-19-1-0268) to M.M.R.; and by grants from the National Institute of Health (NIH) and National Cancer Institute (NCI) grants (R01 CA228216, DP2 CA174499), Department of Defense (DOD) grants (W81XWH-15-1-0124, W81XWH-22-1-0326), Francis Collins Scholar NTAP, Cycle for Survival and Linn Family Discovery Fund to P.C.; the NIH/NCI grants (5R01CA208100-04, 5U54CA224079-03, 5P50CA092629-20) to Y.C.; Geoffrey Beene Cancer Research Fund to P.C.; and the NIH grant P30 CA 008748 to Memorial Sloan Kettering Cancer Center (Core Grant).

References

1. Stucky C-CH, Johnson KN, Gray RJ, Pockaj BA, Ocal IT, Rose PS, et al. Malignant peripheral nerve sheath tumors (MPNST): the Mayo Clinic experience. Ann Surg Oncol. 2012;19:878–85.
2. Meany H, Widemann BC, Ratner N. Malignant Peripheral Nerve Sheath Tumors: Prognostic and Diagnostic Markers and Therapeutic Targets. In: Upadhyaya M, Cooper DN, editors. Neurofibromatosis Type 1: Molecular and Cellular Biology. Berlin, Heidelberg: Springer Berlin Heidelberg; 2012. page 445–67.
3. LaFemina J, Qin L-X, Moraco NH, Antonescu CR, Fields RC, Crago AM, et al. Oncologic outcomes of sporadic, neurofibromatosis-associated, and radiation-induced malignant peripheral nerve sheath tumors. Ann Surg Oncol. 2013;20:66–72.
4. Brennan MF, Antonescu CR, Maki RG. Management of soft tissue sarcoma [Internet]. New York: Springer; 2013 [cited 2017 Jan 10]. Available from: http://public.eblib.com/choice/publicfullrecord.aspx?p=1030375
5. Lee W, Teckie S, Wiesner T, Ran L, Prieto Granada CN, Lin M, et al. PRC2 is recurrently inactivated through EED or SUZ12 loss in malignant peripheral nerve sheath tumors. Nat Genet. 2014;46:1227–32.
6. De Raedt T, Beert E, Pasmant E, Luscan A, Brems H, Ortonne N, et al. PRC2 loss amplifies Ras-driven transcription and confers sensitivity to BRD4-based therapies. Nature [Internet]. 2014 [cited 2017 Mar 6]; Available from: http://www.nature.com/doifinder/10.1038/nature13561
7. Zhang M, Wang Y, Jones S, Sausen M, McMahon K, Sharma R, et al. Somatic mutations of SUZ12 in malignant peripheral nerve sheath tumors. Nature Genetics. 2014;46:1170–2.
8. Malone CF, Fromm JA, Maertens O, DeRaedt T, Ingraham R, Cichowski K. Defining Key Signaling Nodes and Therapeutic Biomarkers in *NF1* -Mutant Cancers. Cancer Discovery. 2014;4:1062–73.
9. Bollag G, Clapp DW, Shih S, Adler F, Zhang YY, Thompson P, et al. Loss of NF1 results in activation of the Ras signaling pathway and leads to aberrant growth in haematopoietic cells. Nat Genet. 1996;12:144–8.
10. Jessen WJ, Miller SJ, Jousma E, Wu J, Rizvi TA, Brundage ME, et al. MEK inhibition exhibits efficacy in human and mouse neurofibromatosis tumors. Journal of Clinical Investigation. 2013;123:340–7.
11. Jousma E, Rizvi TA, Wu J, Janhofer D, Dombi E, Dunn RS, et al. Preclinical assessments of the MEK inhibitor PD-0325901 in a mouse model of neurofibromatosis type 1: MEK Inhibition in Neurofibroma. Pediatr Blood Cancer. 2015;62:1709–16.
12. Dodd RD, Mito JK, Eward WC, Chitalia R, Sachdeva M, Ma Y, et al. NF1 Deletion Generates Multiple Subtypes of Soft-Tissue Sarcoma That Respond to MEK Inhibition. Molecular Cancer Therapeutics. 2013;12:1906–17.
13. Gross AM, Glassberg B, Wolters PL, Dombi E, Baldwin A, Fisher MJ, et al. Selumetinib in children with neurofibromatosis type 1 and asymptomatic inoperable plexiform neurofibroma at risk for developing tumor-related morbidity. Neuro-Oncology. 2022;noac109.

14. Dombi E, Baldwin A, Marcus LJ, Fisher MJ, Weiss B, Kim A, et al. Activity of Selumetinib in Neurofibromatosis Type 1–Related Plexiform Neurofibromas. N Engl J Med. 2016;375:2550–60.
15. Gross AM, Wolters P, Baldwin A, Dombi E, Fisher MJ, Weiss BD, et al. SPRINT: Phase II study of the MEK 1/2 inhibitor selumetinib (AZD6244, ARRY-142886) in children with neurofibromatosis type 1 (NF1) and inoperable plexiform neurofibromas (PN). JCO. 2018;36:10503–10503.
16. Johnson GL, Stuhlmiller TJ, Angus SP, Zawistowski JS, Graves LM. Molecular Pathways: Adaptive Kinome Reprogramming in Response to Targeted Inhibition of the BRAF–MEK–ERK Pathway in Cancer. Clin Cancer Res. 2014;20:2516–22.
17. Lito P, Pratilas CA, Joseph EW, Tadi M, Halilovic E, Zubrowski M, et al. Relief of Profound Feedback Inhibition of Mitogenic Signaling by RAF Inhibitors Attenuates Their Activity in BRAFV600E Melanomas. Cancer Cell. 2012;22:668–82.
18. Montero-Conde C, Ruiz-Llorente S, Dominguez JM, Knauf JA, Viale A, Sherman EJ, et al. Relief of Feedback Inhibition of *HER3* Transcription by RAF and MEK Inhibitors Attenuates Their Antitumor Effects in *BRAF* -Mutant Thyroid Carcinomas. Cancer Discovery. 2013;3:520–33.
19. Dougherty MK, Müller J, Ritt DA, Zhou M, Zhou XZ, Copeland TD, et al. Regulation of Raf-1 by Direct Feedback Phosphorylation. Molecular Cell. 2005;17:215–24.
20. Nazarian R, Shi H, Wang Q, Kong X, Koya RC, Lee H, et al. Melanomas acquire resistance to B-RAF(V600E) inhibition by RTK or N-RAS upregulation. Nature. 2010;468:973–7.
21. Lito P, Saborowski A, Yue J, Solomon M, Joseph E, Gadal S, et al. Disruption of CRAF-Mediated MEK Activation Is Required for Effective MEK Inhibition in KRAS Mutant Tumors. Cancer Cell. 2014;25:697–710.
22. Di Veroli GY, Fornari C, Wang D, Mollard S, Bramhall JL, Richards FM, et al. Combenefit: an interactive platform for the analysis and visualization of drug combinations. Bioinformatics. 2016;32:2866–8.
23. Smith BD, Kaufman MD, Lu W-P, Gupta A, Leary CB, Wise SC, et al. Ripretinib (DCC-2618) Is a Switch Control Kinase Inhibitor of a Broad Spectrum of Oncogenic and Drug-Resistant KIT and PDGFRA Variants. Cancer Cell. 2019;35:738-751.e9.
24. Wang J, Pollard K, Allen AN, Tomar T, Pijnenburg D, Yao Z, et al. Combined Inhibition of SHP2 and MEK Is Effective in Models of NF1-Deficient Malignant Peripheral Nerve Sheath Tumors. Cancer Res. 2020;80:5367–79.
25. Patel AJ, Warda S, Maag JLV, Misra R, Miranda-Roman MA, Pachai MR, et al. PRC2 Inactivating Mutations in Cancer Enhance Cytotoxic Response to DNMT1 Targeted Therapy via Enhanced Viral Mimicry. Cancer Discovery. 2022;cd.21.1671.
26. Dhillon AS, Meikle S, Yazici Z, Eulitz M, Kolch W. Regulation of Raf-1 activation and signalling by dephosphorylation. The EMBO Journal. 2002;21:64–71.
27. Lavoie H, Therrien M. Regulation of RAF protein kinases in ERK signalling. Nat Rev Mol Cell Biol. 2015;16:281–98.

28. Rodriguez-Viciana P, Oses-Prieto J, Burlingame A, Fried M, McCormick F. A Phosphatase Holoenzyme Comprised of Shoc2/Sur8 and the Catalytic Subunit of PP1 Functions as an M-Ras Effector to Modulate Raf Activity. Molecular Cell. 2006;22:217–30.
29. Jones GG, del Río IB, Sari S, Sekerim A, Young LC, Hartig N, et al. SHOC2 phosphatase-dependent RAF dimerization mediates resistance to MEK inhibition in RAS-mutant cancers. Nat Commun. Nature Publishing Group; 2019;10:2532.
30. Adamopoulos C, Ahmed TA, Tucker MR, Ung PMU, Xiao M, Karoulia Z, et al. Exploiting Allosteric Properties of RAF and MEK Inhibitors to Target Therapy-Resistant Tumors Driven by Oncogenic BRAF Signaling. Cancer Discovery. 2021;11:1716–35.
31. Henry JR, Kaufman MD, Peng S-B, Ahn YM, Caldwell TM, Vogeti L, et al. Discovery of 1-(3,3-Dimethylbutyl)-3-(2-fluoro-4-methyl-5-(7-methyl-2-(methylamino)pyrido[2,3-*d*]pyrimidin-6-yl)phenyl)urea (LY3009120) as a Pan-RAF Inhibitor with Minimal Paradoxical Activation and Activity against *BRAF* or *RAS* Mutant Tumor Cells. J Med Chem. 2015;58:4165–79.
32. Peng S-B, Henry JR, Kaufman MD, Lu W-P, Smith BD, Vogeti S, et al. Inhibition of RAF Isoforms and Active Dimers by LY3009120 Leads to Anti-tumor Activities in RAS or BRAF Mutant Cancers. Cancer Cell. 2015;28:384–98.
33. Ramurthy S, Taft BR, Aversa RJ, Barsanti PA, Burger MT, Lou Y, et al. Design and Discovery of *N* -(3-(2-(2-Hydroxyethoxy)-6-morpholinopyridin-4-yl)-4-methylphenyl)-2-(trifluoromethyl)isonicotinamide, a Selective, Efficacious, and Well-Tolerated RAF Inhibitor Targeting RAS Mutant Cancers: The Path to the Clinic. J Med Chem. 2020;63:2013–27.
34. Nakamura A, Arita T, Tsuchiya S, Donelan J, Chouitar J, Carideo E, et al. Antitumor Activity of the Selective Pan-RAF Inhibitor TAK-632 in BRAF Inhibitor-Resistant Melanoma. Cancer Research. 2013;73:7043–55.
35. Hatzivassiliou G, Haling JR, Chen H, Song K, Price S, Heald R, et al. Mechanism of MEK inhibition determines efficacy in mutant KRAS- versus BRAF-driven cancers. Nature. 2013;501:232–6.
36. Ishii N, Harada N, Joseph EW, Ohara K, Miura T, Sakamoto H, et al. Enhanced Inhibition of ERK Signaling by a Novel Allosteric MEK Inhibitor, CH5126766, That Suppresses Feedback Reactivation of RAF Activity. Cancer Research. 2013;73:4050–60.

Figures and Figure Legends

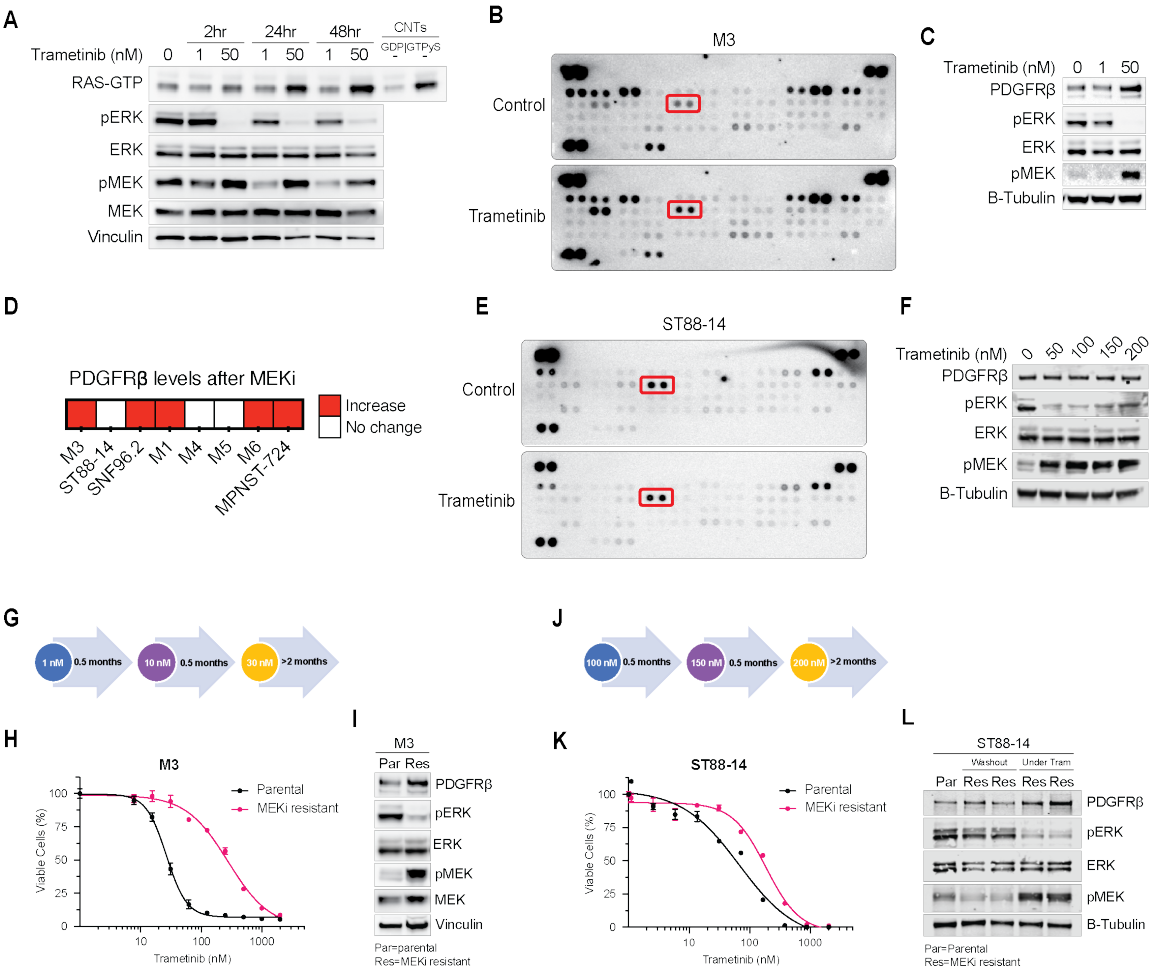

Figure 1. MEK inhibition leads to an increase of PDGFRβ and reactivation of MAPK signaling in NF1-deficient MPNST

A) Western blot analysis of M3 cells were treated with 1 nM or 50 nM Trametinib for 2hr, 24hr, or 48hr.

B,E) Phospho-RTK arrays of M3 (B) and ST88-14 (E) cells treated with DMSO or 50 nM Trametinib for 48hr. PDGFRβ is identified by red squares.

C,F) Western blot analysis of M3 (C) and ST88-14 (F) cells treated with increasing concentrations of Trametinib for 48hr.

D) Summary heatmap highlighting the MPNST cell lines in which PDGFRβ protein levels increase as a response to 48hr *in vitro* Trametinib treatment.

G,J) Schematic of the strategy followed for developing Trametinib resistant M3 (G) and ST88-14 (J) cells.

H,K) Cell viability of parental and Trametinib resistant M3 (H) and ST88-14 (K) cells treated with increasing doses of Trametinib for 5 days. Error bars represent the mean of three measurements ± SEM.
I) Western blot analysis of M3 parental and Trametinib resistant cells.
L) Western blot analysis of ST88-14 parental and Trametinib resistant cells after a 72hr drug washout or under constant MEKi treatment.

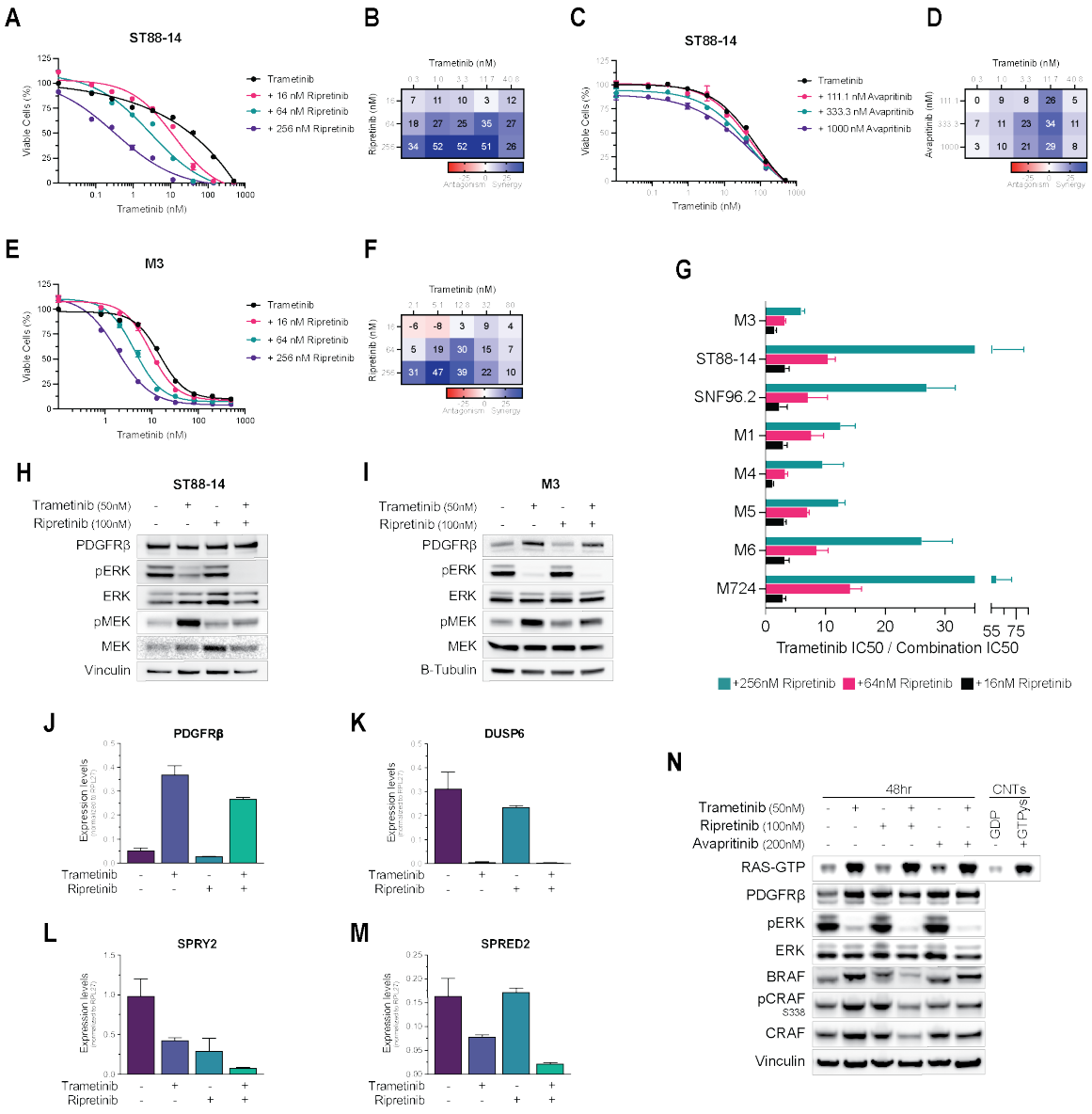

Figure 2. Ripretinib synergizes with MEKi at inhibiting MAPK signaling and MPNST cell viability partially through targeting PDGFRβ

A,C,E) Cell viability of ST88-14 (A,C) or M3 (E) cells treated with increasing doses of Trametinib and Ripretinib (A,E) or Trametinib and Avapritinib (C) for 5 days. Error bars represent the mean of three measurements ± SEM.

B,D,F) Bliss synergy score heat map for the combination treatment of Trametinib and Ripretinib in ST88-14 (B) or M3 (F) cells, or Trametinib and Avapritinib in ST88-14 (D) cells. Data represent the mean from n = 3.

G) Bar graph plot of the cell viability IC50 (nM) fold change of MPNST cells treated for 5 days with Trametinib in combination with Ripretinib.

H,I) Western blot analysis of ST88-14 (H) or M3 (I) cells treated with Trametinib and Ripretinib for 48hr.

J-M) RT-qPCR analysis of the changes of PDGFRβ, DUSP6, SPRY2 or SPRED2 expression levels in M3 cells treated with Trametinib and Ripretinib for 48hr.

N) Western blot analysis of M3 cells treated with Trametinib, Ripretinib and Avapritinib for 48hr.

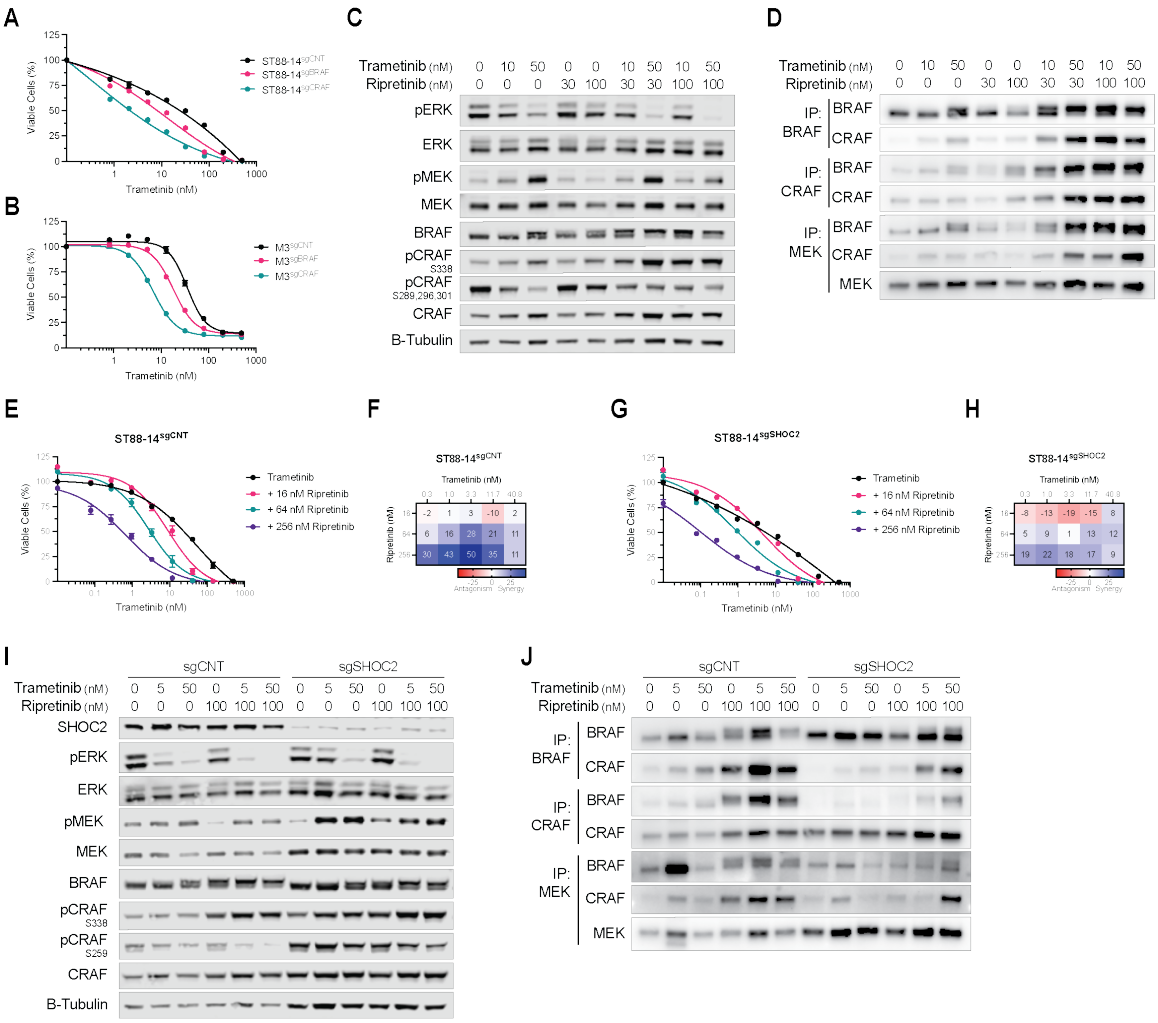

Figure 3. MEKi treatment-induced RAF dimerization mediates synergism with RAF inhibitors in MPNST

A-B) Cell viability of ST88-14 (A) or M3 (B) cells with a CRISPR-cas9 KO of BRAF or CRAF treated with increasing doses of Trametinib for 5 days. Error bars represent the mean of three measurements ± SEM.

C-D) Western blot analysis of ST88-14 cells whole-cell lysate (C) or lysate subjected to immunoprecipitation (D) after 24hr treatment with Trametinib and Ripretinib.

E,G) Cell viability of ST88-14^{sgCNT} (E) and ST88-14^{sgSHOC2} (G) cells treated with increasing doses of Trametinib and Ripretinib for 5 days. Error bars represent the mean of three measurements ± SEM.

F,H) Bliss synergy score heat map for the combination treatment of Trametinib and Ripretinib in ST88-14^{sgCNT} (F) and ST88-14^{sgSHOC2} (H) cells. Data represent the mean from n = 3.

I,J) Western blot analysis of ST88-14^{sgCNT} and ST88-14^{sgSHOC2} cells whole-cell lysate (I) or lysate subjected to immunoprecipitation (J) after 24hr treatment with Trametinib and Ripretinib.

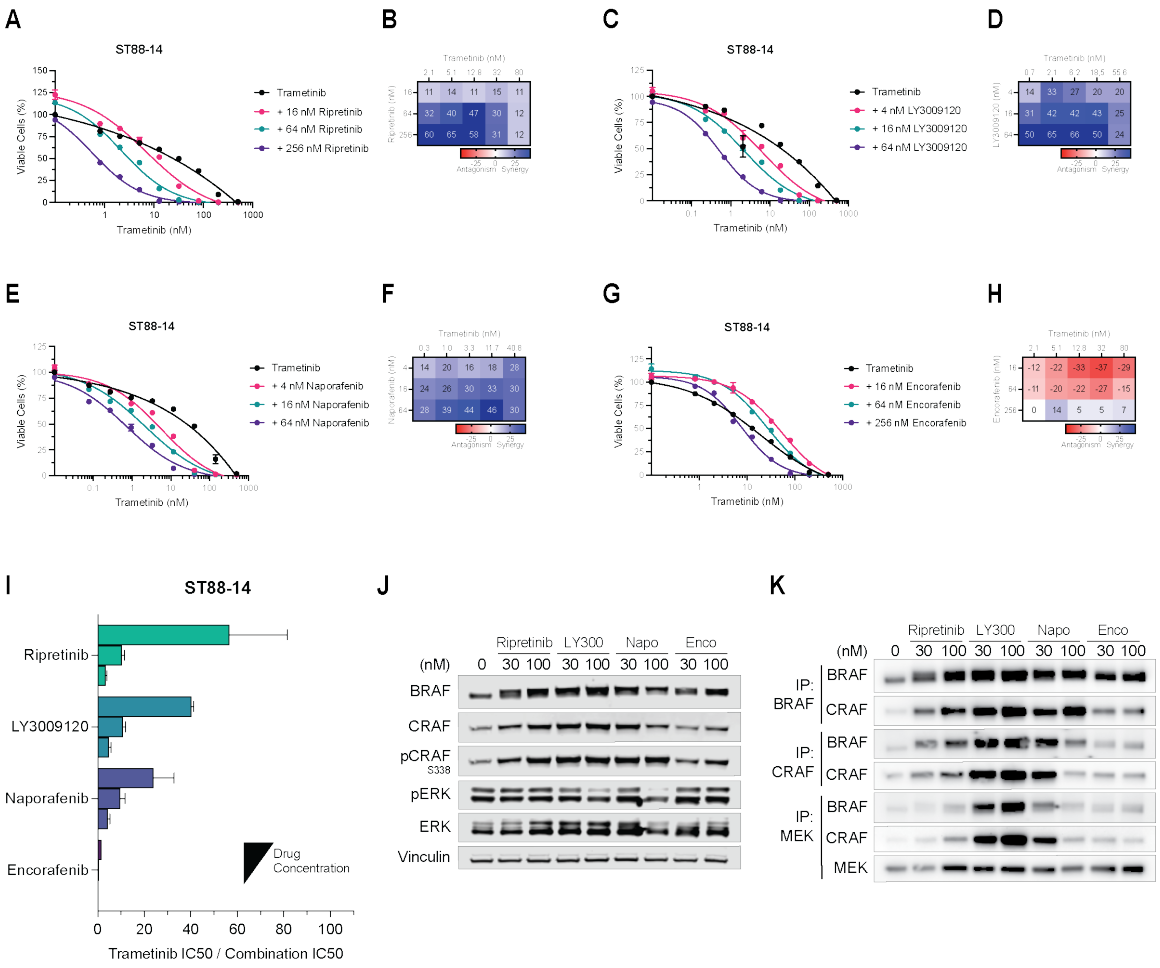

Figure 4. MEKi treatment sensitizes tumor cells to RAF dimer-specific inhibitors in NF1-deficient MPNST

A,C,E,G) Cell viability of ST88-14 cells treated with increasing doses of Trametinib and Ripretinib (A), LY3009120 (C), Naporafenib (E), or Encorafenib (G) for 5 days. Error bars represent the mean of three measurements ± SEM.

B,D,F,H) Bliss synergy score heat map for the combination treatment of Trametinib and Ripretinib (B), LY3009120 (D), Naporafenib (F), or Encorafenib (H) in ST88-14 cells. Data represent the mean from n = 3.

I) Bar graph plot of the cell viability IC50 (nM) fold change of ST88-14 cells treated for 5 days with Trametinib and Ripretinib (16, 64 or 256 nM), LY3009120 (4, 16 or 64 nM), Naporafenib (4, 16 or 64 nM), or Encorafenib (16, 64 or 256 nM).

J-K) Western blot analysis of ST88-14 cells whole-cell lysate (J) or lysate subjected to immunoprecipitation (K) after 24hr treatment with Ripretinib, LY3009120, Naporafenib or Encorafenib.

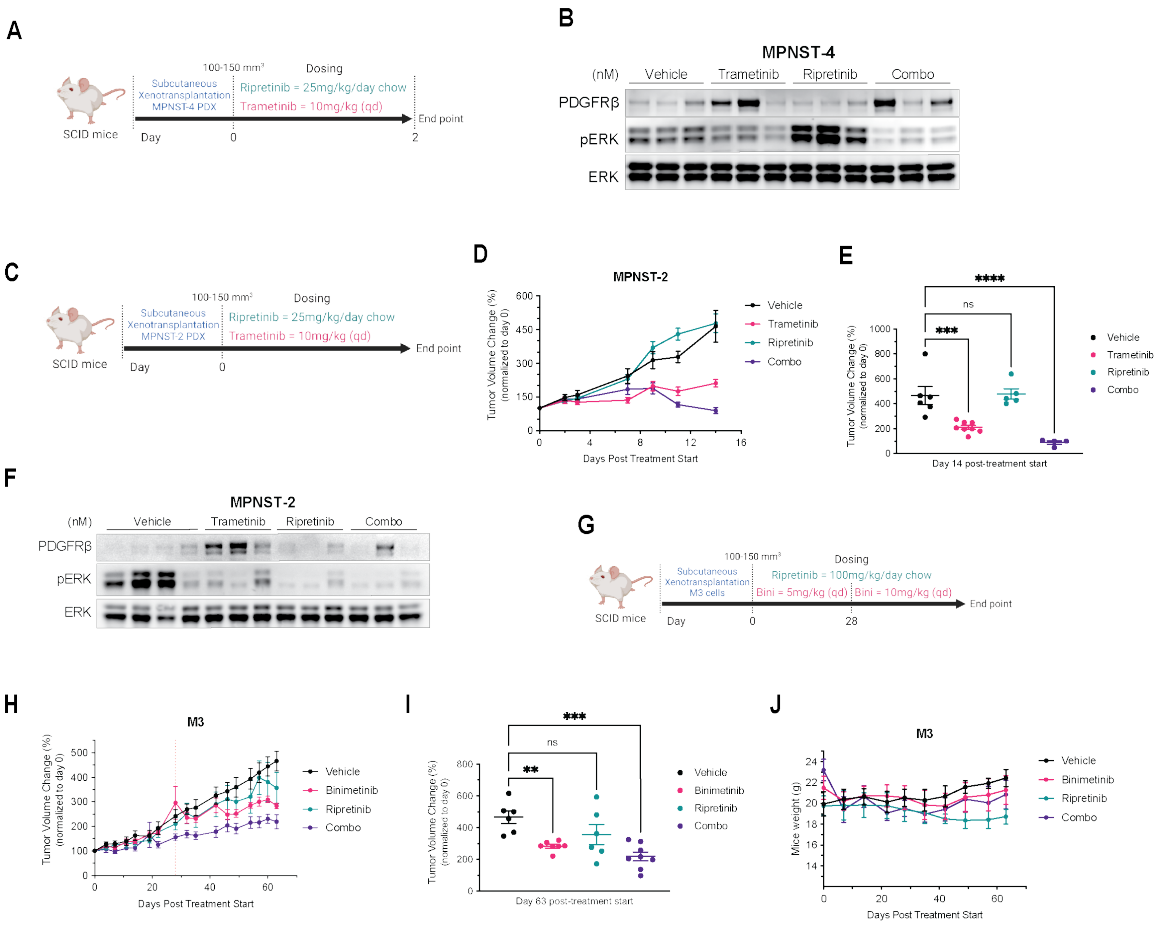

Figure 5. Combined inhibition of PDGFRβ and RAF dimers by Ripretinib enhances the sensitivity of MPNST tumors to MEKi

A) Schematic of the MPNST-4 PDX pharmacodynamic study.
B) Western blot analysis of MPNST-4 PDX tumors after treatment for 48hr.
C) Schematic of the MPNST-2 PDX efficacy study.
D) MPNST-2 PDX tumor volume curves of vehicle, Trametinib, Ripretinib, or the combination cohorts.
E) MPNST-2 PDX tumor volume distribution at the experiment endpoint.
F) Western blot analysis of MPNST-4 PDX tumors collected and the experiment endpoint.
G) Schematic of the M3 cells xenograft efficacy study.
H) M3 xenograft tumor volume curves of vehicle, Binimetinib, Ripretinib, or the combination cohorts.
I) M3 xenograft tumor volume distribution at the experiment endpoint.
J) Body weight measurements of SCID mice treated with vehicle, Binimetinib, Ripretinib, or the combination.

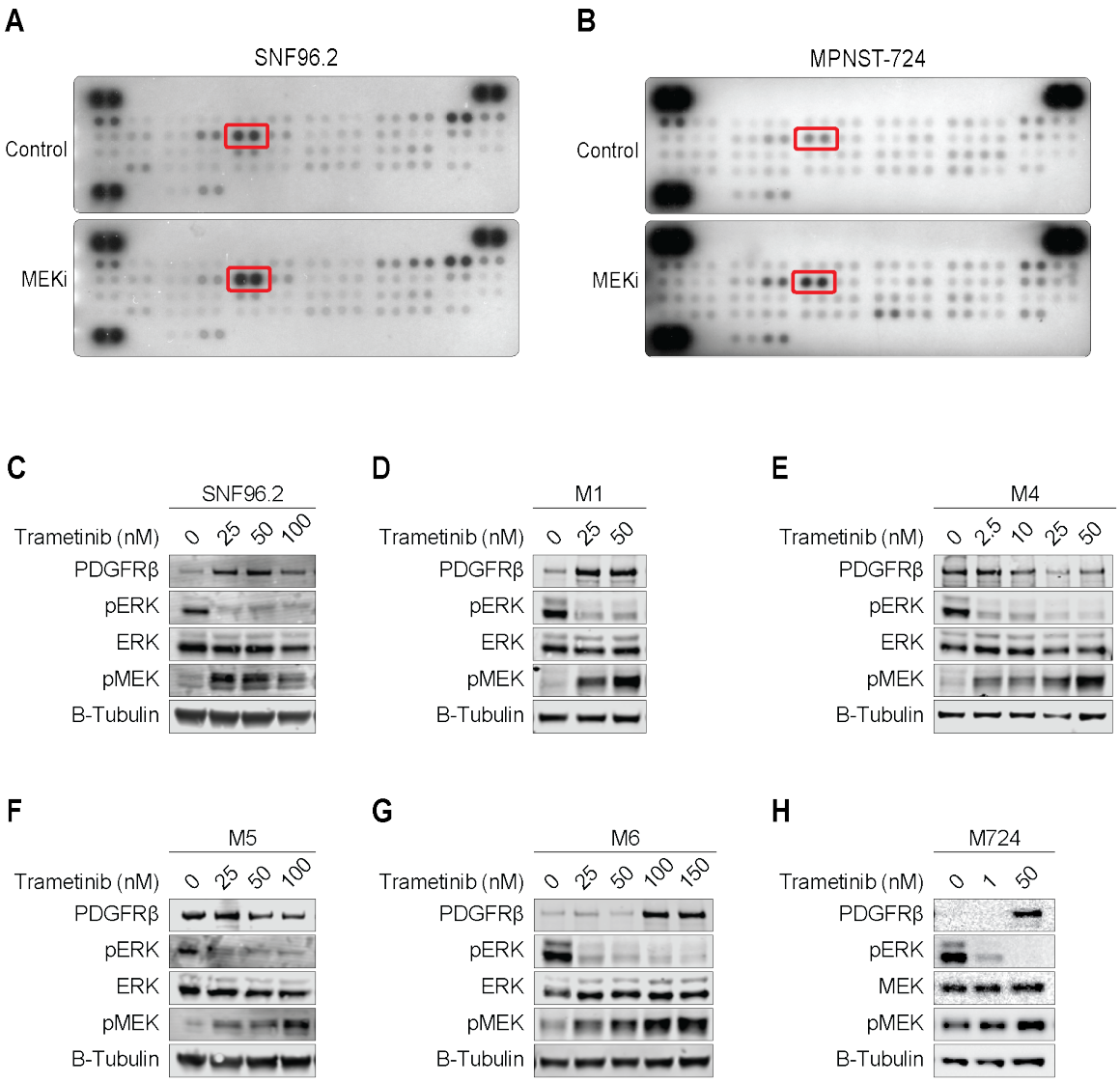

Supplemental Figure S1 (Related to Figure 1)

A-B) Phospho-RTK arrays of SNF96.2 cells treated *in vitro* with DMSO or 500 nM Binimetinib for 2hr (A), or M724 cells treated *in vivo* with vehicle or oral Binimetinib (30mg/kg BID) for 48hr (B). PDGFRβ is identified by red squares.
C-H) Western blot analysis of SNF96.2 (C), M1 (D), M4 (E), M5 (F), M6 (G) or M724 (H) cells treated with increasing concentrations of Trametinib for 48hr.

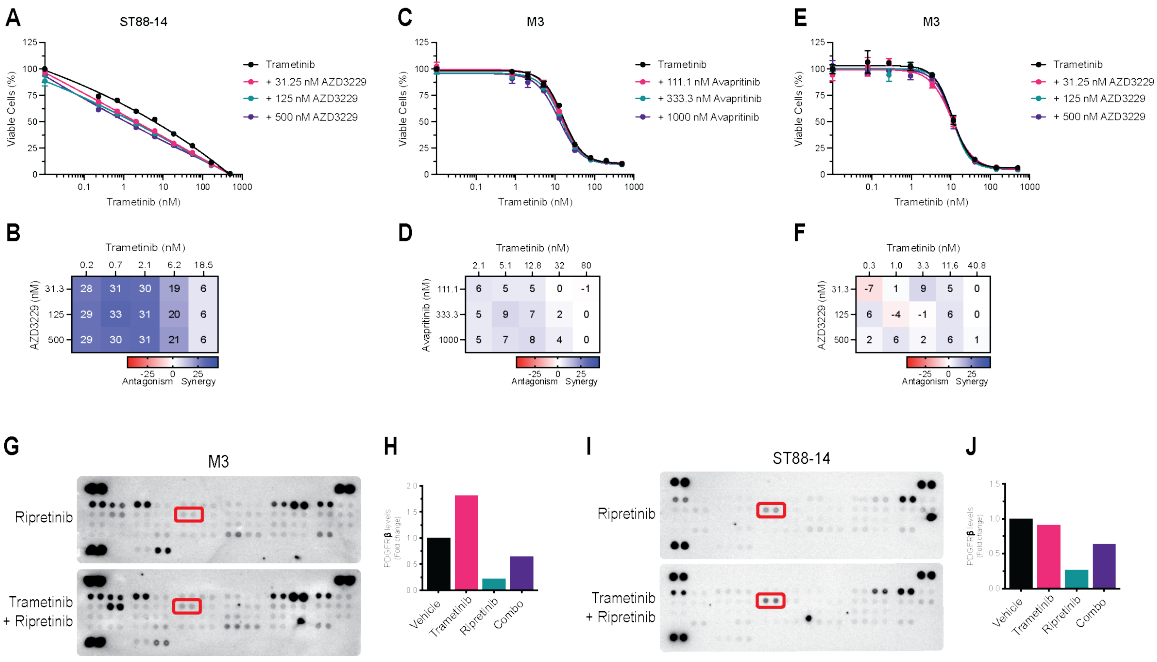

Supplemental Figure S2 (Related to Figure 2)

A,C,E) Cell viability of ST88-14 cells treated with increasing doses of Trametinib and AZD-3229 (A), or M3 cells treated with increasing doses of Trametinib and Avapritinib (C) or Trametinib and AZD-3229 (E) for 5 days. Error bars represent the mean of three measurements ± SEM.

B,D,F) Bliss synergy score heat map for the combination treatment of Trametinib and AZD-3229 in ST88-14 (B) or M3 (F) cells, or Trametinib and Avapritinib in M3 (D) cells. Data represent the mean from n = 3.

G,I) Phospho-RTK arrays of M3 (G) and ST88-14 (I) cells treated with 100 nM Ripretinib or 50 nM Trametinib and 100 nM combination for 48hr. PDGFRβ is identified by red squares.

H,J) Normalized mean pixel intensity quantification of PDGFRβ levels in the Phospho-RTK arrays of M3 (G and Figure 1 B) and ST88-14 (I and Figure 1 E) cells.

A

Cell Line	MPNST Clinical Sub-Type	NF1	CDKN2A	PRC2
M3	NF1	Y2485 (Frame Shift Del) X2624 (Splice)	Homozygous Loss *	WT
ST88-14	NF1	Homozygous Loss *	Homozygous Loss *	Homozygous Loss *
SNF96.2	NF1	Homozygous Loss *	Homozygous Loss *	Homozygous missense mutation
M1	NF1	X1870 (Splice)	Homozygous Loss *	Homozygous Loss *
M4	NF1	X1870 (Splice)	Homozygous Loss *	Homozygous Loss *
M5	NF1	X1870 (Splice)	Homozygous Loss *	Homozygous Loss *
M6	NF1	Q950 (Truncating)	Homozygous Loss *	Homozygous Loss *
M724	Sporadic	WT	Homozygous Loss *	WT

* = Confirmed by western blot

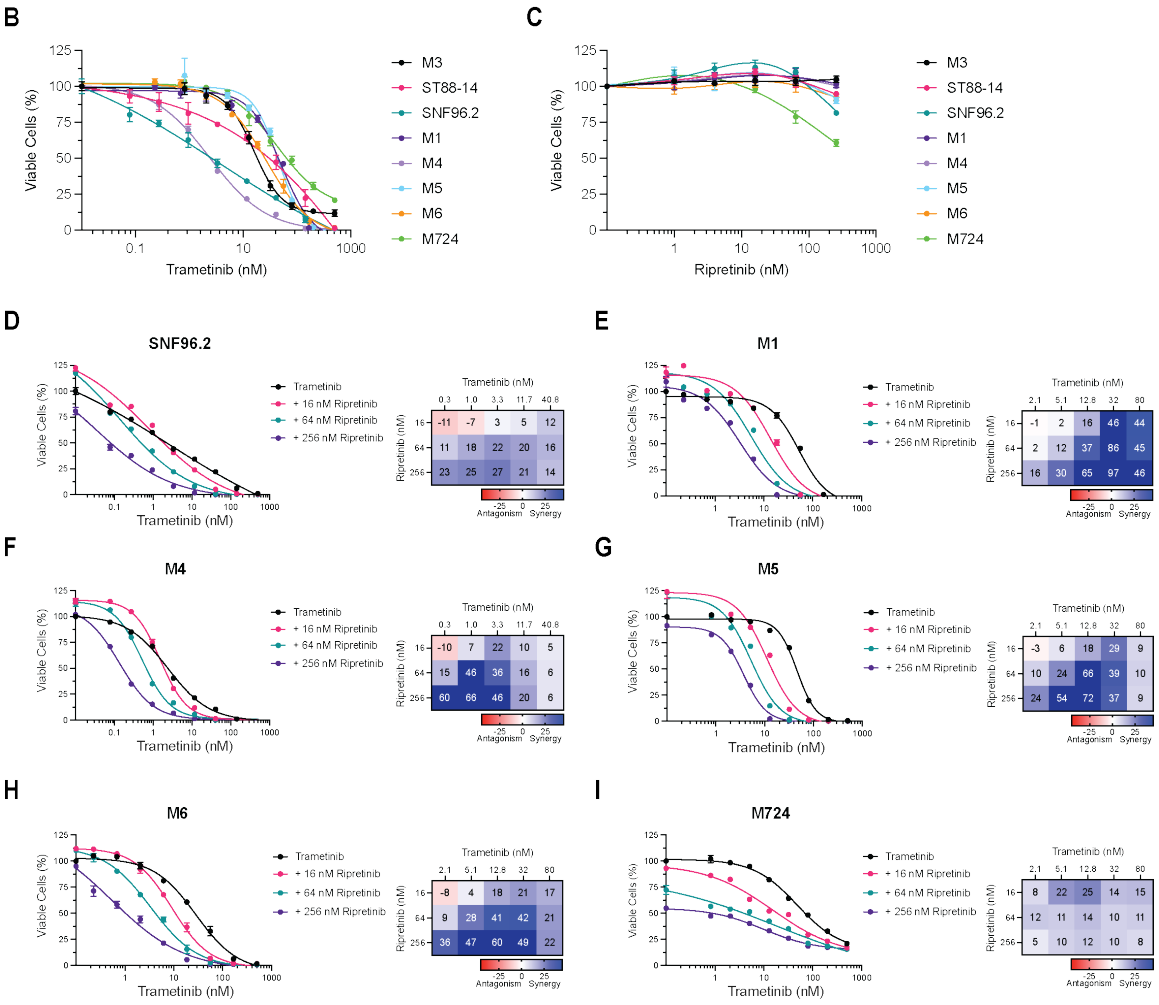

Supplemental Figure S3 (Related to Figure 2)

A) Genetic characteristics of the panel of MPNST cell lines used in the different experiments.

B-C) Cell viability of MPNST cell lines treated with increasing doses of Trametinib (B) or Ripretinib (C) for 5 days. Error bars represent the mean of three measurements ± SEM.

D-I) Cell viability and Bliss synergy score heat map for SNF96.2 (D), M1 (E), M4 (F), M5 (G), M6 (H) or M724 (I) cells treated with increasing doses of Trametinib and Ripretinib for 5 days. Error bars represent the mean of three measurements ± SEM, and Bliss scores represent the mean from n = 3.

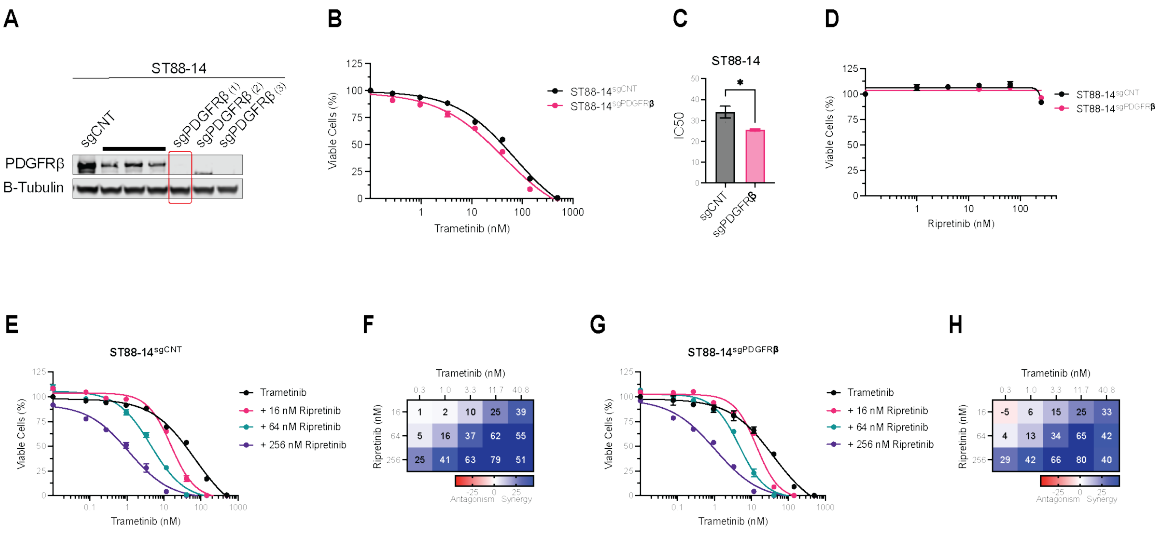

Supplemental Figure S4 (Related to Figure 2)

A) Western blot validation of PDGFRβ KO in ST88-14 cells using CRISPR-Cas9 and three different single guide RNAs.

B,D) Cell viability of ST88-14^{sgCNT} and ST88-14^{sgPDGFRβ} cells treated with increasing doses of Trametinib (B) or Ripretinib (D) for 5 days. Error bars represent the mean of three measurements ± SEM.

C) Bar graph plot of the cell viability IC50 (nM) of ST88-14^{sgCNT} and ST88-14^{sgPDGFRβ} cells treated with increasing doses of Trametinib (B). Error bars represent the mean of triplicate experiments, with internal triplicates, ± SD.

E,G) Cell viability of ST88-14^{sgCNT} (E) or ST88-14^{sgPDGFRβ} (G) cells treated with increasing doses of Trametinib and Ripretinib for 5 days. Error bars represent the mean of three measurements ± SEM.

F,H) Bliss synergy score heat map for the combination treatment of Trametinib and Ripretinib in ST88-14^{sgCNT} (F) or ST88-14^{sgPDGFRβ} (H) cells. Data represent the mean from n = 3.

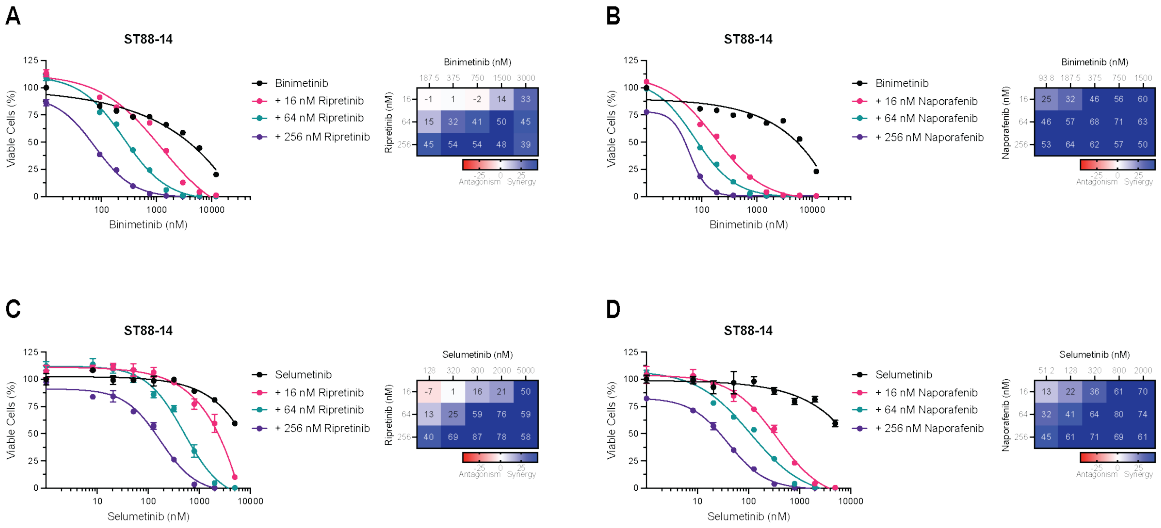

Supplemental Figure S5 (Related to Figure 4)

A-B) Cell viability and Bliss synergy score heat map for ST88-14 cells treated with increasing doses of Binimetinib and Ripretinib (A) or Naporafenib (B) for 5 days. Error bars represent the mean of three measurements ± SEM, and Bliss scores represent the mean from n = 3.

C-D) Cell viability and Bliss synergy score heat map for ST88-14 cells treated with increasing doses of Selumetinib and Ripretinib (C) or Naporafenib (D) for 5 days. Error bars represent the mean of three measurements ± SEM, and Bliss scores represent the mean from n = 3.

Supplementary tables

Supplementary Table 1. Drugs, chemicals, and reagents used in this study

Supplier	Catalog #	Item
Addgene	52962	LentiCas9-Blast plasmid
Addgene	52961	LentiCRISPR v2 plasmid
Addgene	52963	LentiGuide-Puro plasmid
Addgene	8454	pCMV-VSV-G packaging plasmid
Addgene	12260	psPAX2 packaging plasmid
Applied Biological Materials Inc.	G238	Mycoplasma PCR Detection Kit
Bio-Rad	1620115	Nitrocellulose Membrane, Roll, 0.45 µm
Cell Signaling Technology	8821	Active Ras Detection Kit
Cell Signaling Technology	7722	Blue Loading Buffer Pack
Cell Signaling Technology	9803	Cell Lysis Buffer (10X)
Corning	356237	Matrigel Basement Membrane Matrix, Phenol Red-free, LDEV-free
Deciphera Pharmaceuticals	n/a	Ripretinib (DCC-2618)
LI-COR Biosciences	928-60000	Chameleon Duo Pre-stained Protein Ladder
LI-COR Biosciences	927-60001	Intercept (TBS) Blocking Buffer
LI-COR Biosciences	927-85001	Intercept T20 (TBS) Protein-Free Antibody Diluent
Millipore Sigma	4693132001	cOmplete™, EDTA-free Protease Inhibitor Cocktail
Millipore Sigma	WBKLS0500	Immobilon Western Chemiluminescent HRP Substrate
Millipore Sigma	4906837001	PhosSTOP, Phosphatase Inhibitor Cocktail Tablets
MSKCC Pharmacy	n/a	Binimetinib (MEK162) – for *in vivo* studies
New England BioLabs	N3200L	1 kb Plus DNA Ladder
New England BioLabs	R3733L	BsaI-HFv2
New England BioLabs	R0739L	BsmBI-v2
New England BioLabs	B7025S	Gel Loading Dye, Purple (6X), no SDS
New England BioLabs	C3040H	Stable Competent E. coli (High Efficiency)
Omega Bio-Tek	D6492-01	E.Z.N.A. Cycle Pure Kit (V-spin)
Omega Bio-Tek	R6834-01	E.Z.N.A. Total RNA Kit I
Omega Bio-Tek	HCR003	Homogenizer Columns
Promega	G9242	CellTiter-Glo 2.0 Cell Viability Assay
Qiagen	28706	QIAquick Gel Extraction Kit
R&D Systems	ARY001B	Proteome Profiler Human Phospho-RTK Array Kit
R&D Systems	AR002	Resazurin / Alamar Blue
Roche	6365787001	X-tremeGENE™ 9 DNA Transfection Reagent
SelleckChem	S8553	Avapritinib (BLU-285)
SelleckChem	S8780	AZD3229
SelleckChem	S7007	Binimetinib (MEK162) – for *in vitro* studies
SelleckChem	S7108	Encorafenib (LGX818)
SelleckChem	S7842	LY3009120
SelleckChem	S8745	Naporafenib (LXH254)
SelleckChem	S1008	Selumetinib (AZD6244)
SelleckChem	S2673	Trametinib (GSK1120212)
Teknova	M1088	MOPS/SDS Running Buffer
Thermo Fisher Scientific	A1113903	Blasticidin S HCl
Thermo Fisher Scientific	26162	ChIP-grade Protein A/G magnetic beads
Thermo Fisher Scientific	17101015	Collagenase, Type II, powder
Thermo Fisher Scientific	BP172-5	Dithiothreitol (DTT)
Thermo Fisher Scientific	78444	Halt Protease and Phosphatase Inhibitor Cocktail
Thermo Fisher Scientific	4368813	High-Capacity cDNA Reverse Transcription kit
Thermo Fisher Scientific	NP0336BOX	NuPAGE 4-12% Bis-Tris gels
Thermo Fisher Scientific	NP0007	NuPAGE LDS sample buffer
Thermo Fisher Scientific	23225	Pierce BCA Protein Assay Kit
Thermo Fisher Scientific	36978	PMSF Protease Inhibitor
Thermo Fisher Scientific	A25778	PowerUp SYBR Green Master Mix
Thermo Fisher Scientific	A1113803	Puromycin Dihydrochloride
Thermo Fisher Scientific	89900	RIPA Lysis and Extraction Buffer
Thermo Fisher Scientific	26634	Spectra Multicolor Broad Range Protein Ladder
Thermo Fisher Scientific	37542	StartingBlock (TBS) Blocking Buffer
Thermo Fisher Scientific	34578	SuperSignal West Pico PLUS Chemiluminescent Substrate

Supplementary Table 2. sgRNAs for CRISPR/Cas9 used in this study

Species	sgRNA	20-mer Guide Sequence
n/a	sgCNT	GCTGATCTATCGCGGTCGTC
Human	sgBRAF	GGTTTCCGCTGTCAAACATG
Human	sgCRAF	GTGATGCTGTCCACTCGGAT
Human	sgPDGFRβ	GACTAACGTGACGTACTGGG
Human	sgSHOC2	TAGTTATACGATTAAAGCGA

Supplementary Table 3. Primers used for RT-qPCR in this study

Species	Primer	Sequence (5' to 3') [PAM = NGG]
Human	Fw_DUSP6	GGCGAGCTGCTGCTACACGA
Human	Rv_DUSP6	TGCCGGGCGTTCTACCTGGA
Human	Fw_PDGFRβ	ACAGACTCCAGGTGTCATCCA
Human	Rv_PDGFRβ	CCACTTTCTTTGCGGGGGTA
Human	Fw_RPL27	CATGGGCAAGAAGAAGATCG
Human	Rv_RPL27	TCCAAGGGGATATCCACAGA
Human	Fw_SPRED2	GACGTTTTTACAACAGCTACAGACA
Human	Rv_SPRED2	TGTGGGGTATGAGTCGTGGA
Human	Fw_SPRY2	ATTTGCACATCGCAGAAAGAAGA
Human	Rv_SPRY2	AGAACACATCTGAACTCCGTGA

Supplementary Table 4. Antibodies used for WB and IP in this study

Supplier	Catalog #	Target Protein	Host	Application	Dilution
Cell Signaling Technology	2128	B-Tubulin	Rabbit	Western blot	1:1000
Cell Signaling Technology	86298	B-Tubulin	Mouse	Western blot	1:1000
Cell Signaling Technology	9433	BRAF	Rabbit	Western blot	1:1000
Cell Signaling Technology	14814	BRAF	Rabbit	Western blot	1:1000
Santa Cruz Biotechnology	sc-5284	BRAF	Mouse	Western blot, Immunoprecipitation	1:200, 1 µg/IP
Cell Signaling Technology	53745	CRAF	Rabbit	Western blot	1:1000
Millipore Sigma	07-396	CRAF	Rabbit	Immunoprecipitation	1 µg
Cell Signaling Technology	12552	CRAF	Mouse	Western blot	1:1000
Cell Signaling Technology	4695	ERK1/2	Rabbit	Western blot	1:1000
Cell Signaling Technology	4696	ERK1/2	Mouse	Western blot	1:1000
Cell Signaling Technology	5415	Isotype control	Rabbit	Immunoprecipitation	1 µg/IP
Cell Signaling Technology	3900	Isotype control	Mouse	Immunoprecipitation	1 µg/IP
Millipore Sigma	07-641	MEK1	Rabbit	Immunoprecipitation	1 µg/IP
Cell Signaling Technology	9122	MEK1/2	Rabbit	Western blot	1:1000
Cell Signaling Technology	4694	MEK1/2	Mouse	Western blot	1:1000
Cell Signaling Technology	3169	PDGFRβ	Rabbit	Western blot	1:500
Cell Signaling Technology	3175	PDGFRβ	Mouse	Western blot	1:500
Cell Signaling Technology	4370	phospho-ERK1/2	Rabbit	Western blot	1:1000
Cell Signaling Technology	9421	phospho-CRAF-S259	Rabbit	Western blot	1:1000
Cell Signaling Technology	9431	phospho-CRAF-S289, S296, S301	Rabbit	Western blot	1:1000
Cell Signaling Technology	9427	phospho-CRAF-S338	Rabbit	Western blot	1:1000
Cell Signaling Technology	9154	phospho-MEK1/2	Rabbit	Western blot	1:1000
Cell Signaling Technology	53600	SHOC2	Rabbit	Western blot	1:1000
Cell Signaling Technology	13901	Vinculin	Rabbit	Western blot	1:1000
Cell Signaling Technology	7074	Anti-rabbit IgG, HRP-linked	2ry Antibody	Western blot	1:2000
Cell Signaling Technology	7076	Anti-mouse IgG, HRP-linked	2ry Antibody	Western blot	1:2000
LI-COR	926-32211	IRDye® 800CW Goat anti-Rabbit IgG	2ry Antibody	Western blot	1:10,000
LI-COR	926-68070	IRDye 680RD Goat anti-Mouse IgG	2ry Antibody	Western blot	1:20,000

BIBLIOGRAPHY

1. Stucky, C.-C. H., Johnson, K. N., Gray, R. J., Pockaj, B. A., Ocal, I. T., Rose, P. S. & Wasif, N. Malignant peripheral nerve sheath tumors (MPNST): the Mayo Clinic experience. *Ann. Surg. Oncol.* **19,** 878–885 (2012).
2. Carroll, S. L. & Ratner, N. How does the Schwann cell lineage form tumors in NF1? *Glia* **56,** 1590–1605 (2008).
3. Grobmyer, S. R., Reith, J. D., Shahlaee, A., Bush, C. H. & Hochwald, S. N. Malignant peripheral nerve sheath tumor: Molecular pathogenesis and current management considerations. *J. Surg. Oncol.* **97,** 340–349 (2008).
4. Ellison, D. A., Corredor-Buchmann, J., Parham, D. M. & Jackson, R. J. Malignant Triton Tumor Presenting as a Rectal Mass in an 11-Month-Old. *Pediatr. Dev. Pathol.* **8,** 235–239 (2005).
5. Farid, M., Demicco, E. G., Garcia, R., Ahn, L., Merola, P. R., Cioffi, A. & Maki, R. G. Malignant Peripheral Nerve Sheath Tumors. *The Oncologist* **19,** 193–201 (2014).
6. Meany, H., Widemann, B. C. & Ratner, N. in *Neurofibromatosis Type 1 Mol. Cell. Biol.* (eds. Upadhyaya, M. & Cooper, D. N.) 445–467 (Springer Berlin Heidelberg, 2012). doi:10.1007/978-3-642-32864-0_29
7. LaFemina, J., Qin, L.-X., Moraco, N. H., Antonescu, C. R., Fields, R. C., Crago, A. M., Brennan, M. F. & Singer, S. Oncologic outcomes of sporadic, neurofibromatosis-associated, and radiation-induced malignant peripheral nerve sheath tumors. *Ann. Surg. Oncol.* **20,** 66–72 (2013).

8. Brennan, M. F., Antonescu, C. R. & Maki, R. G. *Management of soft tissue sarcoma*. (Springer, 2013). at <http://public.eblib.com/choice/publicfullrecord.aspx?p=1030375>
9. Gupta, G., Mammis, A. & Maniker, A. Malignant Peripheral Nerve Sheath Tumors. *Neurosurg. Clin. N. Am.* **19,** 533–543 (2008).
10. Eilber, F. C., Brennan, M. F., Eilber, F. R., Dry, S. M., Singer, S. & Kattan, M. W. Validation of the postoperative nomogram for 12-year sarcoma-specific mortality. *Cancer* **101,** 2270–2275 (2004).
11. Rodriguez, F. J. Peripheral nerve sheath tumors: the elegant chapter in surgical neuropathology. *Acta Neuropathol. (Berl.)* **123,** 293–294 (2012).
12. Lee, W., Teckie, S., Wiesner, T., Ran, L., Prieto Granada, C. N., Lin, M., Zhu, S., Cao, Z., Liang, Y., Sboner, A., Tap, W. D., Fletcher, J. A., Huberman, K. H., Qin, L.-X., Viale, A., Singer, S., Zheng, D., Berger, M. F., Chen, Y., Antonescu, C. R. & Chi, P. PRC2 is recurrently inactivated through EED or SUZ12 loss in malignant peripheral nerve sheath tumors. *Nat. Genet.* **46,** 1227–1232 (2014).
13. De Raedt, T., Beert, E., Pasmant, E., Luscan, A., Brems, H., Ortonne, N., Helin, K., Hornick, J. L., Mautner, V., Kehrer-Sawatzki, H., Clapp, W., Bradner, J., Vidaud, M., Upadhyaya, M., Legius, E. & Cichowski, K. PRC2 loss amplifies Ras-driven transcription and confers sensitivity to BRD4-based therapies. *Nature* (2014). doi:10.1038/nature13561
14. Zhang, M., Wang, Y., Jones, S., Sausen, M., McMahon, K., Sharma, R., Wang, Q., Belzberg, A. J., Chaichana, K., Gallia, G. L., Gokaslan, Z. L., Riggins, G. J., Wolinksy, J.-P., Wood, L. D., Montgomery, E. A., Hruban, R. H., Kinzler, K.

W., Papadopoulos, N., Vogelstein, B. & Bettegowda, C. Somatic mutations of SUZ12 in malignant peripheral nerve sheath tumors. *Nat. Genet.* **46,** 1170–1172 (2014).

15. Malone, C. F., Fromm, J. A., Maertens, O., DeRaedt, T., Ingraham, R. & Cichowski, K. Defining Key Signaling Nodes and Therapeutic Biomarkers in *NF1* -Mutant Cancers. *Cancer Discov.* **4,** 1062–1073 (2014).
16. Bollag, G., Clapp, D. W., Shih, S., Adler, F., Zhang, Y. Y., Thompson, P., Lange, B. J., Freedman, M. H., McCormick, F., Jacks, T. & Shannon, K. Loss of NF1 results in activation of the Ras signaling pathway and leads to aberrant growth in haematopoietic cells. *Nat. Genet.* **12,** 144–148 (1996).
17. Comet, I., Riising, E. M., Leblanc, B. & Helin, K. Maintaining cell identity: PRC2-mediated regulation of transcription and cancer. *Nat. Rev. Cancer* **16,** 803–810 (2016).
18. Laugesen, A., Højfeldt, J. W. & Helin, K. Role of the Polycomb Repressive Complex 2 (PRC2) in Transcriptional Regulation and Cancer. *Cold Spring Harb. Perspect. Med.* **6,** a026575 (2016).
19. Margueron, R. & Reinberg, D. The Polycomb complex PRC2 and its mark in life. *Nature* **469,** 343–349 (2011).
20. Blackledge, N. P., Rose, N. R. & Klose, R. J. Targeting Polycomb systems to regulate gene expression: modifications to a complex story. *Nat. Rev. Mol. Cell Biol.* **16,** 643–649 (2015).

21. Pasini, D., Bracken, A. P., Jensen, M. R., Denchi, E. L. & Helin, K. Suz12 is essential for mouse development and for EZH2 histone methyltransferase activity. *EMBO J.* **23,** 4061–4071 (2004).
22. O'Carroll, D., Erhardt, S., Pagani, M., Barton, S. C., Surani, M. A. & Jenuwein, T. The polycomb-group gene Ezh2 is required for early mouse development. *Mol. Cell. Biol.* **21,** 4330–4336 (2001).
23. Schumacher, A., Faust, C. & Magnuson, T. Positional cloning of a global regulator of anterior-posterior patterning in mice. *Nature* **384,** (1996).
24. Mysliwiec, M. R., Bresnick, E. H. & Lee, Y. Endothelial Jarid2/Jumonji is required for normal cardiac development and proper Notch1 expression. *J. Biol. Chem.* **286,** 17193–17204 (2011).
25. Harutyunyan, A. S., Krug, B., Chen, H., Papillon-Cavanagh, S., Zeinieh, M., De Jay, N., Deshmukh, S., Chen, C. C. L., Belle, J., Mikael, L. G., Marchione, D. M., Li, R., Nikbakht, H., Hu, B., Cagnone, G., Cheung, W. A., Mohammadnia, A., Bechet, D., Faury, D., McConechy, M. K., Pathania, M., Jain, S. U., Ellezam, B., Weil, A. G., Montpetit, A., Salomoni, P., Pastinen, T., Lu, C., Lewis, P. W., Garcia, B. A., Kleinman, C. L., Jabado, N. & Majewski, J. H3K27M induces defective chromatin spread of PRC2-mediated repressive H3K27me2/me3 and is essential for glioma tumorigenesis. *Nat. Commun.* **10,** 1262 (2019).
26. Lewis, P. W., Müller, M. M., Koletsky, M. S., Cordero, F., Lin, S., Banaszynski, L. A., Garcia, B. A., Muir, T. W., Becher, O. J. & Allis, C. D. Inhibition of PRC2 Activity by a Gain-of-Function H3 Mutation Found in Pediatric Glioblastoma. *Science* **340,** 857–861 (2013).

27. Lulla, R. R., Saratsis, A. M. & Hashizume, R. Mutations in chromatin machinery and pediatric high-grade glioma. *Sci. Adv.* **2,** e1501354 (2016).
28. Stafford, J. M., Lee, C.-H., Voigt, P., Descostes, N., Saldaña-Meyer, R., Yu, J.-R., Leroy, G., Oksuz, O., Chapman, J. R., Suarez, F., Modrek, A. S., Bayin, N. S., Placantonakis, D. G., Karajannis, M. A., Snuderl, M., Ueberheide, B. & Reinberg, D. Multiple modes of PRC2 inhibition elicit global chromatin alterations in H3K27M pediatric glioma. *Sci. Adv.* **4,** eaau5935 (2018).
29. Wassef, M., Rodilla, V., Teissandier, A., Zeitouni, B., Gruel, N., Sadacca, B., Irondelle, M., Charruel, M., Ducos, B., Michaud, A., Caron, M., Marangoni, E., Chavrier, P., Le Tourneau, C., Kamal, M., Pasmant, E., Vidaud, M., Servant, N., Reyal, F., Meseure, D., Vincent-Salomon, A., Fre, S. & Margueron, R. Impaired PRC2 activity promotes transcriptional instability and favors breast tumorigenesis. *Genes Dev.* **29,** 2547–2562 (2015).
30. Ernst, T., Chase, A. J., Score, J., Hidalgo-Curtis, C. E., Bryant, C., Jones, A. V., Waghorn, K., Zoi, K., Ross, F. M., Reiter, A., Hochhaus, A., Drexler, H. G., Duncombe, A., Cervantes, F., Oscier, D., Boultwood, J., Grand, F. H. & Cross, N. C. P. Inactivating mutations of the histone methyltransferase gene EZH2 in myeloid disorders. *Nat. Genet.* **42,** 722–726 (2010).
31. Nikoloski, G., Langemeijer, S. M. C., Kuiper, R. P., Knops, R., Massop, M., Tönnissen, E. R. L. T. M., van der Heijden, A., Scheele, T. N., Vandenberghe, P., de Witte, T., van der Reijden, B. A. & Jansen, J. H. Somatic mutations of the histone methyltransferase gene EZH2 in myelodysplastic syndromes. *Nat. Genet.* **42,** 665–667 (2010).

32. Ntziachristos, P., Tsirigos, A., Vlierberghe, P. V., Nedjic, J., Trimarchi, T., Flaherty, M. S., Ferres-Marco, D., da Ros, V., Tang, Z., Siegle, J., Asp, P., Hadler, M., Rigo, I., Keersmaecker, K. D., Patel, J., Huynh, T., Utro, F., Poglio, S., Samon, J. B., Paietta, E., Racevskis, J., Rowe, J. M., Rabadan, R., Levine, R. L., Brown, S., Pflumio, F., Dominguez, M., Ferrando, A. & Aifantis, I. Genetic inactivation of the polycomb repressive complex 2 in T cell acute lymphoblastic leukemia. *Nat. Med.* **18,** 298–302 (2012).
33. Zhang, J., Ding, L., Holmfeldt, L., Wu, G., Heatley, S. L., Payne-Turner, D., Easton, J., Chen, X., Wang, J., Rusch, M., Lu, C., Chen, S.-C., Wei, L., Collins-Underwood, J. R., Ma, J., Roberts, K. G., Pounds, S. B., Ulyanov, A., Becksfort, J., Gupta, P., Huether, R., Kriwacki, R. W., Parker, M., McGoldrick, D. J., Zhao, D., Alford, D., Espy, S., Bobba, K. C., Song, G., Pei, D., Cheng, C., Roberts, S., Barbato, M. I., Campana, D., Coustan-Smith, E., Shurtleff, S. A., Raimondi, S. C., Kleppe, M., Cools, J., Shimano, K. A., Hermiston, M. L., Doulatov, S., Eppert, K., Laurenti, E., Notta, F., Dick, J. E., Basso, G., Hunger, S. P., Loh, M. L., Devidas, M., Wood, B., Winter, S., Dunsmore, K. P., Fulton, R. S., Fulton, L. L., Hong, X., Harris, C. C., Dooling, D. J., Ochoa, K., Johnson, K. J., Obenauer, J. C., Evans, W. E., Pui, C.-H., Naeve, C. W., Ley, T. J., Mardis, E. R., Wilson, R. K., Downing, J. R. & Mullighan, C. G. The genetic basis of early T-cell precursor acute lymphoblastic leukaemia. *Nature* **481,** 157–163 (2012).
34. Prieto-Granada, C. N., Wiesner, T., Messina, J. L., Jungbluth, A. A., Chi, P. & Antonescu, C. R. Loss of H3K27me3 Expression Is a Highly Sensitive Marker

for Sporadic and Radiation-induced MPNST. *Am. J. Surg. Pathol.* **40,** 479–489 (2016).

35. Schaefer, I.-M., Fletcher, C. D. & Hornick, J. L. Loss of H3K27 trimethylation distinguishes malignant peripheral nerve sheath tumors from histologic mimics. *Mod. Pathol.* **29,** 4–13 (2016).
36. Yan, J., Chen, Y., Patel, A. J., Warda, S., Lee, C. J., Nixon, B. G., Wong, E. W. P., Miranda-Román, M. A., Yang, N., Wang, Y., Pachai, M. R., Sher, J., Giff, E., Tang, F., Khurana, E., Singer, S., Liu, Y., Galbo Jr., P. M., Maag, J. L. V., Koche, R. P., Zheng, D., Antonescu, C., Deng, L., Li, M., Chen, Y. & Chi, P. Tumor-intrinsic PRC2 inactivation drives a context-dependent immune-desert microenvironment and is sensitized by immunogenic therapeutic viruses. *J. Clin. Invest.* (2022). doi:10.1172/JCI153437
37. Nabel, E. G. CDKS and CKIS: Molecular targets for tissue remodelling. *Nat. Rev. Drug Discov.* **1,** 587–598 (2002).
38. Zhao, R., Choi, B. Y., Lee, M.-H., Bode, A. M. & Dong, Z. Implications of Genetic and Epigenetic Alterations of CDKN2A (p16 INK4a) in Cancer. *EBioMedicine* **8,** 30–39 (2016).
39. Serrano, M., Hannon, G. J. & Beach, D. A new regulatory motif in cell-cycle control causing specific inhibition of cyclin D/CDK4. *Nature* **366,** 704–707 (1993).
40. Pomerantz, J., Schreiber-Agus, N., Liégeois, N. J., Silverman, A., Alland, L., Chin, L., Potes, J., Chen, K., Orlow, I., Lee, H.-W., Cordon-Cardo, C. &

DePinho, R. A. The Ink4a Tumor Suppressor Gene Product, p19Arf, Interacts with MDM2 and Neutralizes MDM2's Inhibition of p53. *Cell* **92,** 713–723 (1998).

41. Basu, S. & Murphy, M. E. Genetic Modifiers of the p53 Pathway. *Cold Spring Harb. Perspect. Med.* **6,** a026302 (2016).
42. Quelle, D. E., Cheng, M., Ashmun, R. A. & Sherr, C. J. Cancer-associated mutations at the *INK4a* locus cancel cell cycle arrest by p16 ^{INK4a} but not by the alternative reading frame protein p19 ^{ARF}. *Proc. Natl. Acad. Sci.* **94,** 669–673 (1997).
43. Higham, C. S., Dombi, E., Rogiers, A., Bhaumik, S., Pans, S., Connor, S. E. J., Miettinen, M., Sciot, R., Tirabosco, R., Brems, H., Baldwin, A., Legius, E., Widemann, B. C. & Ferner, R. E. The characteristics of 76 atypical neurofibromas as precursors to neurofibromatosis 1 associated malignant peripheral nerve sheath tumors. *Neuro-Oncol.* **20,** 818–825 (2018).
44. Beert, E., Brems, H., Daniëls, B., De Wever, I., Van Calenbergh, F., Schoenaers, J., Debiec-Rychter, M., Gevaert, O., De Raedt, T., Van Den Bruel, A., de Ravel, T., Cichowski, K., Kluwe, L., Mautner, V., Sciot, R. & Legius, E. Atypical neurofibromas in neurofibromatosis type 1 are premalignant tumors. *Genes. Chromosomes Cancer* **50,** 1021–1032 (2011).
45. Pemov, A., Hansen, N. F., Sindiri, S., Patidar, R., Higham, C. S., Dombi, E., Miettinen, M. M., Fetsch, P., Brems, H., Chandrasekharappa, S. C., Jones, K., Zhu, B., Wei, J. S., National Intramural Sequencing Center (NISC) Comparative Sequencing Program, National Cancer Institute (NCI) Division of Cancer Epidemiology and Genetics (DCEG) Cancer Genomics Research

Laboratory, Mullikin, J. C., Wallace, M. R., Khan, J., Legius, E., Widemann, B. C. & Stewart, D. R. Low mutation burden and frequent loss of CDKN2A/B and SMARCA2, but not PRC2, define premalignant neurofibromatosis type 1–associated atypical neurofibromas. *Neuro-Oncol.* **21,** 981–992 (2019).

46. Chaney, K. E., Perrino, M. R., Kershner, L. J., Patel, A. V., Wu, J., Choi, K., Rizvi, T. A., Dombi, E., Szabo, S., Largaespada, D. A. & Ratner, N. *Cdkn2a* Loss in a Model of Neurofibroma Demonstrates Stepwise Tumor Progression to Atypical Neurofibroma and MPNST. *Cancer Res.* **80,** 4720–4730 (2020).
47. Downward, J. Control of ras activation. *Cancer Surv.* **27,** 87–100 (1996).
48. Nissan, M. H., Pratilas, C. A., Jones, A. M., Ramirez, R., Won, H., Liu, C., Tiwari, S., Kong, L., Hanrahan, A. J., Yao, Z., Merghoub, T., Ribas, A., Chapman, P. B., Yaeger, R., Taylor, B. S., Schultz, N., Berger, M. F., Rosen, N. & Solit, D. B. Loss of NF1 in Cutaneous Melanoma Is Associated with RAS Activation and MEK Dependence. *Cancer Res.* **74,** 2340–2350 (2014).
49. Taylor, B. S., Barretina, J., Maki, R. G., Antonescu, C. R., Singer, S. & Ladanyi, M. Advances in sarcoma genomics and new therapeutic targets. *Nat. Rev. Cancer* **11,** 541–557 (2011).
50. Kahen, E. J., Brohl, A., Yu, D., Welch, D., Cubitt, C. L., Lee, J. K., Chen, Y., Yoder, S. J., Teer, J. K., Zhang, Y. O., Wallace, M. R. & Reed, D. R. Neurofibromin level directs RAS pathway signaling and mediates sensitivity to targeted agents in malignant peripheral nerve sheath tumors. *Oncotarget* **9,** 22571–22585 (2018).

51. Dhillon, A. S., Hagan, S., Rath, O. & Kolch, W. MAP kinase signalling pathways in cancer. *Oncogene* **26,** 3279–3290 (2007).

52. Barbosa, R., Acevedo, L. A. & Marmorstein, R. The MEK/ERK Network as a Therapeutic Target in Human Cancer. *Mol. Cancer Res.* **19,** 361–374 (2021).

53. Zhao, Y. & Adjei, A. A. The clinical development of MEK inhibitors. *Nat. Rev. Clin. Oncol.* **11,** 385–400 (2014).

54. Marais, R., Light, Y., Paterson, H. F. & Marshall, C. J. Ras recruits Raf-1 to the plasma membrane for activation by tyrosine phosphorylation. *EMBO J.* **14,** 3136–3145 (1995).

55. Lavoie, H. & Therrien, M. Regulation of RAF protein kinases in ERK signalling. *Nat. Rev. Mol. Cell Biol.* **16,** 281–298 (2015).

56. Jones, G. G., del Río, I. B., Sari, S., Sekerim, A., Young, L. C., Hartig, N., Areso Zubiaur, I., El-Bahrawy, M. A., Hynds, R. E., Lei, W., Molina-Arcas, M., Downward, J. & Rodriguez-Viciana, P. SHOC2 phosphatase-dependent RAF dimerization mediates resistance to MEK inhibition in RAS-mutant cancers. *Nat. Commun.* **10,** 2532 (2019).

57. Dhillon, A. S., Meikle, S., Yazici, Z., Eulitz, M. & Kolch, W. Regulation of Raf-1 activation and signalling by dephosphorylation. *EMBO J.* **21,** 64–71 (2002).

58. Rodriguez-Viciana, P., Oses-Prieto, J., Burlingame, A., Fried, M. & McCormick, F. A Phosphatase Holoenzyme Comprised of Shoc2/Sur8 and the Catalytic Subunit of PP1 Functions as an M-Ras Effector to Modulate Raf Activity. *Mol. Cell* **22,** 217–230 (2006).

59. Roberts, P. J. & Der, C. J. Targeting the Raf-MEK-ERK mitogen-activated protein kinase cascade for the treatment of cancer. *Oncogene* **26,** 3291–3310 (2007).

60. Shaul, Y. D. & Seger, R. The MEK/ERK cascade: From signaling specificity to diverse functions. *Biochim. Biophys. Acta BBA - Mol. Cell Res.* **1773,** 1213–1226 (2007).

61. Meloche, S. & Pouysségur, J. The ERK1/2 mitogen-activated protein kinase pathway as a master regulator of the G1- to S-phase transition. *Oncogene* **26,** 3227–3239 (2007).

62. Pratilas, C. A., Taylor, B. S., Ye, Q., Viale, A., Sander, C., Solit, D. B. & Rosen, N. V600EBRAF is associated with disabled feedback inhibition of RAF–MEK signaling and elevated transcriptional output of the pathway. *Proc. Natl. Acad. Sci.* **106,** 4519–4524 (2009).

63. Drosten, M. & Barbacid, M. Targeting the MAPK Pathway in KRAS-Driven Tumors. *Cancer Cell* **37,** 543–550 (2020).

64. Samatar, A. A. & Poulikakos, P. I. Targeting RAS–ERK signalling in cancer: promises and challenges. *Nat. Rev. Drug Discov.* **13,** 928–942 (2014).

65. Braicu, Buse, Busuioc, Drula, Gulei, Raduly, Rusu, Irimie, Atanasov, Slaby, Ionescu, & Berindan-Neagoe. A Comprehensive Review on MAPK: A Promising Therapeutic Target in Cancer. *Cancers* **11,** 1618 (2019).

66. Gao, Y., Chang, M. T., McKay, D., Na, N., Zhou, B., Yaeger, R., Torres, N. M., Muniz, K., Drosten, M., Barbacid, M., Caponigro, G., Stuart, D., Moebitz, H., Solit, D. B., Abdel-Wahab, O., Taylor, B. S., Yao, Z. & Rosen, N. Allele-Specific

Mechanisms of Activation of MEK1 Mutants Determine Their Properties. *Cancer Discov.* **8,** 648–661 (2018).

67. Murugan, A. K., Dong, J., Xie, J. & Xing, M. MEK1 mutations, but not ERK2 mutations, occur in melanomas and colon carcinomas, but none in thyroid carcinomas. *Cell Cycle* **8,** 2122–2124 (2009).
68. Adamopoulos, C., Ahmed, T. A., Tucker, M. R., Ung, P. M. U., Xiao, M., Karoulia, Z., Amabile, A., Wu, X., Aaronson, S. A., Ang, C., Rebecca, V. W., Brown, B. D., Schlessinger, A., Herlyn, M., Wang, Q., Shaw, D. E. & Poulikakos, P. I. Exploiting Allosteric Properties of RAF and MEK Inhibitors to Target Therapy-Resistant Tumors Driven by Oncogenic BRAF Signaling. *Cancer Discov.* **11,** 1716–1735 (2021).
69. Markham, A. & Keam, S. J. Selumetinib: First Approval. *Drugs* **80,** 931–937 (2020).
70. Wu, P.-K. & Park, J.-I. MEK1/2 Inhibitors: Molecular Activity and Resistance Mechanisms. *Semin. Oncol.* **42,** 849–862 (2015).
71. Roskoski, R. Classification of small molecule protein kinase inhibitors based upon the structures of their drug-enzyme complexes. *Pharmacol. Res.* **103,** 26–48 (2016).
72. Gilmartin, A. G., Bleam, M. R., Groy, A., Moss, K. G., Minthorn, E. A., Kulkarni, S. G., Rominger, C. M., Erskine, S., Fisher, K. E., Yang, J., Zappacosta, F., Annan, R., Sutton, D. & Laquerre, S. G. GSK1120212 (JTP-74057) Is an Inhibitor of MEK Activity and Activation with Favorable Pharmacokinetic

Properties for Sustained *In Vivo* Pathway Inhibition. *Clin. Cancer Res.* **17,** 989–1000 (2011).

73. Ishii, N., Harada, N., Joseph, E. W., Ohara, K., Miura, T., Sakamoto, H., Matsuda, Y., Tomii, Y., Tachibana-Kondo, Y., Iikura, H., Aoki, T., Shimma, N., Arisawa, M., Sowa, Y., Poulikakos, P. I., Rosen, N., Aoki, Y. & Sakai, T. Enhanced Inhibition of ERK Signaling by a Novel Allosteric MEK Inhibitor, CH5126766, That Suppresses Feedback Reactivation of RAF Activity. *Cancer Res.* **73,** 4050–4060 (2013).
74. Lito, P., Saborowski, A., Yue, J., Solomon, M., Joseph, E., Gadal, S., Saborowski, M., Kastenhuber, E., Fellmann, C., Ohara, K., Morikami, K., Miura, T., Lukacs, C., Ishii, N., Lowe, S. & Rosen, N. Disruption of CRAF-Mediated MEK Activation Is Required for Effective MEK Inhibition in KRAS Mutant Tumors. *Cancer Cell* **25,** 697–710 (2014).
75. Hatzivassiliou, G., Haling, J. R., Chen, H., Song, K., Price, S., Heald, R., Hewitt, J. F. M., Zak, M., Peck, A., Orr, C., Merchant, M., Hoeflich, K. P., Chan, J., Luoh, S.-M., Anderson, D. J., Ludlam, M. J. C., Wiesmann, C., Ultsch, M., Friedman, L. S., Malek, S. & Belvin, M. Mechanism of MEK inhibition determines efficacy in mutant KRAS- versus BRAF-driven cancers. *Nature* **501,** 232–236 (2013).
76. Lito, P., Pratilas, C. A., Joseph, E. W., Tadi, M., Halilovic, E., Zubrowski, M., Huang, A., Wong, W. L., Callahan, M. K., Merghoub, T., Wolchok, J. D., de Stanchina, E., Chandarlapaty, S., Poulikakos, P. I., Fagin, J. A. & Rosen, N. Relief of Profound Feedback Inhibition of Mitogenic Signaling by RAF

Inhibitors Attenuates Their Activity in BRAFV600E Melanomas. *Cancer Cell* **22,** 668–682 (2012).

77. Davies, H., Bignell, G. R., Cox, C., Stephens, P., Edkins, S., Clegg, S., Teague, J., Woffendin, H., Garnett, M. J., Bottomley, W., Davis, N., Dicks, E., Ewing, R., Floyd, Y., Gray, K., Hall, S., Hawes, R., Hughes, J., Kosmidou, V., Menzies, A., Mould, C., Parker, A., Stevens, C., Watt, S., Hooper, S., Wilson, R., Jayatilake, H., Gusterson, B. A., Cooper, C., Shipley, J., Hargrave, D., Pritchard-Jones, K., Maitland, N., Chenevix-Trench, G., Riggins, G. J., Bigner, D. D., Palmieri, G., Cossu, A., Flanagan, A., Nicholson, A., Ho, J. W. C., Leung, S. Y., Yuen, S. T., Weber, B. L., Seigler, H. F., Darrow, T. L., Paterson, H., Marais, R., Marshall, C. J., Wooster, R., Stratton, M. R. & Futreal, P. A. Mutations of the BRAF gene in human cancer. *Nature* **417,** 949–954 (2002).
78. Hodis, E., Watson, I. R., Kryukov, G. V., Arold, S. T., Imielinski, M., Theurillat, J.-P., Nickerson, E., Auclair, D., Li, L., Place, C., DiCara, D., Ramos, A. H., Lawrence, M. S., Cibulskis, K., Sivachenko, A., Voet, D., Saksena, G., Stransky, N., Onofrio, R. C., Winckler, W., Ardlie, K., Wagle, N., Wargo, J., Chong, K., Morton, D. L., Stemke-Hale, K., Chen, G., Noble, M., Meyerson, M., Ladbury, J. E., Davies, M. A., Gershenwald, J. E., Wagner, S. N., Hoon, D. S. B., Schadendorf, D., Lander, E. S., Gabriel, S. B., Getz, G., Garraway, L. A. & Chin, L. A Landscape of Driver Mutations in Melanoma. *Cell* **150,** 251–263 (2012).
79. Subbiah, V., Baik, C. & Kirkwood, J. M. Clinical Development of BRAF plus MEK Inhibitor Combinations. *Trends Cancer* **6,** 797–810 (2020).

80. Corcoran, R. B., Ebi, H., Turke, A. B., Coffee, E. M., Nishino, M., Cogdill, A. P., Brown, R. D., Della Pelle, P., Dias-Santagata, D., Hung, K. E., Flaherty, K. T., Piris, A., Wargo, J. A., Settleman, J., Mino-Kenudson, M. & Engelman, J. A. EGFR-Mediated Reactivation of MAPK Signaling Contributes to Insensitivity of *BRAF* -Mutant Colorectal Cancers to RAF Inhibition with Vemurafenib. *Cancer Discov.* **2,** 227–235 (2012).

81. Hatzivassiliou, G., Song, K., Yen, I., Brandhuber, B. J., Anderson, D. J., Alvarado, R., Ludlam, M. J. C., Stokoe, D., Gloor, S. L., Vigers, G., Morales, T., Aliagas, I., Liu, B., Sideris, S., Hoeflich, K. P., Jaiswal, B. S., Seshagiri, S., Koeppen, H., Belvin, M., Friedman, L. S. & Malek, S. RAF inhibitors prime wild-type RAF to activate the MAPK pathway and enhance growth. *Nature* **464,** 431–435 (2010).

82. Poulikakos, P. I., Zhang, C., Bollag, G., Shokat, K. M. & Rosen, N. RAF inhibitors transactivate RAF dimers and ERK signalling in cells with wild-type BRAF. *Nature* **464,** 427–430 (2010).

83. Peng, S.-B., Henry, J. R., Kaufman, M. D., Lu, W.-P., Smith, B. D., Vogeti, S., Rutkoski, T. J., Wise, S., Chun, L., Zhang, Y., Van Horn, R. D., Yin, T., Zhang, X., Yadav, V., Chen, S.-H., Gong, X., Ma, X., Webster, Y., Buchanan, S., Mochalkin, I., Huber, L., Kays, L., Donoho, G. P., Walgren, J., McCann, D., Patel, P., Conti, I., Plowman, G. D., Starling, J. J. & Flynn, D. L. Inhibition of RAF Isoforms and Active Dimers by LY3009120 Leads to Anti-tumor Activities in RAS or BRAF Mutant Cancers. *Cancer Cell* **28,** 384–398 (2015).

84. Nakamura, A., Arita, T., Tsuchiya, S., Donelan, J., Chouitar, J., Carideo, E., Galvin, K., Okaniwa, M., Ishikawa, T. & Yoshida, S. Antitumor Activity of the Selective Pan-RAF Inhibitor TAK-632 in BRAF Inhibitor-Resistant Melanoma. *Cancer Res.* **73,** 7043–7055 (2013).
85. Lemmon, M. A. & Schlessinger, J. Cell Signaling by Receptor Tyrosine Kinases. *Cell* **141,** 1117–1134 (2010).
86. Yamaoka, T., Kusumoto, S., Ando, K., Ohba, M. & Ohmori, T. Receptor Tyrosine Kinase-Targeted Cancer Therapy. *Int. J. Mol. Sci.* **19,** 3491 (2018).
87. Du, Z. & Lovly, C. M. Mechanisms of receptor tyrosine kinase activation in cancer. *Mol. Cancer* **17,** 58 (2018).
88. Dougherty, M. K., Müller, J., Ritt, D. A., Zhou, M., Zhou, X. Z., Copeland, T. D., Conrads, T. P., Veenstra, T. D., Lu, K. P. & Morrison, D. K. Regulation of Raf-1 by Direct Feedback Phosphorylation. *Mol. Cell* **17,** 215–224 (2005).
89. Montero-Conde, C., Ruiz-Llorente, S., Dominguez, J. M., Knauf, J. A., Viale, A., Sherman, E. J., Ryder, M., Ghossein, R. A., Rosen, N. & Fagin, J. A. Relief of Feedback Inhibition of *HER3* Transcription by RAF and MEK Inhibitors Attenuates Their Antitumor Effects in *BRAF* -Mutant Thyroid Carcinomas. *Cancer Discov.* **3,** 520–533 (2013).
90. Wang, J., Pollard, K., Allen, A. N., Tomar, T., Pijnenburg, D., Yao, Z., Rodriguez, F. J. & Pratilas, C. A. Combined Inhibition of SHP2 and MEK Is Effective in Models of NF1-Deficient Malignant Peripheral Nerve Sheath Tumors. *Cancer Res.* **80,** 5367–5379 (2020).

91. Shawver, L. K., Slamon, D. & Ullrich, A. Smart drugs: Tyrosine kinase inhibitors in cancer therapy. *Cancer Cell* **1,** 117–123 (2002).

92. Reichert, J. M. & Valge-Archer, V. E. Development trends for monoclonal antibody cancer therapeutics. *Nat. Rev. Drug Discov.* **6,** 349–356 (2007).

93. Metibemu, D. S., Akinloye, O. A., Akamo, A. J., Ojo, D. A., Okeowo, O. T. & Omotuyi, I. O. Exploring receptor tyrosine kinases-inhibitors in Cancer treatments. *Egypt. J. Med. Hum. Genet.* **20,** 35 (2019).

94. Smith, B. D., Kaufman, M. D., Lu, W.-P., Gupta, A., Leary, C. B., Wise, S. C., Rutkoski, T. J., Ahn, Y. M., Al-Ani, G., Bulfer, S. L., Caldwell, T. M., Chun, L., Ensinger, C. L., Hood, M. M., McKinley, A., Patt, W. C., Ruiz-Soto, R., Su, Y., Telikepalli, H., Town, A., Turner, B. A., Vogeti, L., Vogeti, S., Yates, K., Janku, F., Abdul Razak, A. R., Rosen, O., Heinrich, M. C. & Flynn, D. L. Ripretinib (DCC-2618) Is a Switch Control Kinase Inhibitor of a Broad Spectrum of Oncogenic and Drug-Resistant KIT and PDGFRA Variants. *Cancer Cell* **35,** 738-751.e9 (2019).

95. Jessen, W. J., Miller, S. J., Jousma, E., Wu, J., Rizvi, T. A., Brundage, M. E., Eaves, D., Widemann, B., Kim, M.-O., Dombi, E., Sabo, J., Hardiman Dudley, A., Niwa-Kawakita, M., Page, G. P., Giovannini, M., Aronow, B. J., Cripe, T. P. & Ratner, N. MEK inhibition exhibits efficacy in human and mouse neurofibromatosis tumors. *J. Clin. Invest.* **123,** 340–347 (2013).

96. Jousma, E., Rizvi, T. A., Wu, J., Janhofer, D., Dombi, E., Dunn, R. S., Kim, M.-O., Masters, A. R., Jones, D. R., Cripe, T. P. & Ratner, N. Preclinical assessments of the MEK inhibitor PD-0325901 in a mouse model of

neurofibromatosis type 1: MEK Inhibition in Neurofibroma. *Pediatr. Blood Cancer* **62,** 1709–1716 (2015).

97. Dodd, R. D., Mito, J. K., Eward, W. C., Chitalia, R., Sachdeva, M., Ma, Y., Barretina, J., Dodd, L. & Kirsch, D. G. NF1 Deletion Generates Multiple Subtypes of Soft-Tissue Sarcoma That Respond to MEK Inhibition. *Mol. Cancer Ther.* **12,** 1906–1917 (2013).

98. Gross, A. M., Glassberg, B., Wolters, P. L., Dombi, E., Baldwin, A., Fisher, M. J., Kim, A., Bornhorst, M., Weiss, B. D., Blakeley, J. O., Whitcomb, P., Paul, S. M., Steinberg, S. M., Venzon, D. J., Martin, S., Carbonell, A., Heisey, K., Therrien, J., Kapustina, O., Dufek, A., Derdak, J., Smith, M. A. & Widemann, B. C. Selumetinib in children with neurofibromatosis type 1 and asymptomatic inoperable plexiform neurofibroma at risk for developing tumor-related morbidity. *Neuro-Oncol.* noac109 (2022). doi:10.1093/neuonc/noac109

99. Dombi, E., Baldwin, A., Marcus, L. J., Fisher, M. J., Weiss, B., Kim, A., Whitcomb, P., Martin, S., Aschbacher-Smith, L. E., Rizvi, T. A., Wu, J., Ershler, R., Wolters, P., Therrien, J., Glod, J., Belasco, J. B., Schorry, E., Brofferio, A., Starosta, A. J., Gillespie, A., Doyle, A. L., Ratner, N. & Widemann, B. C. Activity of Selumetinib in Neurofibromatosis Type 1–Related Plexiform Neurofibromas. *N. Engl. J. Med.* **375,** 2550–2560 (2016).

100. Gross, A. M., Wolters, P., Baldwin, A., Dombi, E., Fisher, M. J., Weiss, B. D., Kim, A., Blakeley, J. O., Whitcomb, P., Holmblad, M., Martin, S., Roderick, M. C., Paul, S. M., Therrien, J., Heisey, K., Doyle, A., Smith, M. A., Glod, J., Steinberg, S. M. & Widemann, B. C. SPRINT: Phase II study of the MEK 1/2

inhibitor selumetinib (AZD6244, ARRY-142886) in children with neurofibromatosis type 1 (NF1) and inoperable plexiform neurofibromas (PN). *J. Clin. Oncol.* **36,** 10503–10503 (2018).

101. Johnson, G. L., Stuhlmiller, T. J., Angus, S. P., Zawistowski, J. S. & Graves, L. M. Molecular Pathways: Adaptive Kinome Reprogramming in Response to Targeted Inhibition of the BRAF–MEK–ERK Pathway in Cancer. *Clin. Cancer Res.* **20,** 2516–2522 (2014).

102. Nazarian, R., Shi, H., Wang, Q., Kong, X., Koya, R. C., Lee, H., Chen, Z., Lee, M.-K., Attar, N., Sazegar, H., Chodon, T., Nelson, S. F., McArthur, G., Sosman, J. A., Ribas, A. & Lo, R. S. Melanomas acquire resistance to B-RAF(V600E) inhibition by RTK or N-RAS upregulation. *Nature* **468,** 973–977 (2010).

103. Di Veroli, G. Y., Fornari, C., Wang, D., Mollard, S., Bramhall, J. L., Richards, F. M. & Jodrell, D. I. Combenefit: an interactive platform for the analysis and visualization of drug combinations. *Bioinformatics* **32,** 2866–2868 (2016).

104. Patel, A. J., Warda, S., Maag, J. L. V., Misra, R., Miranda-Roman, M. A., Pachai, M. R., Lee, C. J., Li, D., Wang, N., Bayshtok, G., Fishinevich, E., Meng, Y., Wong, E. W. P., Yan, J., Giff, E., Pappalardi, M. B., McCabe, M. T., Fletcher, J. A., Rudin, C. M., Chandarlapaty, S., Scandura, J. M., Koche, R. P., Glass, J. L., Antonescu, C. R., Zheng, D., Chen, Y. & Chi, P. PRC2 Inactivating Mutations in Cancer Enhance Cytotoxic Response to DNMT1 Targeted Therapy via Enhanced Viral Mimicry. *Cancer Discov.* cd.21.1671 (2022). doi:10.1158/2159-8290.CD-21-1671

105. Jones, G. G., del Río, I. B., Sari, S., Sekerim, A., Young, L. C., Hartig, N., Areso Zubiaur, I., El-Bahrawy, M. A., Hynds, R. E., Lei, W., Molina-Arcas, M., Downward, J. & Rodriguez-Viciana, P. SHOC2 phosphatase-dependent RAF dimerization mediates resistance to MEK inhibition in RAS-mutant cancers. *Nat. Commun.* **10,** 2532 (2019).

106. Henry, J. R., Kaufman, M. D., Peng, S.-B., Ahn, Y. M., Caldwell, T. M., Vogeti, L., Telikepalli, H., Lu, W.-P., Hood, M. M., Rutkoski, T. J., Smith, B. D., Vogeti, S., Miller, D., Wise, S. C., Chun, L., Zhang, X., Zhang, Y., Kays, L., Hipskind, P. A., Wrobleski, A. D., Lobb, K. L., Clay, J. M., Cohen, J. D., Walgren, J. L., McCann, D., Patel, P., Clawson, D. K., Guo, S., Manglicmot, D., Groshong, C., Logan, C., Starling, J. J. & Flynn, D. L. Discovery of 1-(3,3-Dimethylbutyl)-3-(2-fluoro-4-methyl-5-(7-methyl-2-(methylamino)pyrido[2,3-*d*]pyrimidin-6-yl)phenyl)urea (LY3009120) as a Pan-RAF Inhibitor with Minimal Paradoxical Activation and Activity against *BRAF* or *RAS* Mutant Tumor Cells. *J. Med. Chem.* **58,** 4165–4179 (2015).

107. Ramurthy, S., Taft, B. R., Aversa, R. J., Barsanti, P. A., Burger, M. T., Lou, Y., Nishiguchi, G. A., Rico, A., Setti, L., Smith, A., Subramanian, S., Tamez, V., Tanner, H., Wan, L., Hu, C., Appleton, B. A., Mamo, M., Tandeske, L., Tellew, J. E., Huang, S., Yue, Q., Chaudhary, A., Tian, H., Iyer, R., Hassan, A. Q., Mathews Griner, L. A., La Bonte, L. R., Cooke, V. G., Van Abbema, A., Merritt, H., Gampa, K., Feng, F., Yuan, J., Mishina, Y., Wang, Y., Haling, J. R., Vaziri, S., Hekmat-Nejad, M., Polyakov, V., Zang, R., Sethuraman, V., Amiri, P., Singh, M., Sellers, W. R., Lees, E., Shao, W., Dillon, M. P. & Stuart, D. D.

Design and Discovery of *N* -(3-(2-(2-Hydroxyethoxy)-6-morpholinopyridin-4-yl)-4-methylphenyl)-2-(trifluoromethyl)isonicotinamide, a Selective, Efficacious, and Well-Tolerated RAF Inhibitor Targeting RAS Mutant Cancers: The Path to the Clinic. *J. Med. Chem.* **63,** 2013–2027 (2020).

108. Nichols, R. J., Haderk, F., Stahlhut, C., Schulze, C. J., Hemmati, G., Wildes, D., Tzitzilonis, C., Mordec, K., Marquez, A., Romero, J., Hsieh, T., Zaman, A., Olivas, V., McCoach, C., Blakely, C. M., Wang, Z., Kiss, G., Koltun, E. S., Gill, A. L., Singh, M., Goldsmith, M. A., Smith, J. A. M. & Bivona, T. G. RAS nucleotide cycling underlies the SHP2 phosphatase dependence of mutant BRAF-, NF1- and RAS-driven cancers. *Nat. Cell Biol.* **20,** 1064–1073 (2018).

109. Ishii, N., Harada, N., Joseph, E. W., Ohara, K., Miura, T., Sakamoto, H., Matsuda, Y., Tomii, Y., Tachibana-Kondo, Y., Iikura, H., Aoki, T., Shimma, N., Arisawa, M., Sowa, Y., Poulikakos, P. I., Rosen, N., Aoki, Y. & Sakai, T. Enhanced Inhibition of ERK Signaling by a Novel Allosteric MEK Inhibitor, CH5126766, That Suppresses Feedback Reactivation of RAF Activity. *Cancer Res.* **73,** 4050–4060 (2013).

110. Bennett, D. C., Cooper, P. J. & Hart, I. R. A line of non-tumorigenic mouse melanocytes, syngeneic with the B16 melanoma and requiring a tumour promoter for growth. *Int. J. Cancer* **39,** 414–418 (1987).

111. Shah, M. A. & Schwartz, G. K. The relevance of drug sequence in combination chemotherapy. *Drug Resist. Updat.* **3,** 335–356 (2000).